UNIVERSITÀ DEGLI STUDI DI MESSINA
DIPARTIMENTO DI SCIENZE CHIMICHE, BIOLOGICHE, FARMACEUTICHE ED AMBIENTALI

CORSO DI DOTTORATO DI RICERCA IN
BIOLOGIA APPLICATA E MEDICINA SPERIMENTALE
***XXIX* CICLO**

Amphiphilic biodegradable nanoparticles for optimization of drug delivery and targeting in cancer treatment

TESI DI DOTTORATO:
DOTT.SSA CARLA SERRI

TUTOR:
PROF.SSA ANTONINA SAIJA

CO-TUTOR:
PROF. MARCO BIONDI

COORDINATORE DEL CORSO DI DOTTORATO.
CHIAR.MO PROF. SALVATORE CUZZOCREA

TRIENNIO 2014-2016

Index

Introduction

Cancer is one of the major causes of death worldwide. New cancer diagnoses are about 12 million each year, and about 8.2 million people in 2012 died from this disease in the world (Baban and Seymour, 1998; World Health Organization., 2015). Currently, cancer represents the second cause of death after cardiovascular diseases. According to the World Health Organization (WHO), the most lethal kinds of cancer recognized to date are the cancer of lung (1.59 million deaths), liver (745,000 deaths), stomach (723,000 deaths), colon and rectum (694,000 deaths), breast (521,000 deaths) and esophagus (400,000 deaths) (World Cancer Report., 2014). Cancer may be defined as an abnormal mass of tissue, whose growth exceeds that of normal tissue, and persists in the same excessive manner after cessation of the stimuli which caused it (Willis, 1952; Robbins, 2007). Tumors can be classified according to their biological characteristics in malignant and benign. The latters possess a structure more similar to that of healthy tissue, without invasion of the surrounding tissue and, also, do not metastasize. On the contrary, malignant tumors have an irregular shape and show a strong tendency to invade and infiltrate the surrounding tissues; in particular, metastases are the major cause of death from cancer (Figure 1).

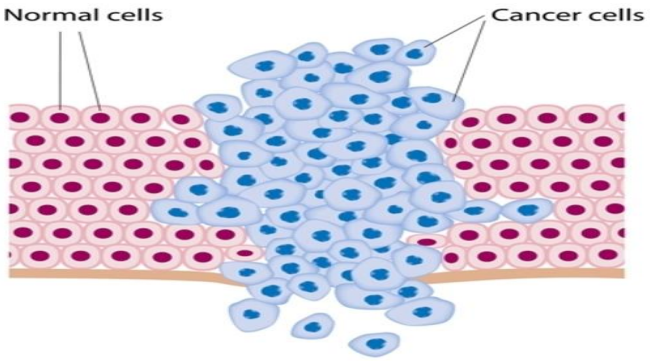

Figure 1: Normal and Cancer cells

There are different possibilities for the treatment of cancer, such as surgery, radiotherapy, chemotherapy and immunotherapy; these options can also be used in combination, simultaneously or sequentially. In particular, chemotherapy is based on the use of antineoplastic drugs (such as irinotecan, cisplatin, 5-fluorouracil, anthracyclines, taxanes, just to name a few) which can be administered by different routes (intravenously, orally, etc.) and aims at killing tumor cells. Ideally, an anticancer drug should exert its cytotoxity selectively against the tumoral tissue. However, many anticancer drugs have low therapeutic indices and generally lack specificity; consequently, they are toxic to both cancer and normal cells, and cause strong non-specific side effects, such as myelosuppression, immunosuppression, gastrointestinal problems (e.g. nausea and vomiting), cardiotoxicity (myocardial ischemia, arrhythmias, more or less severe heart failure) and nephrotoxicity (Willis, 1952; Robbins, 2007). For this reason, pharmaceutical dosage forms with controlled/targeted delivery features have been attracting a great deal of interest, due to their ability to prolong the half-life of the drug, and possibly decrease the therapeutic doses, so improving the patient compliance and the

overall therapeutic response. In this context, the use of nanotechnologies, in particular nanoparticles, may meet this requirement, by improving the pharmacokinetic and pharmacodynamic profiles of the loaded drug(s). (Hardman et al., 2001; Torchilin, 2007; Peer et al., 2007; Gullotti and Yeo, 2009).

Irinotecan and Curcumin in Cancer Treatment

Irinotecan hydrochloride (4,11-diethyl-3,4,12,14-tetrahydro-4-hydroxy-3,14-dioxo1H-pyrano[3',4',6,7]-indolizino[1,2-b]quinolin–9–yl-[1,4'bipiperidine]-1'-carboxylate, or CPT11) (Figure 2) is a semisynthetic derivative of the plant alkaloid camptothecin (isolated from the Chinese tree *Camptotheca acuminate*), which exerts its antitumor activity by inhibiting topoisomerase I enzyme.

In particular, Irinotecan is used as a first-line or second-line agent in the treatment of advanced colorectal, ovarian, cervical, and small cell lung cancer, alone or in combination with other drugs, such as 5-fluorouracil and doxorubicin (Poudel et al., 2016; Saltz, 1999; Biondi et al., 2013a). In particular, Irinotecan is the first-line treatment in combination with fluoropyrimidines for the cure of advanced colorectal cancer in patients who have not previously received a chemotherapy; alternatively, it can be administered alone if a previous treatment with 5-fluorouracil has not produced satisfactory results.

All camptothecins contain a basic structure composed of 5 rings, with a chiral center on the C-20 of the lactone terminal ring. Irinotecan is a prodrug; in

fact its bulky piperidino side chain, located at the C-10 position, must be cleaved enzymatically by a carboxylesterase to form the biologically active metabolite, SN-38, which is 1,000-fold more active in inhibiting topoisomerase I compared to irinotecan. Topoisomerase I acts in the S phase of the cell cycle, when the cell is actively replicating; it forms intermediate complexes with DNA by cutting one of the two strands of the double helix, then relaxing and reannealing the strand. During this process, topoisomerases stabilize the DNA break by forming a covalent bond between the enzyme (via a tyrosine hydroxyl group) and the phosphate at the break site. Camptothecins bind and stabilize the DNA-topoisomerase I complex, thus preventing the subsequent DNA repair, thereby causing accumulation of single filaments of broken DNA that interferes with the replication and thus lead to cell death (Kehrer et al., 2001; Lavergne et al, 1998; Garcia-Carbonero and Supko, 2002).

Several *in vitro* studies have demonstrated numerous mechanisms of resistance to topisomerase inhibitors and in particular to irinotecan. The following general mechanisms of resistance have been suggested: variable levels of the enzymes involved in the conversion of irinotecan; reduced cellular accumulation from active drug efflux; reduced levels of topoisomerase I expression and genetic alterations in its structure; alterations in the cellular response to camptothecin–topoisomerase I-DNA complex formation, which involves proteasome degradation of topoisomerase I and/or enhanced DNA repair; activation of the transcription factor nuclear factor kappa B by DNA damage and subsequent suppression of apoptosis (Xu and Villalona-Calero. 2002).

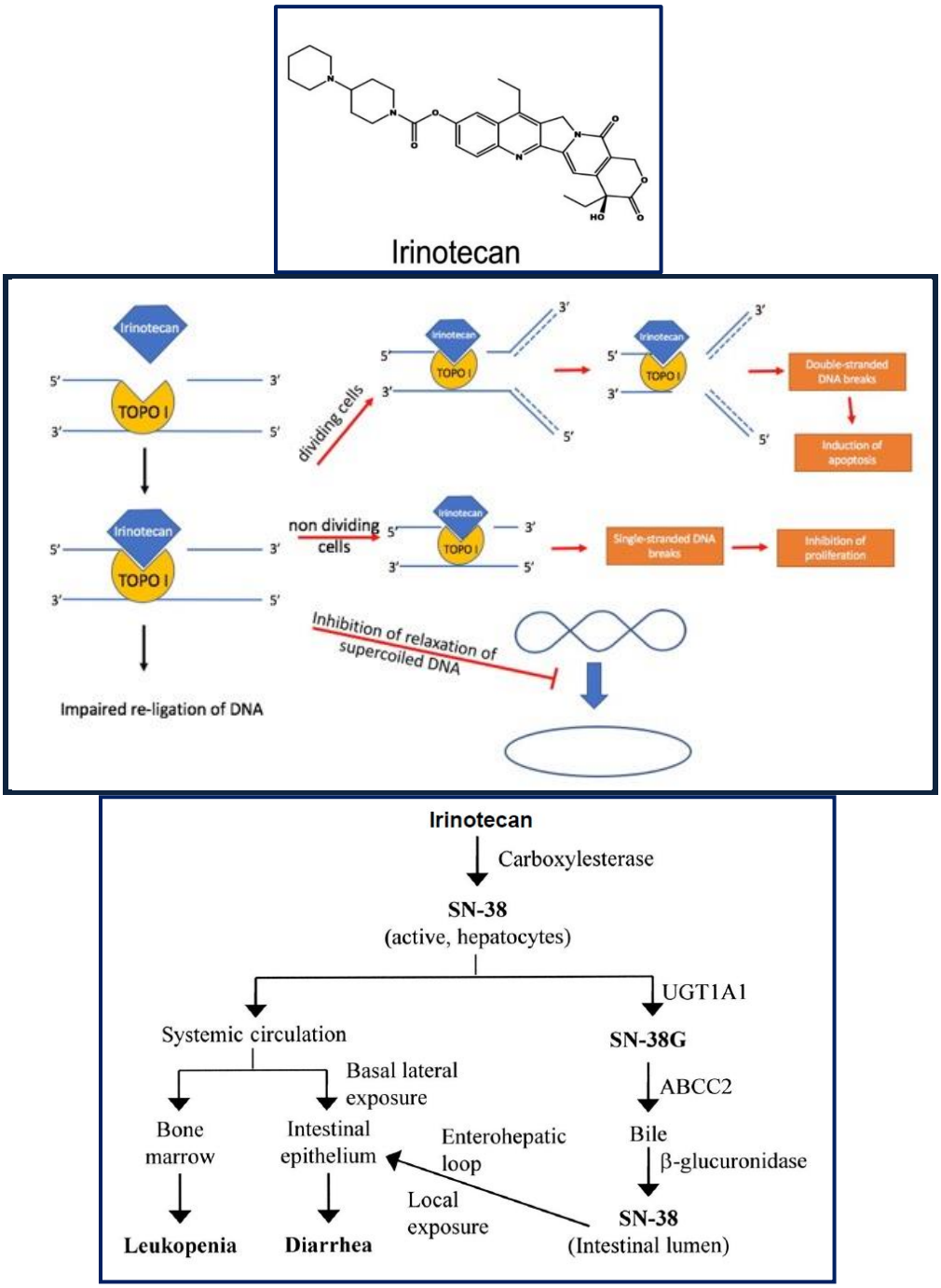

Figure 2. Chemical structure of irinotecan; effects due to irinotecan inhibition of topoisomerase; metabolism of irinotecan.

Irinotecan is metabolized by carboxylesterase in the liver to SN-38, which is glucuronidated mainly by UGT1A1 and, in this form, secreted into the bile through ABCC2. A large part of SN-38 glucuronide (SN-38G) is reconverted in the intestine to SN-38 by β-glucuronidase. Intestinal SN-38, once reabsorbed, is sent back to the liver (enterohepatic circulation loop), therefore increasing the possibility to develop leucopenia and diarrhea.

The active drug SN-38 is, in turn, glucuronidated by the enzyme uridine diphosphate glucuronosyl 1A transferase 1 (UGT1A1); this metabolite is then eliminated into the bile. Polymorphisms of UGT1A1 are related to defects in SN-38 metabolism and are associated to an increased risk of toxicity. The major dose-limiting toxicity of irinotecan is represented by a delayed diarrhea emerging 7-10 days after the end of the treatment, with or without neutropenia. Further unwanted effects include myelosuppression, cholinergic syndrome, diaphoresis, hypersalivation, abdominal cramps, watery eyes, runny nose and bradycardia, nausea, vomiting, fatigue, vasodilatation, increased liver transaminases (Morton et al., 1999; Gupta et al., 1997).

Topoisomerase I inhibitor irinotecan has been commercially available since 1996 for the treatment of colorectal cancer. Despite the fact that TOP1 inhibitors are widely used chemotherapeutic agents, limitations hamper broad clinical utility. Irinotecan and its active metabolite SN-38 have the propensity to damage healthy tissues, but also have short circulation half-lives, neither sufficiently exposing the tumor to the therapeutic agent nor adequately maintaining TOP1 clevage complexes for subsequent DNA damage.

Nanotechnology and polymer-based chemistry is transforming the field of drug delivery systems and is playing an increasingly important role in modern therapeutics. Pegylation defines the modification of a protein, peptide, or nonpeptide molecule by the linking of one or more poly(ethylene glycol) (PEG) chains. PEG is highly soluble, nontoxic, and nonimmunogenic. This technology increases the bioavailability of a pegylated drug, decreases the degradation of the drug, decreases uptake of the PEG–drug compound through the reticuloendothelial system, and decreases its immunogenicity.

Pegylation of certain drugs has facilitated an increase in the general therapeutic efficacy of certain biomolecules.

The first agent approved by the US Food and Drug Administration (FDA) was pegademase bovine in 1990, for the treatment of severe combined immunodeficiency disease, and 4 years later pegaspargase (pegylated L-asparaginase) was approved for the treatment of acute lymphoblastic leukemia. Since then the FDA has approved ten other drugs in which pegylation technology is used to deliver a specific therapeutic agent to treat not only certain types of malignancies, but also certain chronic infections such as chronic hepatitis C virus infection (pegylated interferon alpha), to treat macular degeneration (pegaptanib), and to stimulate erythropoiesis (peginesatide) and myelopoiesis (pegfilgrastim).

Etirinotecan pegol (pegylated irinotecan), also known as NKTR-102, is a uniquely structured, long-acting polymer conjugate that contains a large-chain polyethylene glycol (PEG) core to which four molecules of irinotecan are attached via a cleavable ester-based linker (Alemany, 2014; López-Miranda and Cortés et al., 2016). The linker slowly hydrolyses in vivo to release irinotecan, which is subsequently converted to SN-38, the active metabolite of irinotecan. The high molecular weight of etirinotecan pegol (nominal molecular weight 22 kDa) limits its ability to freely cross intact vasculature into healthy tissues but promotes extravasation through the leaky tumour microvasculature, consistent with the enhanced permeation and retention effect shown for macromolecules. Etirinotecan pegol was developed and engineered to reduce maximal exposure to SN-38 in systemic concentrations while providing continuous exposure in tumors, even when

administered in 14- or 21-day cycles. The half-life of SN-38, after administration of irinotecan, is approximately 12-17 h, in contrast to the half-life of SN-38 after etirinotecan pegol administration of approximately 50 days. In murine xenograft models, pharmacokinetic studies of etirinotecan pegol showed lower plasma clearance and greater exposure to irinotecan and SN-38 in comparison with irinotecan. Given its prolonged bioavailability, it was hypothesized that etirinotecan pegol would have a better antineoplastic effect. Actually, this new irinotecan formulation has shown promising activity for treatment of patient with metastatic breast cancer.

Onivyde, also known as MM-398 (pegylated liposomal irinotecan hydrochloride trihydrate), has been designed and developed as a nanoliposomal formulation of irinotecan, which employs a modified gradient-loading method using sucrose octasulfate (Ur Rehman et al., 2016; Ko, 2016). It improves the pharmacokinetics of the drug by increasing drug encapsulation and loading efficiency, protecting the drug in the active lactone configuration, prolonging circulation time, providing sustained release, rerouting the drug from sites of toxicity such as the gastrointestinal tract, increasing tumor accumulation via the EPR effect, and reducing host toxicity. Based on the encouraging data available from the phase 3 NAPOLI-1 study, Onivyde was approved by the US Food and Drug Administration (FDA) in October 2015 and by EMA in 2016 as for treatment, in combination with 5-fluorouracil and leucovorin, of patients with gemcitabine-based chemotherapy-resistant metastatic pancreatic cancer. Onivyde has been designated as an orphan medicinal product on 9 December 2011 for the treatment of this rare kind of patients.

Curcumin (1,7-bis-(4-hydroxy-3-methoxyphenyl)-hepta-1,6-diene-3,5-dione) is a polyphenol extracted from the rhizome of *Curcuma Longa* Linn (turmeric) and has a long history as a remedy in Ayurveda, Unani, and Siddha medicine for the treatment of various diseases. Curcumin was first isolated by Vogel et al. in an impure form, then its properties were clarified by Milobedeska et al. and was synthesized chemically by Lampe et at (Vogel Pelletier., 1815; Milobedeska et al., 1910; Lampe et al., 1913). Turmeric contains a mixture of three different analogues, curcumin, demethoxycurcumin (DMC), and bisdemethoxycurcumin (BDMC). These three compounds, called curcuminoids, differ in terms of methoxy substitution on the aromatic ring. Curcumin has two symmetrical methoxy-phenol bound through the α,β-diketoneβ-unsaturated portion; also BDMC is a symmetrical molecule but lacks two o-methoxy substitutions, while DMC has an asymmetric structure with one of the phenyl rings with methoxy substitution (Anand et al., 2008; Kiuchi et al., 1993; Mehanny et al., 2016) (Figure 3).

Figure 3: Tumeric (*Curcuma longa*), the curcuma rhizome and the three different analogues extracted from it

A great scientific interest has recently been focused on curcumin, since it possesses different pharmacological activities, such as antioxidant, anti-inflammatory and antimicrobial properties, and so it is effective against different diseases, such as cardiovascular (e.g. atherosclerosis, thrombosis), neurodegenerative (e.g. Parkinson and Alzheimer disease) and autoimmune (e.g. rheumatoid arthritis) diseases, gastrointestinal disorders, gastroduodenal ulcers and pulmonary illnesses, as well as viral and bacterial infections (Apetz et al., 2014; Kochi et al., 2015; Lv et al., 2014; Chiu et al., 2013; Hasan et al., 2014; Pari, et al., 2008; Kerdsakundee et al., 2015; Yadav et al., 2013; Jiang et al., 2013; Prakash et al., 2011; Srivastava et al., 1985; Shah et al., 1999; Ferreira et al., 2015; Gandapu et al., 2011). It is also well known that curcumin can be potentially used in cancer treatment taking advantage of its ability to kill tumor cells, and, more interestingly, it seems to exert a selective cytotoxic effect against tumoral cells (Jurenka et al., 2009; Sarkar et al., 2016). Not only in vitro but also in vivo preclinical studies have pointed at the ability of curcumin to block tumor progression. Cancer progression and growth are governed by multiple signaling pathways (e.g. NF-κB, Akt, MAPK, Wnt, Notch, p53) (Li et al., 2011; Sahin et al., 2016) (Figure 4).

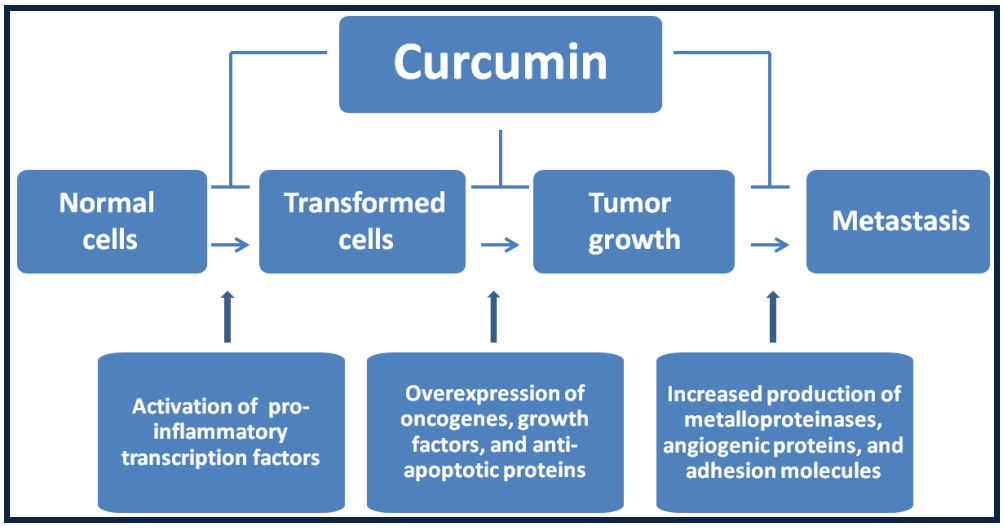

Figure 4: Potential anti-cancer functions of curcumin
(see also Shanmugam et al., 2015**)**

In this context, curcumin has multiple molecular targets and may intervene in different phases of the cell cycle, and for this reason a fluorishing interest of research in the medical field has been recently raised for the use of curcumin in cancer treatment. Curcumin also modulates the activities of many cell key molecules, such as kinases (e.g., EGFR, ERK, JAK, and AAPK), enzymes (e.g., MMP, iNOS, GST, and ATPase), transcription factors (e.g., NF-κB, STAT3, AP-1, NRF-2, PPAR-γ, and HIF-1), receptors (e.g., HER-2, IL-8, and CXCR-4), growth factors (e.g., EGF, NGF, HGF, and PDGF) and cytokines (e.g., TNF, IL, MIP, and MCP) (Goel et al., 2008). In particular, a main role in the anticancer activity of curcumin is ascribed to its capability to inhibit the transcription factor NF-kB, which has a key role (Figure 5).

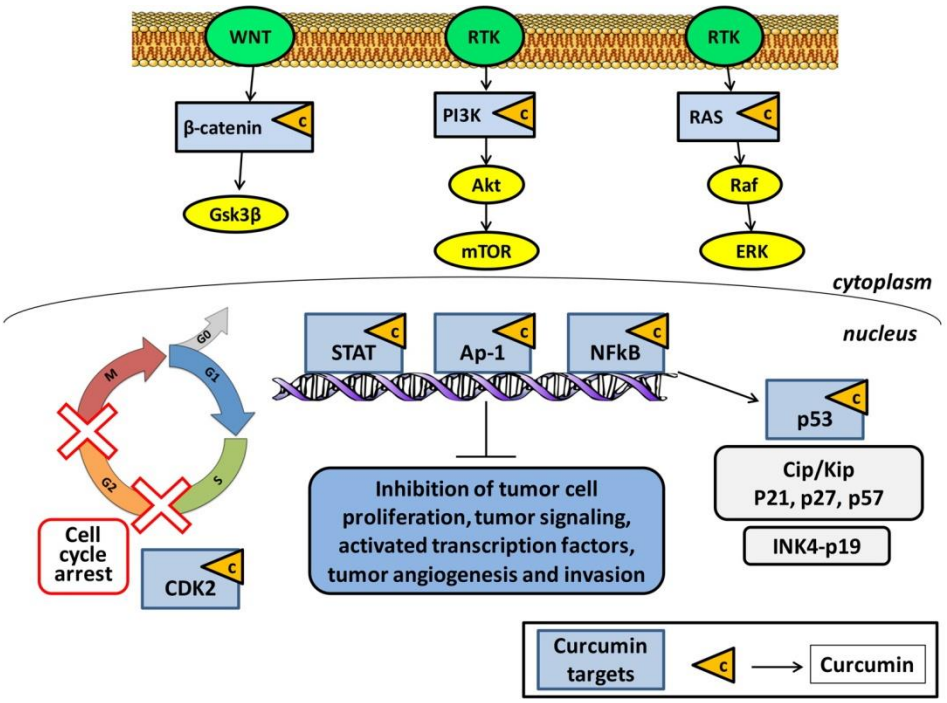

Figure 5: Molecular targets of curcumin in cancer cells (see also Kasi et al., 2016) activator protein-1 (Ap-1); CDK interacting protein/Kinase inhibitory protein (cip/kip); cyclin-dependent kinases (CDK); extracellular signal–regulated kinase (ERK); glycogen synthase kinase 3 (Gsk3); inhibitors of CDK4 (INK4); mammalian target of rapamycin (mTOR); nuclear factor kappa-light-chain-enhancer of activated B cells (NF-kB); phosphoinositide 3-kinase (PI3K); protein kinase B (Akt); receptor tyrosine kinases RTK); signal transducer and activator of transcription (STAT)

Malignant pleural mesothelioma (MPM) arises from the mesothelial cells that line the pleural cavity, pericardium, and peritoneum and is a relatively rare but aggressive malignancy with a dismal prognosis and very limited therapeutic strategies (Bonelli et al., 2016). In fact, despite the recent advances in the combination treatment of surgery, chemotherapy, radiotherapy, immunotherapy, targeted molecular therapy and gene therapy, the prognosis is still poor, with a life expectancy of 9–12 months from time of diagnosis. Since MPM is considered to be linked at least in part to exposure to asbestos, and due to the 20-40 year delay between exposure to asbestos and the development of MPM, the incidence of the disease is

expected to continuously increase over the next decades. Thus, novel treatment strategies are urgently required to improve survival of these patients. Although the anticancer efficacy of curcumin was investigated in a large number of solid malignancies, there is a paucity of data about its possible effects on MPM cells. Wang investigated the biological and molecular responses of MPM cells (human H2373, H2452, H2461 and H226 cells and murine AB12 cells) to curcumin and the mechanisms involved (Wang et al. 2011). Curcumin inhibited MPM cell growth in a dose- and time-dependent manner, while pretreatment of MPM cells with curcumin enhanced cisplatin efficacy. Curcumin activated the stress-activated p38 kinase, caspases 9 and 3, caused elevated levels of proapoptotic proteins Bax, stimulated PARP cleavage, and apoptosis. In addition, curcumin treatments stimulated expression of novel transducers of cell growth suppression. Furthermore in female BALB/c mice oral administration of curcumin inhibited growth of murine MPM cell-derived tumors in part by stimulating apoptosis. Thus, curcumin targets cell cycle and promotes apoptosis to suppress MPM growth *in vitro* and *in vivo*. Yamauchi examined the effects of curcumin on ACC-MESO-1, a human derived mesothelioma cell line (Yamauchi et al., 2012). Curcumin could reduce cell viability in a dose-dependent manner, but did not induce apoptosis. The authors suggested that induction of autophagy is one of the mechanisms in the reduction of cell viability by curcumin, as demonstrated by the increased LC3B-II/LC3B-I expression and the formation of autophagosomes on el MPM ectron microscopy. More recently, Miller demonstrated that curcumin may have a double effect on malignant mesothelioma human and mouse cells, through

induction of pyroptosis and subsequently protecting cells against inflammation (Miller et al., 2014). Using *in vitro* models with mouse and human malignant mesothelioma cells, curcumin was shown to induce pyroptosis through activation of caspase-1 and increased release of the high-mobility group box 1 protein; furthermore curcumin significantly downregulated levels of inflammasome-related gene expression involved in inflammation, such as NF-κB and IL-1β. Finally, Mahajanakatti analyzed the inhibitory properties of curcumin towards virulent proteins for various cancers by computer aided virtual screening (Mahajanakatti et al., 2014). Curcumin showed good towards the virulent protein for mesothelioma platelet-derived growth factor alpha (PDGFA), compared with its natural ligands. Moreover, curcumin has a relatively low cost and a low toxic profile if compared to standard chemotherapeutic drugs (Wang et al., 2011). Unfortunately, the pharmacological potential of curcumin is severely restricted by its low water solubility/absorption, low stability and short half-life, resulting in an extremely poor bioavailability. To overcome these issues, nanotechnologies, especially those based on nanoparticles, may help to improve the bioavailability of curcumin and, thus, its anticancer effects. Curcumin activity is limited by its poor bioavailability and some possible adverse effects. Although still in its early stages, the development of curcumin formulations in the form of nanosystems (nanoparticles, liposomes, micelles, phospholipid complexes, etc.) represent an interesting and useful approach to enhance its bioavailability and efficacy (Chen et al., 2015; Yallapu et al., 2015; Shome et al., 2016). Just a few examples of curcumin loaded nanosystems tested for anticancer activity are listed below: polymeric

nanoparticles (50 nm) for pancreatic cancer (Bisht et al., 2007), liposomes (80-90 nm) for skin cancer (Chen et al., 2012), solid lipid nanoparticles (190-200nm) for breast cancer (Mulik et al, 2010), nanogels (74 nm) for cervical cancer (Gonçalves et al., 2012), metallic nanoparticles (10.5 nm) for pancreatic cancer (Yallapu et al., 2013), dendrimers (150 nm) for breast cancer (Falconieri et al., 2016), quantum dots (100 nm) for colon cancer (Some et al., 2014), cyclodextrin inclusions (60–65 nm) for cervical cancer (Sawant et al., 2014), superparamagnetic iron oxide nanoparticles (~ 200 nm) for leukaemia (Dilnawaz et al., 2012).

Nanoparticles as Drug Delivery Systems

Nanotechnology is an emerging branch of science in the design, fabrication and application of nanostructures or nanomaterials that include devices with a sub-micron size. The definition by the American physicist Richard Feynman, in a famous lecture given in December 1959 at the California Institute of Technology and entitled "There's plenty of room at the bottom", suggested that he could build many devices able to direct the arrangement of atoms in the matter. The modern term "nanotechnology" was first, however, invented in 1974 by Norio Taniguchi, a researcher at the University of Tokyo, to describe the precise manipulation of atoms and molecules for the production of new materials. According to Eric Drexler, in his book "Engines of Creation: the coming era of nanotechnology" (1986), nanotechnology was defined as a molecular technology allowing the positiong of every single

atom in a desired position (Cao, 2004; Feynman, 1960; Whatmore, 2006). Recent advances in nanotechnology have revolutionized various research fields such as engineering, medicine and pharmaceutical technology. Actually, in recent years, nanotechnology has emerged as one of the greatest challenges of modern medicine and, in particular, has been focusing on the production of nanoscale devices for the controlled release of drugs. In 1995, less than 1% of scientific publications were focussed on the study of nanoparticles. In less than a decade, this proportion rose to 16%. In 2002, moreover, the global market for nanotechnology has a turnover of 406 million dollars, with an increase of 28% over the previous year (Freitas, 2005). The administration of drugs with the aid of nanotechnology-based devices is finding practical application in the biomedical field. In this context, the term "nanomedicine" refers to the use of nanotechnology aiming to improve medical diagnosis and drug therapy. In particular, in the therapeutic field, polymeric nanocarriers can be used to achieve alternative approaches to the targeting of drugs in specific cells and tissues. In fact, it must be considered that standard chemotherapeutic drugs generally generate strong unwanted side effects and, for this reason, there is a strong need to selectively attack tumor cells (Ehdaie, 2007). Nanoparticles are also able to protect the unreleased drug from degradation and thus early inactivation, thereby helping to improve drug efficacy. Moreover, properly designed NPs also allow the controlled release of active molecules by different mechanisms (e.g. sustained, delayed or pulsatile delivery), thereby in principle being able to modulate drug release in both time and space. All these properties of nanoparticles allow to improve the efficacy and reduce the toxic side effects

of highly potent drugs, such as chemotherapeutics (Mohanraj and Chen, 2006; De Jong and Borm, 2008; Aziz, 1996).

Nanoparticles can be carried to tumors by both passive and/or active targeting. Passively targeted nanoparticles exploit the well known enhanced permeability and retention (EPR) effect of tumors, which consists of leaky vessels feeding the tumor mass along with a hampered lymphatic drainage. Nanoparticles exposing a hydrophilic surface can thwart serum protein adsorption and possess stealth properties, being able to circulate in the bloodstream for prolonged times. This, in principle, increases the chances of a preferential device accumulation in solid tumor tissue (Figure 6).

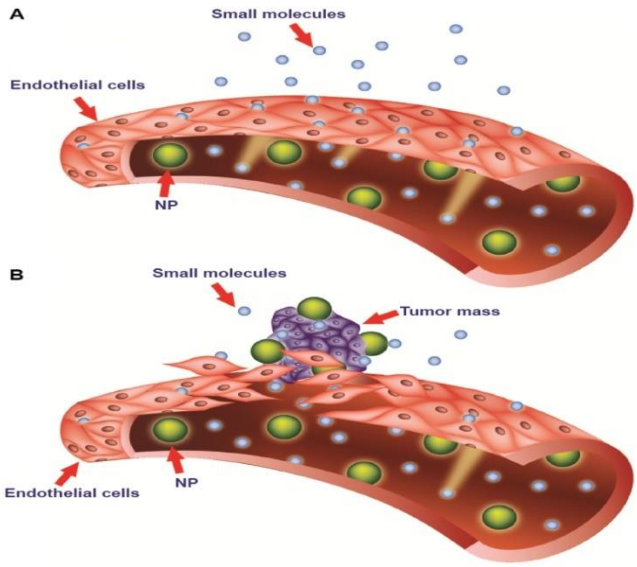

Figure 6: Passive targeting strategy of nanoparticles and Enhanced Permeability and Retention (EPR) effect (from Bozzuto and Molinari, 2015). Vessel endothelium in normal tissue (A) presents tight junctions between cells avoiding nanoparticle diffusion from blood to tissue. Conversely, endothelium of tumor vessels (B) presents large fenestrations so that nanoparticles can reach the tumoral tissue (EPR effect)

On the other hand, active targeting can be obtained if nanoparticle surface is functionalized by suitable modifications with specific ligands for the tumors,

such as nucleic acids, proteins, ligands and antibodies. (Zhang et al., 2016; Jee et al., 2012).

Among the materials used to produce nanoparticles, the ones approved by Food and Drug Administration (FDA) play a prominent role. In particular, polylactic-co-glycolic acid (PLGA) is a biodegradable polyester widely employed to produce nanoparticles. PLGA is a synthetic copolymer of lactic acid and glycolic acid, and its chain is formed by a hydrophilic (the polyglycolic acid, PGA) and a hydrophobic portion (the polylactic acid, PLA, unit) (Figure 7).

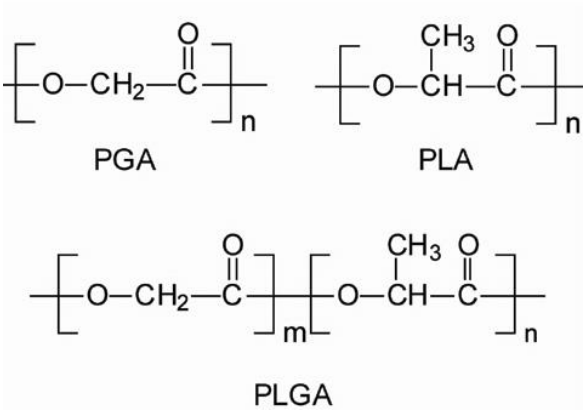

Figure 7: Chemical structure of Poly(glycolic acid) (PGA), Poly(lactic acid) (PLA) and poly(lactic-co-glycolic acid) (PLGA)

The wide PLGA use has been prompted by its well known biocompatibilty, biodegradabilty and non-toxicity, along with its mechanical strength. Properly formulated PLGA-based nanoparticles are able to control the release of drugs over time (days to weeks/months) (Jain, 2000; Peresa et al., 2016; Doty et al., 2016). Drugs encapsulated in biodegradable PLGA nanoparticles

may remain in the bloodstream for prolonged times and, therefore, their half-life, resistance to metabolic degradation and release times can be improved. It must be underlined that nanoparticle pharmacokinetics are strongly affected by the control of their size, surface charge and hydrophilicity. For example, if a hydrophilic polymer such as poly(ethylene oxide) (PEO) is superficially exposed on nanoparticles, the adsorption of opsonins is hampered, thus conferring the desired stealth properties to nanoparticles (Mainardes et al., 2009).

Other polymeric material of pharmaceutical interest are poloxamers, which are amphiphilic tri-block copolymers of poly(ethylene oxide) - poly(propylene oxide) - poly(ethylene oxide) (PEO-PPO-PEO). In particular, PEO segments are hydrophilic, while the amphiphilic features are due to the central PPO portion of the polymer (Santander-Ortega et al., 2006) (Figure 8).

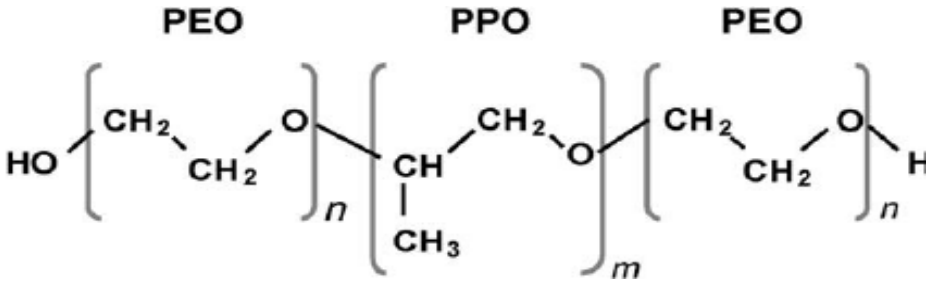

Figure 8: Chemical structure of a poloxamer (PEO-PPO-PEO)

Poloxamers form micelles in aqueous solution, with a lipophilic core, and a predominantly hydrophilic shell. When their molecular weight is < 15 kDa, they are generally eliminated by kidneys into the urine. Among poloxamers,

Pluronic F127 (also known as poloxamer 407) has been approved by FDA as a pharmaceutical excipient for medical use (FDA., 2013; Rao et al., 2014).

Another polymer which has drawn great scientific interest in the biomedical field is hyaluronic acid (HA). HA is known for its ease of chemical modification and, in its native state, possesses unique properties such as biocompatibility, nonimmunogenicity and biodegradability. HA is a natural polysaccharide composed of repeating disaccharide units of D-glucuronic acid and N-acetyl-D-glucosamine. Discovered in 1934 by Karl Meyer and John Palmer in the vitreous body in bovine eyes (Meyer and Palmer, 1934), it is ubiquitously present in the extracellular matrix of connective tissues of mammals (Weissman and Meyer, 1954) (Figure 9).

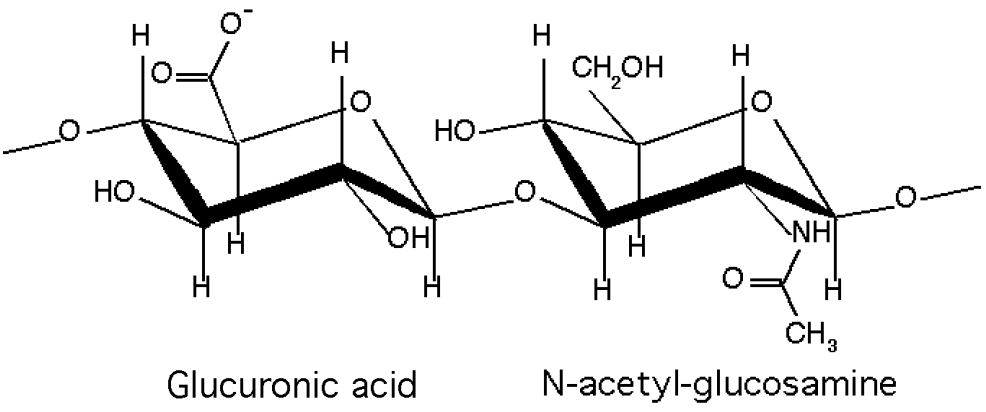

Figure 9: Chemical structure of Hyaluronic Acid

HA is an important structural element in the skin and is also present at high concentration in synovial fluid, vitreous humor, hyaline cartilage, disc core and umbilical cord (Monheit and Coleman, 2006; Borzacchiello et al., 2000; Barbucci et al., 2000; Barbucci et al., 2002). The unique biological as well as

chemico-physical properties of HA are attracting a great deal of interest among researchers and, to date, HA is being used in various biomedical applications such as regenerative medicine and drug delivery (Mironov et al., 2005).

HA actively influences cell differentiation, proliferation and migration by binding to cells with specific interactions. In fact, these processes are mediated by proteins, called hyaladherins, which act as cellular receptors for HA. Examples of HA receptors are the cluster determinant 44 (CD44), the receptor for hyaluronan-mediated motility (RHAMM), the HA receptor for endocytosis (HARE), and the lymphatic vessel endothelial hyaluronan receptor-1 (LYVE-1), capable of recognizing and selectively bind HA (Alho and Underhill, 1989; Aruffo et al., 1990; Entwistle et al.,1996; Asayama et al., 1998; Takei et al. 2004; Schledzewski et al., 2006). In particular, CD44 and RHAMM receptors are being increasingly investigated because involved in tumor metastasis. CD44 is the best characterized transmembrane HA receptor because it is expressed on the surface of several cells, such as leucocytes, fibroblasts, keratinocytes and epithelial and endothelial cells, and it also involved in many cellular processes, such as cell adhesion, migration, proliferation and activation, as well as HA degradation and uptake (Ahrens et al., 2001; Noble, 2002; Toole et al., 2002; Isacke and Yarwood, 2002). In tumor therapy, there is a strong interest on the employment of HA due to its tumor targeting ability, since it shows a strong tropism toward many tumor cells which naturally overexpress CD44 receptor. Therefore, nanoparticles which superficially expose HA may be better endocytosed by target tumor cells through receptor-mediated pathways and, hence, can be endowed with

active targeting capability. In this panorama, HA-decorated nanoparticles can be considered as interesting candidate devices for drug targeting to tumors.

Aim of the Thesis

The present research work has been focused on the design of amphiphilic biodegradable nanoparticles for optimization of drug delivery and targeting in cancer treatment. The drugs that we have taken into consideration are the natural compound curcumin (Chapter 1 and 2) and the synthetic chemotherapic drug irinotecan (Chapter 3). Curcumin has many pharmacological properties and a recognized anti-tumor activity, but its pharmacological potential is severely limited due to its low water solubility, short half-life and poor bioavailability. The topoisomerase I inhibitor irinotecan is used, as a first-line or second-line agent, in the treatment of advanced colorectal, ovarian, cervical, and small cell lung cancer, alone or in combination with other drugs, such as 5-fluorouracil and doxorubicin. Unfortunately cancer cells can present and develop resistance to irinotecan through numerous mechanisms. To this aim, biodegradable PLGA-based nanoparticles for the release of curcumin and irinotecan have been produced. In particular, curcumin has been loaded in nanoparticles made of an amphiphilic blend of poloxamers and PLGA, produced by a double emulsion and nanoprecipitation technique, so as to confer stealth properties to the nanoparticles and take advantage of the EPR effect. The produced nanoparticles were tested for their stability and investigated for their *in vitro* ability to be internalized by mesothelioma cells and affect their growth. A development of this formulation was performed by targeting it to tumor cells by HA moieties on the surface of PLGA-based nanoparticles loaded with irinotecan. This has been accomplished by directing HA arrangement on

nanoparticle surfaceby means of a lipophilicity gradient between the oil and water phases of the emulsion used to produce the nanoparticles, and using poloxamers as a bridging molecule between PLGA and HA. The obtained devices were characterized for their technological and thermodynamic features as well as by ELISA tests to support the hypothesis of polymer assembly in nanoparticle formulations. *In vitro* biologic studies were carried out on CD44-overexpressing breast carcinoma cells (HS578T) to verify nanoparticle ability to target CD44 receptor.

Chapter 1

PLGA/Poloxamer Nanoparticles for Intracellular Curcumin Delivery Induce a Cell Cycle Arrest in Mesothelioma Cells

Introduction

Curcumin (CURC) is a polyphenol extracted from the rhizome of *Curcuma longa Linn*, possessing numerous pharmacological activities, such as anti-inflammatory, antioxidant and antimicrobial (Hatcher et al., 2008;). CURC can be potentially used in cancer treatment taking advantage of its ability to block the proliferation of many tumor cells (Bhattacharyya et al., 2007a; Bhattacharyya et al., 2007b). Even more interestingly, CURC seems to induce a selective cytotoxic effect mainly towards cancer cells, even in the presence of healthy cells. This activity was correlated with both a downregulation of the nuclear factor NF-κB and to its ability to react with thioredoxin reductase, which is an enzyme overexpressed in tumor cells. This interaction leads to an increased production of H_2O_2 in tumor, thus promoting cancer cell cytotoxicity (Fang et al., 2005). Furthermore, CURC triggers both downregulation of AP-1, cyclin D1, cyclin E and upregulation of p21, p27 and p53 proteins, thus repressing tumor cell proliferation/migration and promoting cell cycle arrest and apoptosis (Balasubramanian and Eckert, 2007; Banerjee et al., 2010). Another very attractive feature of CURC is its ability to overcome the multidrug resistance (MDR) of cancer cells, most likely due to its ability to down-regulate the expression of P-glycoprotein (P-gp), multidrug resistance associated protein-1 (MRP-1) and mitoxantrone resistance protein (ABCG2), which are three major proteins responsible for the high drug efflux in multidrug-resistant cancer cells (Limtrakul et al., 2007). Unfortunately, the pharmacological potential of CURC is severely restricted, mainly owing to its low water solubility/absorption, short half-life

and extremely poor bioavailability (Aggarwal and Sung, 2009; Anand et al., 2007). To overcome solubility problems, CURC has been complexed with different cyclodextrins (CDs), which are cyclic oligosaccharides with a hydrophilic outer surface and a lipophilic cavity that can incorporate hydrophobic drugs/compounds (Yadav VR et al., 2010; Yallapu et al., 2010). Moreover, CURC encapsulation in biodegradable nanoparticles (NPs) made up of poly(lactic-co-glycolic acid) (PLGA) allows to increase its circulation times/half life, cell permeability and resistance to metabolic degradation, and also promotes controlled release and targeting (Anand et al., 2010; Farokhzad et al., 2008; Shaikh, et al., 2009; Tsai et al., 2011). Drug-loaded PLGA NPs generally possess low toxicity and also a high specificity and tolerability compared to the free drug. It must also be underlined that size, surface charge and hydrophilicity of the NPs in which CURC is loaded strongly affect its bioavailability. For example, depending on their surface properties, the NPs can be either short-circulating to reach the macrophages in liver and spleen, or long-circulating to passively accumulate in tumor tissues, which are normally characterized by the enhanced vascular permeability and retention (EPR) effect (Fang et al., 2011). For these reasons, the hydrophobic surface of PLGA NPs causes short circulation times after e.v. injection due to a rapid in vivo opsonization while, if a hydrophilic polymer such as poly(ethylene oxide) (PEO) is superficially exposed, it hampers the adsorption of opsonin proteins, thus conferring stealth properties to NPs and increasing their probability of reaching tumor sites (Mainardes et al., 2009; Owens and Peppas., 2006).

Aim of the Work

The aim of the work reported in this first chapter was to study the possibility to formulate PLGA–based NPs coated with hydrophilic PEO moieties without a chemical reaction between the two polymers, therefore avoiding the presence of chemical reaction solvents and wastes. In particular, the basic idea of this work was to formulate stealth NPs by a double emulsion-solvent evaporation technique, in which the organic phase is composed of a blend of PLGA and poloxamers instead of employing them as surfactants in the external aqueous phase, as is usually performed. Poloxamers (Polox) are triblock copolymers made up of poly(ethylene oxide)-poly(propylene oxide)-poly(ethylene oxide) (PEO–PPO–PEO), displaying amphiphilic properties taking advantage of the presence of hydrophilic EO and hydrophobic PO segments on polymer backbone (Mayol et al., 2011; Ranall et al., 2011). The obtained NPs have been loaded with CURC which, for the solubility problems mentioned above, was preliminarily complexed with hydroxylpropyl-β-CDs (HPβCDs). The obtained NPs have been characterized in terms of size, morphology, zeta potential, yield and drug entrapment efficacy. NP stability was evaluated by measuring their size over time at 4 °C in aqueous media (i.e. storage condition) and at 37 °C in serum (i.e. the same conditions of *in vitro* cell experiments). Moreover, *in vitro* drug release studies have been carried out to assess the capacity of the formulated NPs to prolong CURC release. Furthermore, malignant mesothelioma cell line MSTO-211H was used to exploit the biological efficacy of CURC-loaded NPs by investigating NP cellular uptake and CURC-loaded NP effect on cell proliferation and cell cycle progression.

Materials and Methods

Materials

Poloxamers (PEO_a-PPO_b-PEO_a) are a group of amphiphilic triblock polymers, possessing variable numbers of oxyethylene (a) and oxypropylene (b) units. Poloxamer F127 (a = 100 and b = 65) and F68 (a = 76 and b = 29) were obtained from Lutrol (Basf, Germany). Equimolar uncapped poly(D,L-lactide-coglycolide) (PLGA) (Resomer RG504H, Mw: 40 kDa, inherent viscosity: 0.16-0.24 dL g^{-1} in acetone at 25 °C) was purchased from Boehringer Ingelheim (Ingelheim, Germany); Curcumin ((E,E)-1,7-bis(4-hydroxy-3-methoxyphenyl)-1,6-heptadiene-3,5-dione) (purity > 90%) from Cayman Chemical Company, USA), ultrapure sucrose from Riedel-deHaen (Germany) and potassium chloride (KCl) from Carlo Erba (Italy) were used. Polyvinyl alcohol (PVA, Mowiol® 40-88), 2-Hydroxypropyl-β-cyclodextrin (HPβCD; CD in the text), ethanol (EtOH), acetone, dimethylsulfoxide (DMSO), Tween-80, dibasic sodium phosphate (Na_2HPO_4), sodium chloride (NaCl), 1,6-diphenyl-1,3,5-hexatriene (DPH), Trypan blue, propidium iodide (PI) and RNase were obtained from Sigma-Aldrich (USA). Ascorbic and citric acid from J-Baker (USA) were used. Human mesothelioma (MSTO-211H) cell line was obtained from the American Type Culture Collection (Rockville, MD, USA); Roswell Park Memorial Institute (RPMI-1640) medium, Fetal Bovine Serum (FBS), penicillin 50 UI/mL, streptomycin 0.05 mg/mL, penicillin/streptomycin 10 UI/mL, trypsin-ethylenediamine tetra-acetic acid (Trypsin-EDTA) 1mM, sodium pyruvate and 4-(2-hydroxyethyl)-1-piperazineethanesulfonic acid (HEPES) from Euroclone (Italy) were

employed. All chemicals and media were used as received without any further purification.

Preparation of Nanoparticles

Prior to NP preparation, to enhance CURC solubility and allow a higher drug loading in NPs, CD-CURC complex was prepared by dissolving CURC in EtOH (1 mg/mL) and adding CD (8 mg/mL). The resulting solution was placed under magnetic stirring for 20 min at 80 °C until complete evaporation of the solvent. The obtained solid was found to be soluble at > 50 μg/mL in PBS, i.e. at a higher concentration than CURC solubility (about 10 μg/mL), thus proving the formation of the CD-CURC complex. Blank and CURC-loaded NPs were prepared by a modified double emulsion-solvent evaporation technique. Briefly, the internal phase, composed by 640 μL of EtOH, or the same volume of a 1.4 mg/mL solution of CD-CURC in EtOH, was emulsified with 5 mL of a 30 mg/mL PLGA or PLGA/poloxamer (50/50 mass ratio) solution in acetone (NP formulations have been named P or PP, correspondingly). The resulting emulsion was sonicated for 5 min at 4 °C (Branson 3510 ultrasonic bath, 100% power, operating at 42 kHz ± 6%). The resulting water-in-oil emulsion was immediately poured into 18 mL of 1% w/v aqueous PVA and further sonicated (5 min, 4 °C). The resulting double emulsion was stirred overnight for complete acetone evaporation. The obtained NP suspension was washed three times by centrifugation (Hettich Zentrifugen, Germany; 13,000 rpm, 30 min) and, once the supernatant was eliminated, NPs were stored at -80 °C. Fluorescent NPs were also prepared

by adding 10 mg of the fluorescent dye 1,6-diphenyl-1,3,5-hexatriene (DPH) to the organic phase containing PLGA or PLGA/poloxamer blend. DPH was chosen since it is fluorescent only in a hydrophobic environment with an intensity related to the hydrophobicity of the solution (Ranall et al., 2011).

Nanoparticle Morphology

NP morphology was studied by using a transmission electron microscope (TEM, EM208S, Philips, The Netherlands). TEM observations were carried out by spraying 100 μL of ultradiluted NP suspensions in water on a copper TEM grid (300 meshes, 3 mm diameter).

Nanoparticle Size, and ζ-Potential Analyses

NP mean size, size distribution and ζ-potential were determined by laser light scattering (ZetaSizer Nano ZS, Malvern Instruments, Malvern, UK) on a 0.1 mg/mL suspension of NPs in water (12 runs each sample).

Nanoparticle Stability

The evolution of the hydrodynamic diameters and ζ-potential of P and PP NPs was monitored at 4 °C up to 30 days in bidistilled water (i.e. in storage conditions) and in RPMI-1640 cell culture medium supplemented with 10% FBS at 37 °C up to 72 hours, i.e. the period of exposure used for *in vitro* cell

uptake/growth experiments. Size measurements were also performed on bare cell culture medium to verify possible self-aggregation. Results were averaged on at least five measurements.

Nanoparticle Yield and Drug Entrapment Efficacy

NP yield and CD-CURC entrapment efficiency were calculated from previously freeze-dried NPs (0.01 atm, 24 hours; Modulyo, Edwards, UK). In particular, NP yield was gravimetrically obtained from the entire mass of recovered freeze-dried NPs. For the loading efficiency, lyophilized NPs were dissolved in acetone (0.1% w/v) under gentle agitation for 1 h at room temperature to completely leach out CD-CURC from NPs. The obtained solution was centrifuged for 15 minutes at 13,000 rpm and CD-CURC quantified by spectrophotometric assay (UV-1800, Shimadzu Laboratory World, Japan) at 420 nm. The linearity of the response was verified over the concentration range 0.2 - 50 μg/mL ($r^2 > 0.99$). Results are expressed as mean ± standard deviation (SD) of values collected from three different batches.

Drug Release Kinetics

The release of CD-CURC from NPs was determined by loading P and PP NP suspension (at 15.74 mg/mL and 6.60 mg/mL, respectively) in a dialysis membrane (Spectra/Por® Biotech Cellular ester; molecular cut-off 12 kDa)

and placing them in 50 mL of a release medium composed by PBS 90% v/v, ethanol 10% v/v, Tween 80 0.5% w/v, acetic acid 0.01 % w/v and ascorbic acid 0.01% w/v; the pH was adjusted to 7.4. Acetic and ascorbic acid were added to the release medium to improve CD-CURC stability over time. Indeed, prior to the release experiments, CD-CURC stability was assessed by spectrophotometric assay at λ = 428 nm at 37 °C in the dark with or without the antioxidant agents. Regarding the release kinetics, at predetermined time intervals, aliquots of medium were withdrawn and replaced with fresh medium and the CD-CURC content determined by reverse phase high performance liquid chromatography (RP-HPLC). The chromatograph was equipped with a HPLC LC-10AD pump (Shimadzu, Milano, Italy), a 7725i injection valve (Rheodyne), a SPV-10A UV-Vis detector (Shimadzu) set at the wavelength of 420 nm and a C-R6A integrator (Shimadzu). Analyses were performed on a Phenomenex Luna C18 (2) 100Å column (250 mm × 4.6 mm, 5 μm). The mobile phase was a mixture of methanol, acetonitrile and bidistilled water (40:40:20 v/v). The flow rate was 1 mL/min, and the run time was set at 7 min. The experiments were performed in triplicate and under sink conditions.

Cell Cultures

Human mesothelioma MSTO-211H cells were cultured as monolayer in culture dishes using RPMI-1640 medium, supplemented with 10% FBS, 50 UI/mL penicillin and 0.05 mg/mL streptomycin, 1 mM sodium pyruvate and 10 mM HEPES. Cell cultures were maintained in a humidified atmosphere

containing 5% CO_2 at 37 °C. Prior to the experiments, cells were seeded in complete growth medium for 16 hours, in order to allow cell attachment but not cell doubling. Afterwards, cells were treated with free or NP-encapsulated drug. Different treatment times were used according to the experimental conditions. Untreated cells were used as a control.

Nanoparticle Cellular Uptake

NP cellular uptake was followed by means of a fluorescence microscope (Leica Microsystems, Germany). Fluorescent P and PP NPs were formulated as described in the Preparation of Nanoparticles section. NP cellular uptake by MSTO-211H cells was analyzed by treating for 6, 12, 24 and 48 hours 2 x 10^5 cells/well in a 6-well plate with 1 mg/mL of fluorescent P and PP NPs. At the end of the treatment, cells were rinsed with PBS and fixed with 95% ethanol for 20 min. The nuclei were stained using 2.5 µg/mL PI for 5 min. Images of stained cells were acquired and DPH blue fluorescence was monitored at λ = 428 nm, while PI fluorescent red signal was followed at λ = 610 nm. P and PP NP fluorescence intensity was quantified by Image J software on 10 cells/picture. Fluorescence intensity was normalized to the cytoplasmic area after subtracting the nucleus area from the total. Three pictures for each sample were analyzed. Experiments were performed in triplicate.

Cell Viability/Growth

To evaluate the cell viability, 1 x 10^6 MSTO-211H cells per well were seeded in 100 mm diameter culture dish for 16 hours. In a preliminary series of experiments, cells were treated for 12, 24, 48 and 72 hours with free CURC ranging from 10 to 100 μM, in order to find out the best working concentration of the drug in terms of cell viability. Free CURC at 20 μM decreases up to 50% cell viability after 72 h of exposure. So, in the subsequent experiments, cells were exposed for 12, 24, 48 and 72 hours to 20 μM of free CD-CURC or CD-CURC-loaded NPs or with the same amount of void NPs to assess NP biocompatibility and CURC-loaded NP biological effectiveness. In all experiments untreated cells were used as a control. Experiments were performed in triplicate.

At predetermined time points, the Crystal Violet (CV) staining method was performed to assess cell viability by culturing 2x10^4 cells/well in a 24-well plate and treating them as above reported. CV is a triphenylmethane dye (4-[(4-dimethylaminophenyl)-phenyl-methyl]-N,N-dimethyl-aniline), also known as gentian violet (or hexamethyl pararosaniline chloride). CV stains DNA and, upon solubilization, the amount of dye taken-up by the monolayer and the intensity of the color produced are proportional to cell number. Samples were washed in PBS after the treatment and fixed with 10% v/v formaline solution for 10 min at room temperature. Afterwards, cells were washed twice in bidistilled water and stained with 0.05% v/v CV aqueous solution for 20 minutes at room temperature. Cells were further washed twice with water and incubated for 15 minutes with 10% acetic acid solution to

dissolve the stain. Colorimetric assay, carried out in triplicate, was quantified measuring OD595 by using a TECAN instrument (Switzerland).

Cell Cycle Analysis.

Evaluation of the cell cycle distribution was performed by analyzing the DNA content in each cycle phase. Analyses were carried out by treating 1.5 x 10^6 cells for 12, 24, 48 or 72 hours with free or NP-encapsulated CD-CURC at a final concentration of 20 μM. After the treatment, cells were harvested and washed with cold PBS and centrifuged at 400 rpm for 8 min at 4 °C. The treated cells were fixed in 1 mL chilled 70% v/v EtOH and incubated for 30 minutes at 4 °C. Cells were centrifuged again (400 rpm, 8 min) and washed twice with cold PBS. Pellets were redissolved in 500 μL of cold PBS and incubated with 100 μg/mL RNaseA for 30 minutes at 37 °C. PI was added to a final concentration of 20 μg/mL and the cells were incubated on ice for 30 minutes in the dark. Flow cytometry was performed using a FACScan™ flow cytometry system (Becton Dickinson, San Jose, CA). For each sample, $5x10^4$ events were recorded and the cells fractions in each different phase of the cell cycle calculated.

Statistical Analysis.

Data were reported as mean value ± SD. Results were analyzed by using GraphPad Prism 5.0H statistical software (GraphPad Software Inc., La Jolla, CA). Paired *t* test was used for comparison of two paired groups. Results

were analyzed by one way or two way analysis of variance (ANOVA), followed by Bonferroni adjustment.

Results and Discussion

Nanoparticle Characterization

NPs made up of PLGA alone (P) or blended with poloxamers (PP) were prepared by the double emulsion–solvent evaporation technique. In a previous work, PP micro/nanoparticles for the controlled release of growth factors in tissue engineering were produced, aiming to protect the encapsulated protein from acidic degradation products of PLGA (Parajo et al., 2010). Here, we have employed the PP blend aiming to establish a rapid method to provide NPs with a hydrophilic surface. In figure 1.1, representative TEM images of NPs are reported while in table 1.1 the technological features of NPs are displayed. As it can be noted from Figures 1.1A and 1.1B, both P and PP NPs are spherical in shape with a regular surface.

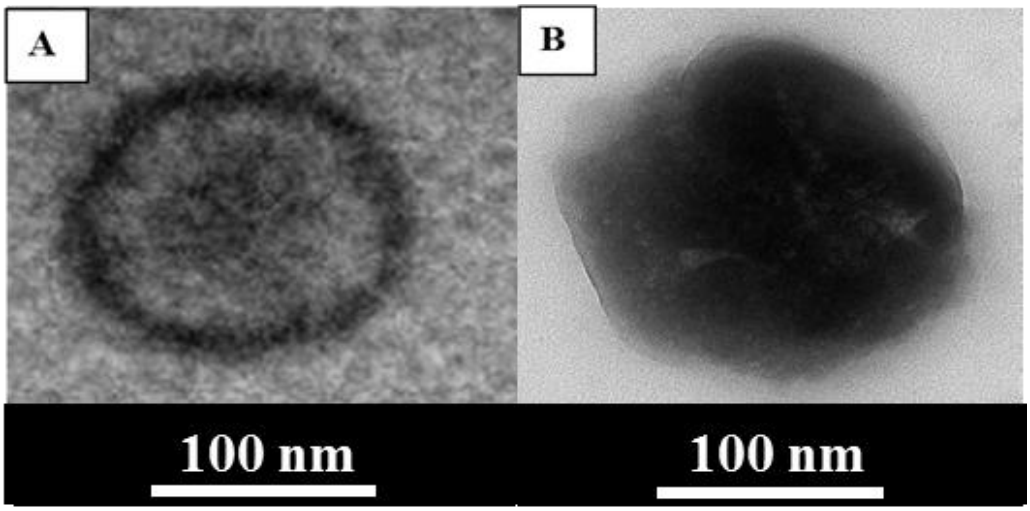

Figures 1.1: Representative TEM images of CURC-loaded P (A) and PP (B) NPs

As for NP diameters, NP yield and ζ-potential, no significant effect of poloxamer presence could be evidenced, as displayed in Table 1.1.

Forms	Particle mean diameter (nm)	Polydispersity Index (PDI)	Zeta potential (mV)	Entrapment efficiency (%)	Yield (%)
P	189 ± 37	0.258 ± 0.02	-15.7 ± 0.9	72.1 ± 3.2	79.6 ± 1.9
PP	160 ± 31	0.671 ± 0.03	-18.7 ± 1.3	90.0 ± 2.1	76.9 ± 1.4

Table 1.1: Size, polydispersity index (PDI), zeta potential entrapment efficiency and yield of CD-CURC– loaded NPs

A high entrapment efficiency was found in both formulations, in particular for PP NPs, which showed about 90% of encapsulated drug. This suggests a slightly higher affinity of the CD-CURC complex for the polymeric PLGA-poloxamers blend compared to the bare PLGA solution. In order to investigate NP storage condition, size distribution and ζ-potential of P and PP NPs were monitored as a function of time, up to 30 days, at 4 °C in double distilled water while, to reproduce the time frame of cellular experiments, after the washing step, NPs were placed in RPMI-1640 medium supplemented with 10% FBS at 37 °C up to 72 hours. Results are reported in Table 1.2, where it can be observed that the presence of poloxamers in the organic blend does not substantially affect the stability of NP suspension in comparisons with P formulation in water.

Forms.	Water, 4 °C				RPMI, 37 °C		
	Day 0	Day 10	Day 20	Day 30	Day 1	Day 2	Day 3
d_P	189 ± 37	233 ± 11	243 ± 76	265 ± 36	226 ± 9	221 ± 19	234 ± 15
d_{PP}	160 ± 31	167 ± 17	153 ± 13	180 ± 24	161 ± 4	157 ± 13	164 ± 11

Table 1.2: Time evolution of NP diameter in water at 4 °C and in cell culture medium (RPMI) at 37 °C

On the contrary, when facing serum proteins, the presence of poloxamers on the NP surface does make the difference. Actually, while the diameters of P NPs rapidly increased to about 230 nm in only 8 hours (data not shown), thus indicating a strong interaction with serum protein due to their hydrophobic surface, PP NPs diameters were basically stable within the time frame of the experiment. The interaction of NPs with serum proteins is a critical issue since it is known to strongly affect the pharmacokinetics of devices and hence their *in vivo* fate/activity, since long circulating NPs weakly interact with serum proteins (Fang et al., 2011). Actually, the strong difference in the NP/protein interaction indicates different surface properties between P and PP formulations. This can be reasonably ascribed to a spontaneous interaction between PLGA and poloxamers in the organic phase of the emulsion used for NP preparation. In particular, it can be easily grasped that

the hydrophobic PPO segments of the poloxamer dissolve in the organic phase of the emulsion together with PLGA, while the most of hydrophilic PEO segments orient themselves towards the external aqueous phase. By this way, a spontaneous cover of hydrophilic PEO is expected to arrange themselves on PLGA NP surface. Therefore, the use of an amphiphilic polymeric blend in the organic phase of the emulsion seems to be a promising alternative method to obtain stealth NPs without the economical and purification issues related to chemical reaction used for standard PEGylation.

Curcumin Stability Studies

It is well known that CURC is highly unstable at 37 °C at both neutral and neutral/basic pH. Actually, CURC undergoes extensive degradation within 24 hours and the mechanism is believed to be mainly oxidative (Subhashini et al., 2013; Pan et al., 1999). For this reason, prior to release experiments, CD-CURC stability has been assessed by measuring the absorbance of a solution of CD-CURC complex in the release medium at 25 μg/mL and 37 °C (Figure 1.2). We found that CD-CURC absorbance in the release medium dropped down of approximately 90% within only 24 hours. For this reason, we added ascorbic and citric acid (0.01% w/v for both substances) as anti-oxidant agents. In these conditions, the measured absorbance was found to be stable for at least 5 days.

In Vitro Drug Release Kinetics

In vitro CD-CURC release profiles from P and PP NPs, at 37 °C and physiological conditions are shown in Figures 1.2A and 1.2B.

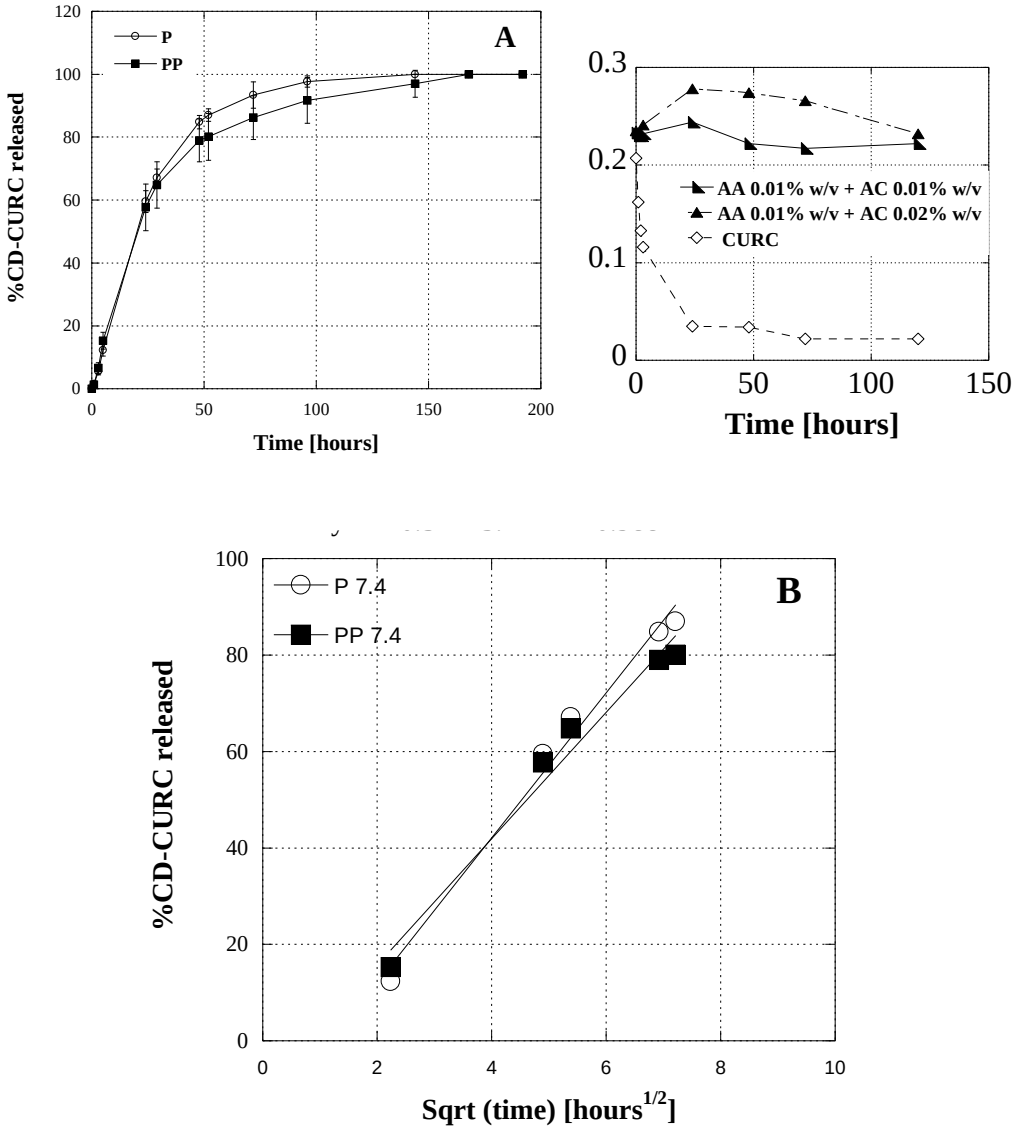

Figures 1.2: CD-CURC release kinetics. A) Release profile of CD-CURC from P and PP NPs at 37 °C and pH=7.4, and CURC stability in the release medium at 37 °C in the dark with and without antioxidants (i.e. acetic acid (AA) and ascorbic acid (AC)). B) Percentage of released CD-CURC as a function of square root of time (○ y = -18.1 + 15.0x R= 0.992; ■ y = -10.5 + 13.1x R= 0.988).

Release profiles were found to be reproducible and evidenced the ability of NPs to control and sustain CD-CURC release. A 24 h burst, in which about

60% of drug was released, followed by a slower release phase was found. The release was completed within approximately 4 days with no significant difference between the two formulation. To investigate the mechanisms of NP unloading, CD-CURC release profiles were plotted as a function of $t^{1/2}$ (Fig. 1.2B). In all cases, after the initial burst, a second linear region followed, with a slope relatively constant and basically independent on the formulation, thus indicating that the release is mainly driven by drug diffusion (Biondi et al., 2013b).

Nanoparticle Cellular Uptake

P and PP NP cellular uptake results are reported in Figures 1.3. Representative pictures, after 48 hours of treatment, are shown in Figure 1.3A. Untreated MSTO-211H cells were used as a control to assess the absence of any background fluorescence. Results indicated that both P and PP formulations are able to enter the cells. In particular, the fluorescent blue signal of DPH is localized throughout the cytoplasm, prevalently in the perinuclear space. As depicted in Figure 1.3B, a time-dependent increase of the fluorescent signal of DPH was observed, which is directly related to the total amount of internalized NPs and is qualitatively the same for both P and PP NPs. On the contrary, from a quantitative point of view, P NP accumulation in the cytoplasm was found to be significantly higher compared to PP NPs in the time frame of the experiment. A fast uptake of both formulations was found in the first 24 hours of treatment, while no significant differences in fluorescence intensity were found for each formulation from 24

to 48 hours, thus suggesting a saturation uptake. Actually, NP cellular uptake is a process mediated by endocytosis rather than by passive diffusion (Rosen and Abribat, 2005), thus resulting into a saturable process (Li et al., 2010). Since internalization is an active process involving the interaction of membrane proteins with NP surface, the lower internalization of PP NPs compared to P NPs is indicative of different surface properties between the two formulations and, in particular, of a lower affinity between the PP NP surface and the cellular membrane. This further confirms the presence of hydrophilic moieties on NP surface.

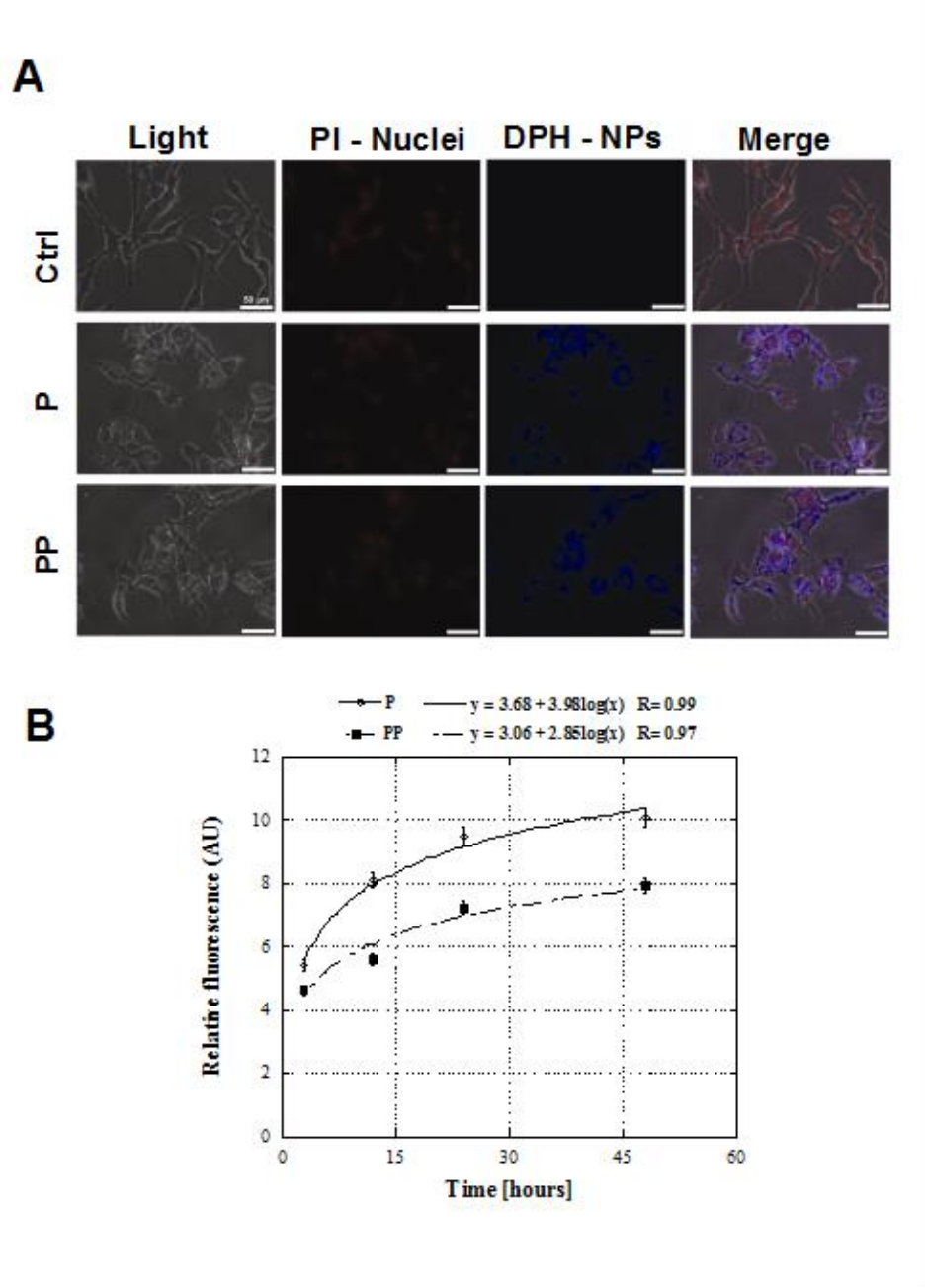

Figure 1.3. NP cellular uptake. A) Representative fluorescent microscopy images of NP uptake by MSTO-211H cells after 48h of treatment. Control untreated cells (Ctrl) did not show any background signal referred to the blue DPH emission, while P and PP NPs labeled with DPH were located in the perinuclear region as evidenced by the merged images from PI and DPH labeling. Scale bar represents 50 µm. B) Relative fluorescence intensity referred to cellular uptake of fluorescent NPs in MSTO-211H cells, from 3 to 48 hours after the treatment showing that the fluorescent signal from the NPs increased during time until the process is saturated. Data represent the mean ± SD of at least three different experiments.

Preliminary dose-response experiments using free CD-CURC were performed to assess the best working concentration of drug, as it has been mentioned above. CD-CURC 20 μM treatment has been chosen to perform all the subsequent experiments since this concentration showed ~ 50% of cell viability after 72 hours of treatment (data not shown). CD-CURC concentration higher than 20 μM caused massive cell death within 72 hours. Cell growth was followed at regular time intervals up to 72 hours of treatment with free CD-CURC and CURC-loaded P and PP NPs, using unloaded NPs as a control. Results are reported in Figures 1.4. No statistically significant differences on cell growth were found between control and unloaded NPs (Figure 1.4A), thus indicating the biocompatibility and the non-toxicity of both the formulations. On the other hand, interesting results were obtained by using free or entrapped CD-CURC (Figure 1.4B). In particular, free CD-CURC was found to inhibit cell growth after only 24 hours of treatment and, after 72 hours, the inhibition was about 40% compared to control. CD-CURC-loaded NPs showed a statistically significant lower inhibition effect compared to the free drug, probably due to the sustained release of CD-CURC from NPs. In particular, the inhibition was less pronounced in the case of the P NPs than the PP NPs, especially between 24 and 48 hours of treatment demonstrating the improved bioactivity of the novel CURC-loaded PP NPs compared to the bare PLGA NPs.

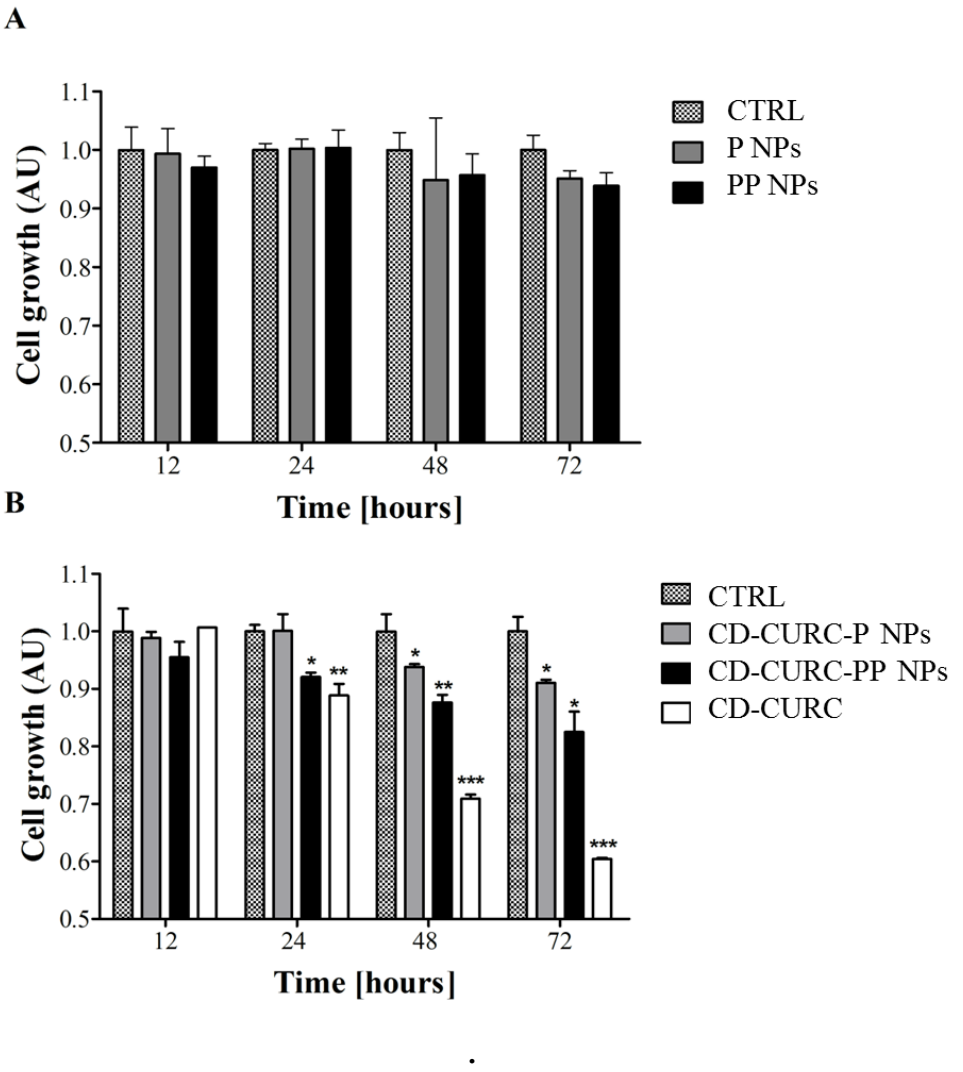

Figure 1.4: Cell growth inhibition induced by CURC-loaded NPs. A) MSTO-211H cell growth after treatment with placebo NPs. No statistically significant difference among the treatments was found. B) MSTO-211H cell growth effects induced by 20 μM of free or encapsulated CURC. Results are expressed as Arbitrary Units (AU) and the control group (untreated MSTO-211H cells, CTRL) is fixed as 1.0 cell growth at each time point. Data represent the mean ± SD of three different experiments (*P < 0.05, **P < 0.01 and ***P < 0.001 are referred to the different treatments in comparison to CTRL).

Analysis of Cell Cycle Distribution

The anti-proliferative activity of CD-CURC is related to its ability to interact with several transcription factors and signaling proteins, such as the tumor suppressor p53, the tumor necrosis factor, inflammatory enzymes, cyclines

and protein kinases (Shishodia et al., 2005). In particular, it is known that an effect of CD-CURC is the modification of cell cycle phases distribution (Sa and Das, 2008). Therefore, we performed a FACS analysis to test the response of the PI-positive MSTO-211H cells to free CD-CURC or CD-CURC-loaded PP NPs (Figure 1.5).

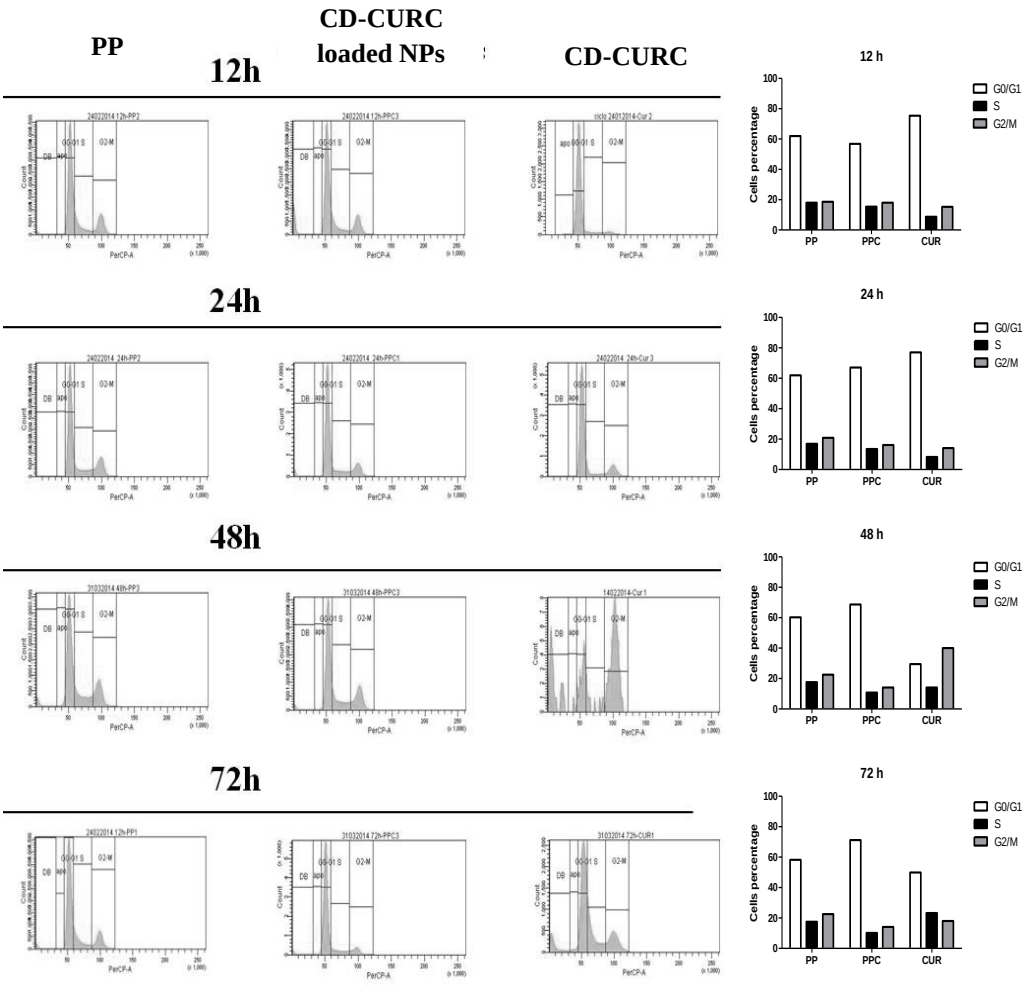

Figure 1.5. CD-CURC and CD-CURC loaded NPs treatment induces cell block. A) MSTO-211H cells were exposed to 20 μM of free CD-CURC or CD-CURC loaded in NPs and cell cycle was analyzed by flow cytometry analysis from 12 hours to 72 hours. Cells treated with naked NPs (PP) were considered as controls. B) Data summary of the cell cycle arrest. Data were performed on three independent experiments with comparable results and standard error was less than 3%.

Only PP NPs were selected to perform cell cycle experiments due to their higher inhibition effect as evidenced in cell growth studies. Unloaded PP NPs were used as a control. DNA staining analysis with PI showed no differences in cell cycle distribution in comparison with untreated cells (data not shown). MSTO-211H cells treated with CD-CURC 20 μM had a relevant alteration of cell cycle profile compared to the controls (untreated cells and unloaded PP NP-treated cells). As shown in Figure 1.5, at 12 and 24 hours free CD-CURC determined an increase in the number of cells blocked in the G0/G1 phase from ~ 60% to ~ 80%, while a slight decrease in the S and G2/M phases was found, in accordance with literature data (Shishodia et al., 2005). At 48 hours, we observed a release of the block in G0/G1 phase, probably due to a CD-CURC tolerance acquired by the cells. Actually, drug tolerance is a well known phenomenon characterized by a reduced response of the cells to a drug, which often occurs when the drug is used for a prolonged time period (Shen et al., 2013; Mikami et al., 1997). This condition induces a shift in cell cycle phase distribution, causing a significant decrease in G0/G1 phase, accompanied by an accumulation of cells blocked in G2/M (40%). This subsequent arrest could be due to a considerable DNA damage induced by the continuous exposure to CD-CURC and can be viewed as a normal cellular response. This hypothesis is also supported by the inhibition of cell growth observed after 72 hours, when most of the cells arrested in G2/M may undergo apoptosis since they are unable to repair the DNA anymore. This fraction is unsuitable for cell cycle analysis. Although this effect regards the majority of the cells, the viable cell population is able to recover a normal profile of the cell cycle, which was found to be very similar to that of

controls after 72 hours of exposure. We can suggest two possible explanations to this phenomenon. On the one side, the viability and the restoration of the cell cycle may be related to the reduction over the time of the CD-CURC bioavailability, thus resulting into a lower efficacy. Otherwise, recovered cells, previously resulted arrested in G2, may repair the damaged DNA, thus starting a new cell cycle. Taken all together, these results confirm the anti-proliferative and cytotoxic activity of free CD-CURC, showing that it is able to reduce both the uncontrolled cell proliferation, as well as DNA synthesis of DNA if used for a prolonged time period.

CD-CURC-loaded PP NPs on MSTO-211H cells showed a growing induction of G0/G1 block in a time-dependent manner associated to a reduction of S and G2/M phase populations. The percentage of cells arrested in G0/G1 ranged from 56.8% to 71.1% from 12 hours to 72 hours. At this time point PP NPs produced a similar molecular bioactivity as the free CD-CURC at 24 h. It must be underlined that a continuous block in G0/G1 after 72 hours can promote cell apoptosis in a later time.

These results clearly indicate that the effect of CD-CURC-loaded NPs appears better and more prolonged than that of the free CD-CURC and, even if the internalization of PP NPs is lower compared to that of P NPs, PP NPs can achieve a persistent G0/G1 cell block. This can be explained by considering that NPs, once internalized, are able to release the active molecule for a prolonged period. Thus, the PP NPs can be useful to overcome the bioavailability and tolerance issues related to CD-CURC.

Conclusions

In this work we propose a novel method to produce stealth NPs coated with hydrophilic polyethylene oxide (PEO) by simply blending poloxamers and PLGA in the organic phase of the emulsion used to produce the NPs. Indeed, taking advantage of the amphiphilic properties of the blends, a hydrophilic coating of the NPs can spontaneously form, thus avoiding the drawbacks of the chemical reaction normally needed to confer stealth properties to NPs. The different surface properties of P and PP NPs were confirmed both by the different interactions of these NPs with serum proteins and also by their ability to be endocytosed by mesothelioma cells. In particular, although PP NPs are internalized to a lower extent within MSTO-211H cells, they are able to induce a persistent block in G0/G1 phase of the cell cycle up to 72 hours, thus overcoming the drug tolerance phenomenon, normally evidenced when free CD-CURC is used. This interesting result is probably related to NP ability to sustain the drug release up to at least 100 hours by a prevalently diffusive release mechanism.

Chapter 2

Nano-Precipitated Curcumin Loaded Particles: Effect of Carrier Size And Drug Complexation With (2-Hydroxypropyl)-B-Cyclodextrin on Their Biological Performances

Introduction

In the previous chapter, it was shown that the produced NPs made up of a blend of polylactic-co-glycolic acid (PLGA) and poloxamer and loaded with curcumin (CURC) have shown a propensity to be internalized by mesothelioma MSTO-211H cells. In particular, the hypothesis of NP effectiveness has been corroborated by the persistence of the block of cell cycle in the G0/G1 phase. Unfortunately, we also found out that the cellular internalization of PP NPs was lower compared to internalization features of P NPs, which, however, have a strong tendency to aggregation and therefore are not promising vectors.

In an advancement of this work, we aimed to improve the internalization amount of PP NPs by optimizing NP formulation so as to achieve a more effective control of size and size distributions of the produced nanocarriers.

Actually, there is a strong research interest in the proper engineering of CD-CURC-loaded NPs since CURC safety and intrinsic non-toxicity to humans, even at high doses, are well established (Lao et al., 2006; Mehanny et al., 2016). It must also be highlighted that a constantly increasing number of clinical trials of CD-CURC have been published or are currently in progress, therefore evidencing the flourishing research interest of the scientific community on the therapeutic potential of CD-CURC (Martin et al., 2015).

Aim of the Work

In this chapter, we propose a method to produce amphiphilic PLGA NPs coated with hydrophilic polyethylene oxide (PEO), which exhibit a high dimensional stability and could take advantage of enhanced permeability and retention (EPR) effect. In particular, although PEO-coated PLGA NPs were internalized to a low extent within MSTO-211H cells compared to PLGA NPs, they were able to induce a persistent block in G0/G1 phase of the cell cycle up to 72 hours, thus overcoming the drug tolerance phenomenon, normally evidenced when free CD-CURC is used (Mayol et al., 2015).

In this study, we aimed to improve the cellular uptake of these amphiphilic NPs, by reducing their diameter using nanoprecipitation as a production technique. Moreover, in this study we have also investigated into more depth the host-guest complex that CURC forms with hydroxypropyl-β-cyclodextrin (HPβCD) by means of ^{1}HNMR and differential scanning calorimetry (DSC).

Materials and Methods

Materials

The chemical substances used for the experiments are the same as described in Chapter 1.

Preparation of Curcumin-Hydroxypropyl-β–Cyclodextrin Inclusion Complex and Nanoparticles

Different formulations of placebo NPs and CURC-loaded NPs were prepared using nanoprecipitation technique. In particular, to prepare NPs loaded with free CURC, 5 mL of a PLGA/poloxamer (1:1 mass ratio) solution in acetone at different polymer concentrations (1.5, 3.0 and 6.0% w/v; the CURC-loaded formulations were named PPFC1.5, PPFC3 and PPFC6, respectively) were forced through the needle of a syringe (inner diameter: 11.99 mm) at 333.3 μl/min flow rate, and poured into 40 mL of an aqueous solution of F127 and F68 as surface active agents (1:1 w/w; 0.375 mg/mL overall concentration). Table 2.2 reports the composition of NP formulations. Subsequently, acetone was evaporated overnight for NP hardening, and the resulting NP suspension was washed three times by centrifugation (Hettich Zentrifugen, Germany; 10,000 rpm, 30 min). Finally, the supernatant was removed and the NPs were stored at -80 °C.

Thereafter, the CD-CURC inclusion complex to be loaded in the dispersed aqueous phase was prepared by dissolving 1 mg of CURC and 8 mg of CD in

1 mL EtOH. The resulting solution was stirred for 1 h at 70 °C for EtOH evaporation and, afterwards, 1 mL of double-distilled water (DDW) was added and evaporated under stirring. Finally, 2 mL of DDW were added and the obtained solution was centrifuged (10,000 rpm, 15 min). The supernatant was freeze-dried at -60 °C (24 h, 0.01 atm; Modulyo, Edwards, UK) and the obtained dried mass stored at 4 °C.

The NPs encapsulating CD-CURC inclusion complex were obtained by precipitating a water-in-oil emulsion in the same external aqueous phase described above (containing the poloxamers as surface active agents, 1:1 weight ratio, 0.375 mg/mL). The internal phase of the emulsion was composed of 640 μL of EtOH or, for placebo NPs, of the same volume of a 1.4 mg/mL solution of CD-CURC in EtOH. This phase was emulsified with the same organic phase described in the previous section at different polymer concentrations by sonication for 5 min at 4 W (Sonicator 3000, Misonix, USA) using a microtip 419 probe. The resulting water–in–oil emulsion was precipitated in the same conditions described above. Placebo nanodevices were named PP1.5, PP3 and PP6, while the CD-CURC-loaded formulations were named PPC1.5, PPC3 and PPC6. For cell uptake experiments, fluorescent NPs were prepared by adding 1 mg of DPH to the organic phase of the primary emulsion.

^{1}H NMR Study of the Host-Guest Complex

All spectra were recorded in deuterated DMSO-d6 using Varian Mercury-400 apparatus (Palo Alto, CA, USA). ^{1}H NMR spectra are reported in parts *per* million (ppm) referred to specific signals due to deuterated solvents as internal references. The following abbreviations are used to describe peaks: s (singlet), d (doublet), dd (double double), t (triplet), q (quadruplet) and m (multiplet). CD, CURC and CD-CURC complex were dissolved in DMSO and then tested. HP-β-Cyclodextrin ^{1}H NMR (500 MHz, DMSO-d6) δ 5.71 (br s, 2-OH and 3-OH), 5.01 (s, H8), 4.83 (br s, H1), 4.43 (br s,6-OH and 8-OH), 3.74 (s, H3), 3.61 (3.61, H6), 3.56 (H5), 3.33–3.44 (br, H2, H4, H7), 1.02 (s, H9) (Danel, Azaroual et al., 2013).

Curcumin ^{1}H NMR (500 MHz, DMSO-d6) δ 3.84 (s, 6H), 6.06 (s, 1H), 6.75 (d, J = 15.8 Hz, 2H), 6.82 (d, J = 8.2 Hz, 2H), 7.15 (dd, J = 8.1 and 1.2 Hz, 2H), 7.32 (d, J = 1.2 Hz, 2H), 7.54 (d, J = 15.8 Hz, 2H), 9.65 (s, -OH) (Koo, Shin et al., 2015).

Differential Scanning Calorimetry (DSC)

Thermoanalytical tests were carried out on CD, CURC, and CD-CURC complex, to investigate on the formation of the host guest complex. The heat involved in the phase transitions of the materials was determined by a differential scanning calorimeter (DSC; DSC Q20, TA Instruments, USA), calibrated with a pure indium standard. The samples were placed in flat aluminum pans and heated from 25 to 300 °C at a constant rate of 10 °C/min.

Measurements were carried out under an inert nitrogen atmosphere, purged at 50.0 mL/min. The heat evolved during polymer crystallization and fusion (W/g) was calculated from DSC thermograms by integrating the exothermic/endothermic peaks, while the glass transition temperatures (T_g) were obtained from the inflection points of DSC spectra.

Characterization of Nanoparticles

TEM Analyses

A transmission electron microscope (TEM, EM208S, Philips, The Netherlands) was used to study NP morphology. TEM observations were carried out by spraying 100 µl of an aqueous suspension of nanocarriers onto a TEM copper grid (300 mesh, diameter: 3 mm).

Size and ζ-Potential Analyses of Nanoparticles

The average diameter, diameter distribution and ζ-potential of NPs were obtained by laser light scattering (Zetasizer Nano ZS, Malvern Instruments, Malvern, UK) carried out at room temperature on a NP suspension in water at 0.1 mg/mL. Twelve runs were performed for each sample.

Stability of Nanoparticles

The stability of NP formulations was studied in terms of trend of the hydrodynamic diameter and ζ-potential in storage conditions for 30 days (i.e. at 4 °C in double distilled water) and in the conditions of *in vitro* cellular uptake and cytotoxicity experiments (i.e., at 37 °C for 72 h in RPMI-1640 supplemented with 10% FBS). Size measurements were also carried out in bare culture medium to check for possible self-aggregation phenomena. Results are expressed as average values obtained from at least five independent measurements.

Yield and Drug Loading Efficacy of Nanoparticles

The yield of NP formulations was obtained gravimetrically by weighing the entire mass of lyophilized nanodevices (0.01 atm, 24 hours; Modulyo, Edwards, UK). The loading efficiency of CD-CURC, η, was found by the indirect method. In detail, immediately after production, NPs were centrifuged (10,000 rpm, 10 min) and 300 μL of the supernatant were withdrawn and mixed with an equal volume of acetone. The obtained samples were analyzed by spectrophotometric assay (Shimadzu UV-1800 World Laboratory, Japan) at 444 nm. The linearity of the response has been verified between 0.2 and 50 μg/mL ($r^2 > 0.99$). CD-CURC loading efficiency was calculated with the following equation:

$$\eta = 100 \cdot \frac{CD - CURC_{entrapped}}{CD - CURC_{initial}} . \quad (1)$$

Drug Release Kinetics

The release of CD-CURC from NPs was determined by loading 5 mL of NP suspension (at 1.2, 2.61 and 7.4 mg/mL for PPC1.5, PPC3 and PPC6 formulations, respectively) in a dialysis membrane (Spectra/Por® Biotech Cellular ester; molecular cut-off 12 kDa). The NP-containing membrane was plunged in 50 mL of a release medium composed by PBS and EtOH 90:10 v/v, and containing surfactant Tween 80 (0.5% w/v), and acetic acid (0.01 % w/v) and ascorbic acid (0.01 % w/v) as CURC stabilizers [20]; pH was adjusted to 7.4. At scheduled time points, the release medium was withdrawn and completely replaced with fresh medium. Released CD-CURC was determined by reverse phase ultra-high performance liquid chromatography (UHPLC). The chromatograph was equipped with a UHPLC LC-10AD pump (Shimadzu, Milano, Italy), a 7725i injection valve (Rheodyne), a SPV-10A UV–Vis detector (Shimadzu) set at the wavelength of 425 nm and a C-R6A integrator (Shimadzu). Chromatographic separation was realized by a gradient elution applied at a flow rate of 1 mL/min in a Phenomenex Luna C18(2) 100Å column (250 mm × 4.6 mm, 5 μm; injection volume: 20 μl: λ = 425 nm). Mobile phase A was deionized water and mobile phase B was methanol. The following gradient was applied: B 10% (0-4 min), 20–95% B 10-90% (4-5 min), B 90% (5-11 min); B 90-10% (11.5–12.5 min).

Cell Cultures

Human mesothelioma MSTO-211H cells were grown in RPMI-1640 medium supplemented with 10 % FBS, 10 UI/mL penicillin/streptomycin, 10 mM HEPES and 1 mM sodium pyruvate in a humidified incubator at 37 °C and 5 % CO_2. After reaching confluence, cells were enzymatically detached with Trypsin- EDTA and subcultured into new cell culture dishes. The medium was replaced every two days, and the cells were used for experiments between passages 7-13.

Cell Viability Assay

The CV test was used to determine the dose-response curves of free CURC and of CD-CURC inclusion complex, and also to assess the biocompatibility/cytotoxicity of placebo and CD-CURC-loaded NPs, respectively. For each experiment, $1x10^4$ MSTO-211H cells were allowed to attach in 96-multiwell plates. Twenty-four hours post-seeding, cells were treated with different concentrations of CURC and CD-CURC (10, 20 and 40 μM), with placebo PP NPs and with PPC NPs at a 2.5 mg/mL, corresponding to 20 μM CD-CURC loading. NPs were suspended in complete culture medium, and untreated cells were used as control. The experiments were performed at 24, 48 and 72 h. After incubation, cells were fixed with formaldehyde 3.7 % for 10 min, then washed with PBS and stained for 10 min with 0.1% crystal violet (Sigma Aldrich, St Louis, MO). Acetic acid

10% was used to dissolve crystal violet and the absorbance was read at 595 nm with a microplate reader (Tecan, USA). The intensity of the measured absorbance directly correlates with the number of living cells.

Cell Uptake Experiments

NP cellular uptake was visualized by means of an inverted fluorescence microscope (Leica Microsystem, Germany). For each experiment, $3x10^4$ cells/well were plated in 12-well plates and treated with 100 μg/mL fluorescent PP NPs containing DPH (λ_{ex} = 350 nm, λ_{em} = 452 nm); the uptake was monitored over time at 0.2 and 2, 12, 24 and 48 h. Then, cells were washed with PBS and fixed with formaldehyde as described in Section 2.11. Cell nuclei were counterstained with 2.5 μg/mL PI (λ_{ex} = 540 nm, λ_{em} = 608 nm) for 5 min. Images were randomly acquired. The kinetics of cell internalization were determined by spectrofluorimetric assay following a previously describe procedure (Forte et al., 2016) with some modifications. Briefly, $1x10^3$ cells/well were seeded in 96-well white clear bottom plates (Perkin Elmer Milano, Italy). Afterwards, fluorescent NPs were added (100 μg/mL) and the uptake was quantified at the same time points indicated above. At each time point, to eliminate non-internalized NPs, cells were rinsed twice with PBS for 5 min, and cells were lysed with 0.1% Triton X - 100 to allow the release of the internalized nanoparticles in the solution (Xiao et al., 2011) . Cell lysates were analyzed with a VictorTM X3 microplate reader (Perkin Elmer) at 350 nm and 452 nm.

Statistical Analysis

Results are reported as mean values ± SD of three independent experiments, unless otherwise indicated. Statistical analyses were performed using Graph Pad Prism 5.0 (GraphPad Software, San Diego, CA, USA). For crystal violet assay, the significance was evaluated using the Two Way ANOVA with Bonferroni's multiple comparison test and differences were considered statistically significant for $P < 0.05$.

Results and Discussion

[1]HNMR and DSC Analyses

[1]H NMR spectroscopy results are summarized in Table 2.1, and the spectra of CURC, CD and CD-CURC inclusion complex are shown in Figure 2.1.

Hydrogen	HP-β-CD	CD-CURC complex	Δδ[(a)]
H-1	4.8318	4.8329	+0.0011
H-2[(b)]	-	-	-
H-3	3.7484	3.7501	+0.0017
H-4[(b)]	-	-	-
H-5[(c)]	3.5637	3.5719	+0.0082
H-6	3.6194	3.6233	+0.0039
H-7[(b)]	3.3270	3.3270	-
H-8	5.0177	5.0207	+0.0030
H-9	1.0237	1.0244	+0.0007

Table 2.1: [1]H chemical shifts of free HP-β-CD and in the presence of CURC

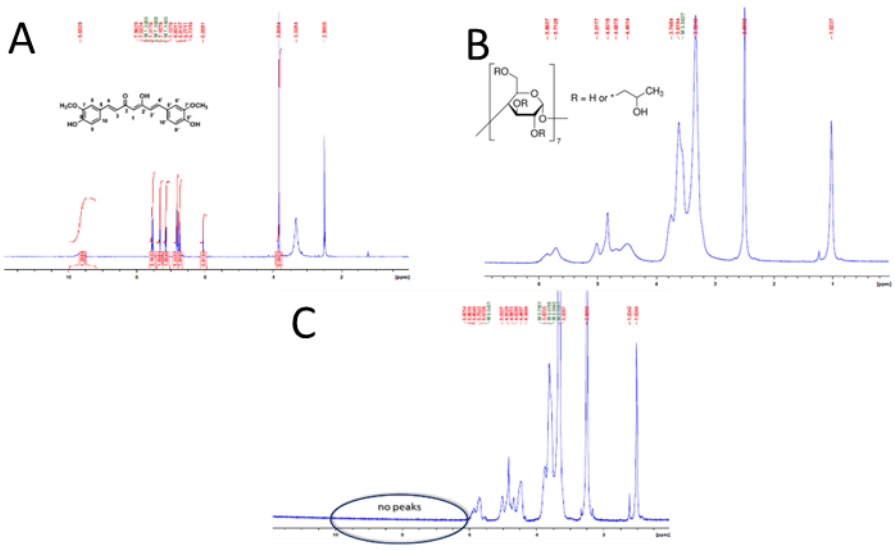

Figure 2.1: [1]H NMR spectrum of (A) CURC, (B) HP-β-Cyclodextrin and (C) CD-CURC complex: [1]H NMR spectrum was recorded on a Varian Mercury-400 spectrometer at 25 °C with DMSO-d6 as the solvent.

Here it can be observed that CD-CURC inclusion complex showed all the peaks belonging to HPβCD but their proton signal peaks were shifted to low field region. In particular, all CD hydrogens are de-shielded in the presence of CURC molecules, and this behavior can be associated with a decrease in the electronic density around HPβCD hydrogens, probably due to van der Waals forces, dipole-dipole interactions and/or hydrogen bonds between CURC and CD molecules (Masson et al., 1998; Ventura et al., 1998). Moreover, specific peaks of CURC between 8 and 6 ppm are not visible. Thus, these data strongly suggest a successful formation of an inclusion complex between CD and CURC. Figure 2.2 shows the result of the thermal analyses of CD, CURC and CD-CURC inclusion complex. CD and CURC showed individual endothermic peaks at 82 °C and 181 °C, due to their melting; in the case of CD-CURC inclusion complex, the peak associated to CURC melting at 181 °C was not evidenced, while the melting temperature of CD was lowered to 71 °C, therefore further confirming the formation of the inclusion complex.

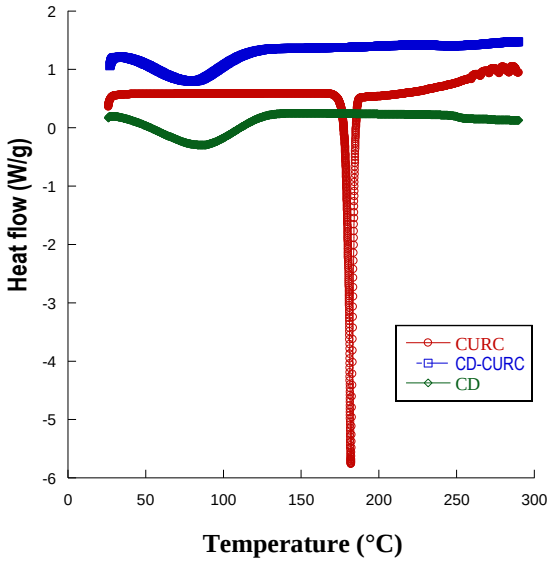

Figure 2.2: DSC thermograms endothermic curves of CURC, CD and CD-CURC inclusion complex. Results were obtained from at last three independent experiments.

Preparation and Characterization of Nanoparticles

As a first attempt, PPFC NPs encapsulating free CD-CURC have been produced by precipitating an organic solution of PLGA, poloxamers and the active molecule (as shown in Table 1 and Table 2.2).

Acronym	Water phase (W0)		Oil phase (O)			Water phase (W0)	
	CD-CURC (w/v %)	CURC (w/v %)	PLGA (w/v %)	F68 (w/v %)	F127 (w/v %)	F68 (w/v %)	F127 (w/v %)
PPFC1.5	-	0.2	0.75	0.375	0.375	0.05	0.05
PPFC3	-	0.2	1.5	0.75	0.75	0.05	0.05
PPFC6	-	0.2	3	1.5	1.5	0.05	0.05
PPC1.5	1.4	-	0.75	0.375	0.375	0.05	0.05
PPC3	1.4	-	1.5	0.75	0.75	0.05	0.05
PPC6	1.4	-	3	1.5	1.5	0.05	0.05

Table 2.2: Composition and acronyms of the nanoparticle formulations loaded with free CURC (PPFC NPs) and CD-CURC inclusion complex.

The major technological features of the obtained NPs are shown in Table 2.3. It can be observed that, by using the technique of nanoprecipitation, it was possible to obtain smaller NPs as well as values of the polydispersity index significantly lower compared to those obtained when producing NPs by the double emulsion/solvent evaporation method, as previously published (Mayol et al., 2015). However, in this case the entrapment efficiency of CURC in PP-NPs was dramatically low (3, 16 and 35% for PPC1.5, PPC3 and PPC 6 formulations, respectively). This result indicates the need to produce NPs with an internal phase containing CD-CURC inclusion complex, separated from the outer aqueous phase. For this reason, NPs have been produced by precipitating a water-in-oil emulsion in a second, external aqueous phase. This method allows to hinder the extraction of the active molecule in the dispersing phase. Actually, CD-CURC encapsulation efficiency in the NPs was terrifically increased (up to 93 - 95%), as shown in Table 2.3.

Forms	Particle mean diameter (nm)	Polydispersity Index (PDI)	Zeta potential (mV)	Entrapment efficiency (%)	Yield (%)
PPFC1.5	92±6	0.14±0.03	-22.1±1	3±1	54±6
PPFC3	109±2	0.09±0.03	-23.1±2	16±1	55±7
PPFC6	117±3	0.30±0.09	-22.5±4	35 ±1	58±3
PPC1.5	83 ± 4	0.10 ± 0.03	-25.5 ± 1	93 ± 1	25 ± 1
PPC3	96 ± 1	0.08 ± 0.03	-27.4± 2	93 ± 1	44 ± 2
PPC6	115 ± 1	0.07 ± 0.04	-28.5 ± 1	95 ± 0.1	59 ± 2

Table 2.3: Size, polydispersity index (PDI), zeta potential entrapment efficiency and yield of different NP formulations loaded with free CURC (PPFC) CD-CURC inclusion complex (PPC).

Interestingly, this noteworthy increase of the entrapment efficiency was not accompanied by a significant change in NP dimension, polydispersity index, zeta potential and yield. Consequently, CD-CURC loaded PP NPs were selected for a further technological and biological characterization. As shown in Figure 2.3, all the NPs possess a spherical shape with a regular surface. Recently, the diameters of PP NPs have been shown to be constant over time both in water and in cell culture medium (Mayol et al., 2015). This is due to the hydrophilic nature of nanodevice surface, which discourages the adsorption of serum proteins.

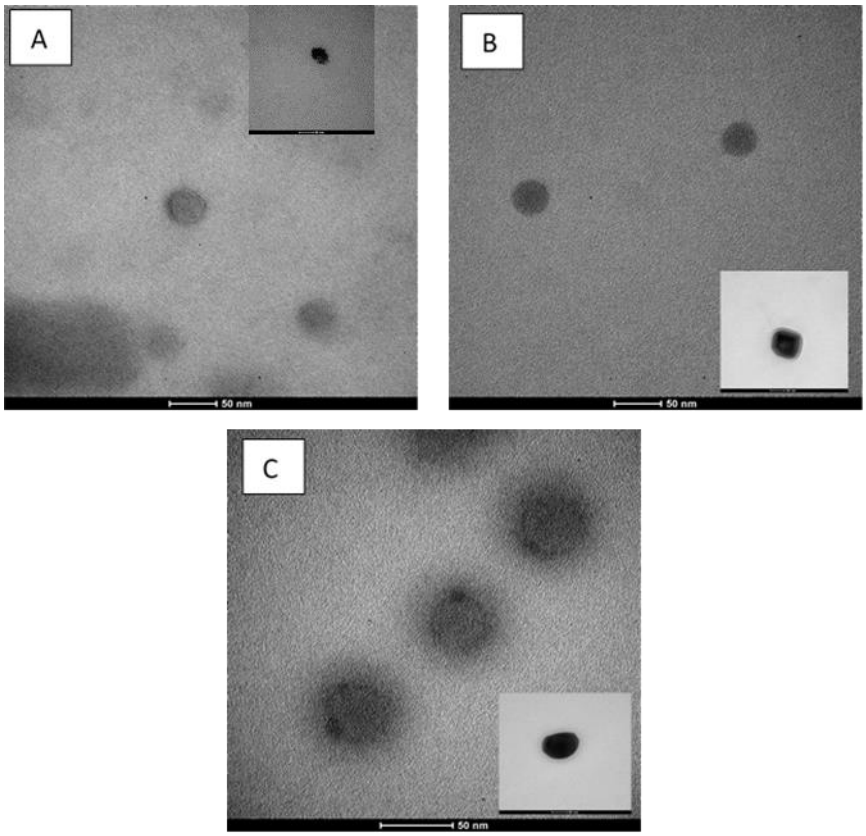

Figure 2.3: Representative TEM images of PPC1.5 (A), PPC3 (B) and PPC6 (C) NPs**.**

Form.	Water, 4 °C			RPMI, 37 °C		
	day 10	**day 20**	**day 30**	**day 1**	**day 2**	**day 3**
PPC1.5	93 ± 1	90 ± 1	93 ± 1	81± 1	92 ± 3	86 ± 3
PPC3	100 ± 1	98 ± 1	99 ± 1	103 ± 2	113 ± 1	111 ± 2
PPC6	122 ± 1	111± 5	138 ± 1	116 ± 1	133 ± 3	134 ± 2

Table 2.3: Time evolution of NP diameter in water at 4 °C and in cell culture medium (RPMI) at 37 °C of different nanoparticle formulations loaded with CD-CURC inclusion complex.

This behavior was confirmed for all the formulations produced since, as reported in Table 2.4, they are very stable, in water at 4 °C up to 30 days and in cell culture medium (RPMI) at 37 °C up to 3 days.

The *in vitro* release profile of CD-CURC from PPC1.5, PPC3 and PPC6 NPs was performed in the release medium described before at pH = 7.4, and the results are reported in Figure 2.4.

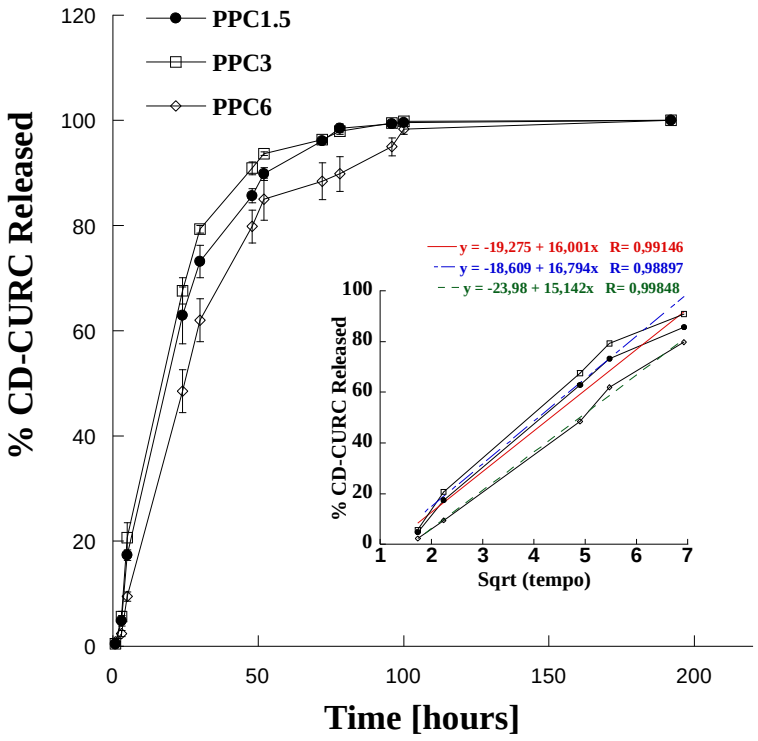

Figure 2.4: *In vitro* release profile of CD-CURC from PPC1.5, PPC3 and PPC6 NPs in PBS at 37 °C. Inset: released CD-CURC percentage as a function of the square root of time.

All the formulations were able to sustain the release of CD-CURC for about 4 days, with 60-80 % of the active molecule being released in the first 2 days.

The drug release mechanism seems to be prevalently diffusive since, as depicted in the inset of Figure 2.4, the released percentage of CD-CURC is a linear function of the square root of time (de Gennaro et al., 2015). More in detail, Figure 4 shows that release kinetics of CD-CURC from PPC6 NPs is significantly slower compared to the others. In particular, a burst effect as low as 10% after five hours was envisaged, compared to about 20% of CURC released from PPC1.5 and PPC3 NPs.

In-Vitro Biocompatibility and Cell Uptake of Nanoparticles

The biocompatibility of placebo PP NPs was verified by means of the crystal violet assay. As shown in Figure 2.5a, the three produced formulations caused no cytotoxic effect against MSTO-211H cells at all the times of treatment. As shown in Figure 2.5b, both CURC and CD-CURC elicited a cytotoxic activity against MSTO-211H, which lead a cell viability which was decreasing with increasing active molecule concentration and culture time. Treatment for 48 h with both 20 μM free CURC or CD-CURC inclusion complex decreased cell viability by about 50%, in comparison with controls, with no significant difference between free CURC and CD-CURC treatment. Figure 2.5c reports the cytotoxic activity of the three CD-CURC loaded PPC NPs, obtained by treating the cells for 24, 48 and 72 h with an NP amount equivalent to 20 μM CD-CURC. Results evidence that cell treatment with PPC1.5 and PPC3 NPs lead to a 24% and 16% reduction of cell viability after 24 h respectively. On the contrary, no significant effect was shown for PPC6 NPs at the same time, probably due to the slower release of the active

molecule from this NP formulation. After 48 and 72 hours, the effect of PPC1.5 and PPC3 was found to be still persistent, and, at the same time points, also PPC6 NPs evidenced their ability to decrease cell viability by approximately 20%.

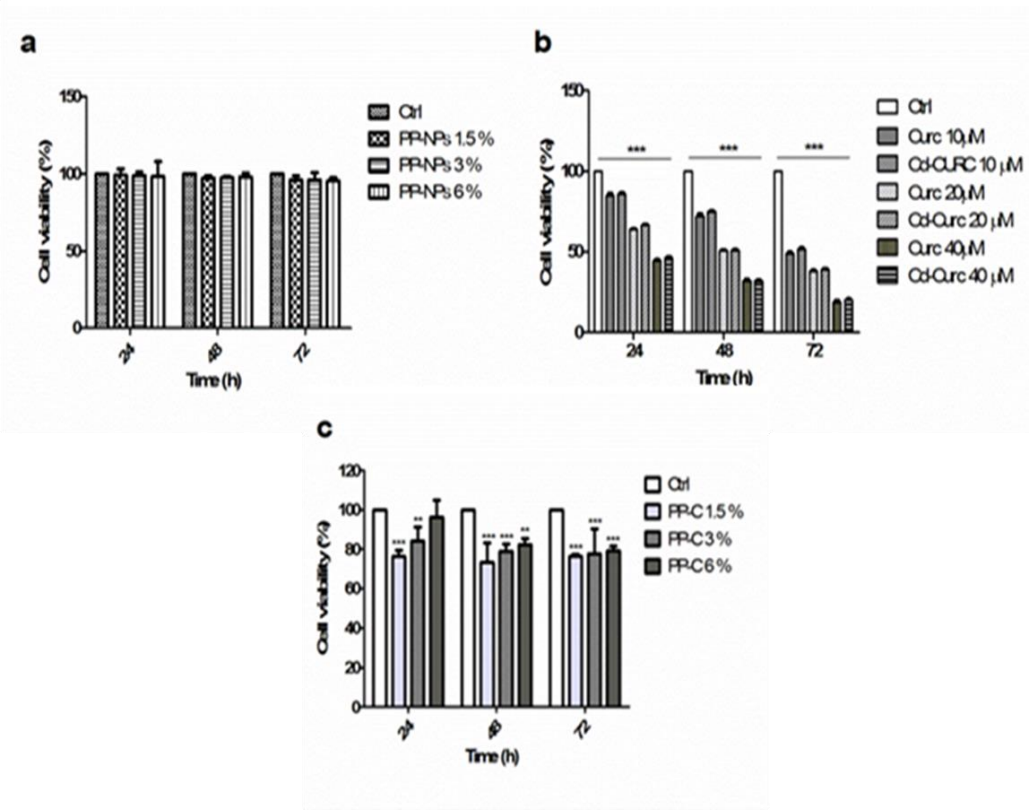

Figure 2.5: MSTO-211H cells were used to evaluate biocompatibility of unloaded PP NPs at different times (a); toxicity of curcumin (CURC) and CD-CURC at different concentrations and times (b); citotoxicity of 20 µM CD-CURC loaded PP-NPs (PPC1.5, PPC, PPC6) after 24, 48 and 72 hours of treatment of MST0-211H (c). All the formulations of placebo PP NPs did not cause any effect on cell viability (**a**). Both CURC and CD-CURC reduced MSTO-211H growth of 50 % at 20 µM (**b**). PP-C affected the cell viability, causing a significant reduction after 24 and 48 hours (PPC1.5 and PPC3) and 72 hours (PPC1.5, PPC3, PPC6) (**c**). **P < 0.01, *** P < 0.001 related to control group (Ctrl).

In order to quantify NP uptake in MSTO-211H cells, cells were incubated with fluorescent PP NPs containing DPH dye (100 µg/mL) for 48 h. The fluorescence images of the cells, seeded in the presence of DPH-loading NPs,

showed that the nanodevices were rapidly internalized after times in order of minutes (Figure 2.6).

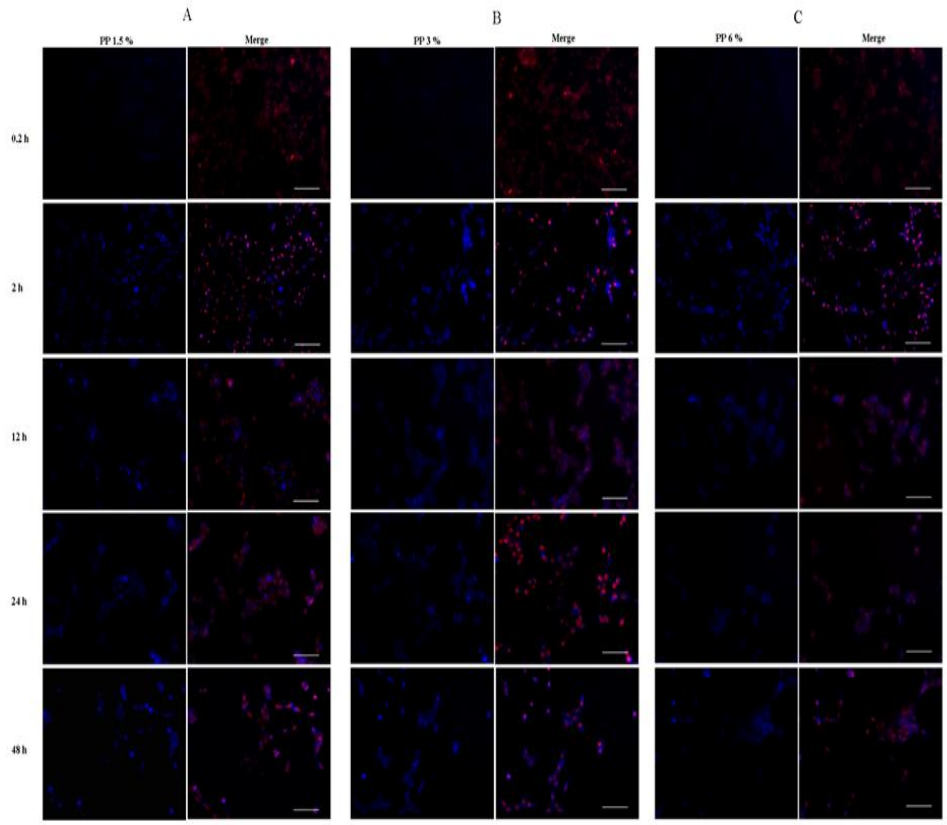

Figure 2.6: Time course analysis of fluorescent PP NPs uptake (PP1.5, panel A; PP3, panel B; PP6, panel C) in MSTO-211H cells. PP-NPs were labeled with diphenylhexatriene (DPH). Cells were incubated with PP NPs for different times (0.2, 2, 12, 24 and 48 hours) and then analyzed with fluorescence microscopy. Cell nuclei were stained with propridium iodide (red). Scale bar: 100μm.

In particular, the fluorescent signal of DPH was found as discrete spots in the cytoplasmatic space, being mostly distributed in the proximity of the perinuclear region after 12 and 24 hours, without reaching the cell nucleus. Furthermore, as indicated by spectrofluorimetry results, the number of internalized NPs was found to be increasing with time (Figure 2.7).

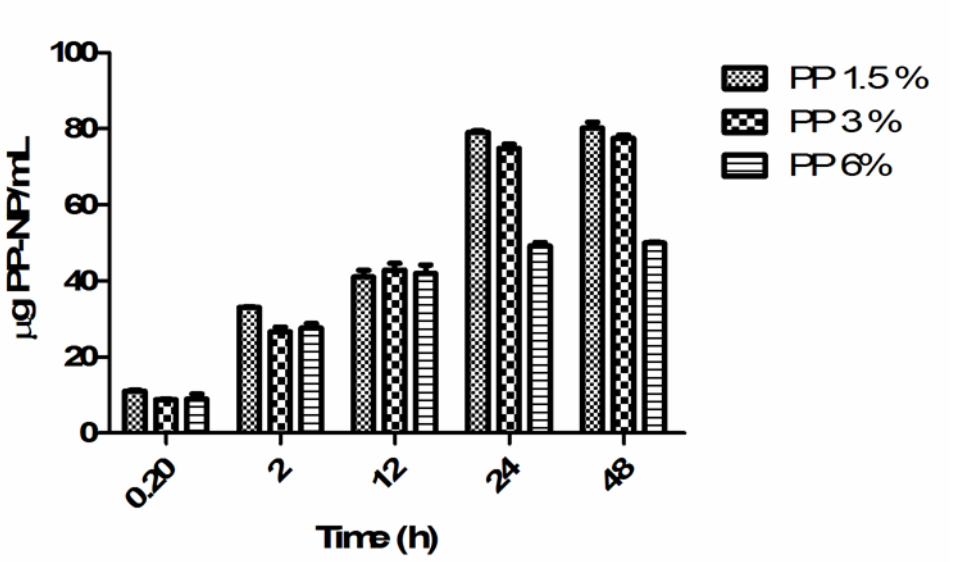

Figure 2.7: Spectrofluorimetric analysis of PP NPs (PP1.5, PP3, PP6) and uptake kinetics in MSTO-211H cells. Cells were treated with 100 µg/ml of fluorescent NPs. NPs showed the highest rate of uptake after 24 hours of incubation with a plateau between 24 and 48 h of internalization.

In all cases, the trends of internalization kinetic profile were qualitatively similar for all the formulations, with an initial fast transient internalization followed by a slower uptake in 48 h. In particular, the uptake was higher and similar for PP1.5 and PP3 NPs compared to PP6 NPs, which is clearly lower and reached a plateau after 24 h. This was ascribed to the effect of PPC6 NP size, which is about 20 nm higher compared to PPC3 formulation. This result shows that the reduction of NP size, even if by 20 nm only, strongly enhances their internalization in MSTO-211H cells. Therefore, this outcome underlines the importance of the control of both size and polydispersity index to guide NP cell uptake and thus CURC bioavailability.

Conclusions

An efficient uptake of PP NPs in MSTO-211H cells is strongly affected by the size and the polydispesity index of the nanodevices. Actually, uptake results indicate that a size reduction of only 20 nm leads to an evident increase in NP internalization. In this panorama, nanoprecipitation allowed to improve the control over NP size and size distribution of the NPs that, in turns, encourage cell internalization in MSTO-211H cells, and can reasonably lead to an improvement of CURC *in vivo* bioavailability.

Furthermore, the formation of an inclusion complex between CURC and CD allows its encapsulation in an internal aqueous phase of the emulsion used to produce the NPs, thereby reducing the possibility of extraction of the active molecule and, hence, increasing its loading efficiency.

Chapter 3

Arrangement of a Hyaluronic Acid Shell on Irinotecan Loaded PLGA Nanoparticles to Target CD44-Overexpressing Breast Carcinoma Cells

Introduction

Over the last couple of decades, NPs have been attracting a great deal of interest in the field of cancer therapy (Cho et al., 2008; Ross et al., 2004; Brigger et al., 2002) thanks to their ability to encapsulate a wide range of poorly water-soluble anticancer drugs and release them in a sustained manner at the target site; in this way, from one side they can enhance the intracellular concentration of drugs in cancer cells and, on the other side, they allow to avoid toxicity in normal cells, therefore overcoming the lack of specificity of conventional chemotherapeutic therapy (Cho et al., 2011; He et al., 2011; Vergara et al., 2012; Malam et al., 2009). Furthermore, NPs can accumulate into tumor cells and tissues by taking advantage of passive and/or active targeting (Bae et al., 2011; Gao et al., 2008; Tang et al., 2007; Wang et al., 2005). The passive tumor targeting phenomenon of NPs is known as the enhanced permeability and retention (EPR) effect that is the property by which NPs tend to accumulate in tumor tissue much more than they do in normal tissues. The general explanation that is given for this phenomenon is that, in order for tumor cells to grow quickly, they must stimulate the production of blood vessels. The newly formed tumor vessels are usually abnormal in form and possess an aberrant architecture (leaky, non-organized and hyperpermeable). Consequently, NPs can passively accumulate at target sites and a preferential extravasation of circulating nanodevices occurs (Wang et al., 2012; Davis et al., 2008; Cho et al., 2008; Ferrari, 2005; Peer et al., 2007; Duncan et al., 2006; Duncan et al., 2003). However, this passive targeting strategy of NPs is limited by the possible lack of cell internalization

and/or by the release of the loaded drugs before NP uptake and, in addition, EPR accounts only for a few percent of the administered dose (Choi et al., 2010). To overcome these limitations, in recent years an important research focus has been devoted to modify NP interface so as to achieve an active biomolecular targeting by the propr functionalization with antibodies (Lukyanov et al., 2004; Park et al., 2001), nucleic acids (Sapra and Allen, 2002; Farokhzad et al., 2006), proteins (Farokhzad et al., 2004; Bies et al., 2004; Minko, 2004; Qian et al., 2002; Sahoo et al., 2005) and various ligands (Lee and Low, 1994; Lu and Low, 2002; Eliaz and Szoka, 2001). Functionalized NPs can recognize tumor cells and can specifically bind to the target tissues, and they can be internalized by means of receptor-mediated endocytosis (Peer et al., 2007; Torchilin, 2006; Byrne et al., 2008). Of the different ligands studied, antibody fragments have been extensively used for NPs funzionalization. However, the use of antibodies for therapeutic purposes suffers from their occasionally potent immunogenicity and as a consequence of the binding affinity for the target is often deteriorated (Stacy, 2005). In this frame, hyaluronic acid (HA) has attracted a significant research attention as a material for tumor-targeted delivery since it can specifically bind to those cancer cells overexpressing CD44 receptor (Toole, 2004; Jaracz et al., 2005; Gotte and Yip, 2006; Choi et al., 2009; Ambrosio et al., 1999a and 1999b). HA is a naturally occurring polysaccharide mainly present in the extra-cellular matrix of the mammalian connective tissues. It plays a major role in several functions *in vivo* such as lubrification of arthritis joints, viscoelastic properties of soft tissues and it is involved in important cell functions such as cell motility, cell matrix adhesion and cell organization

(Xuejun et al., 2004; Mori et al., 2004; Borzacchiello et al., 2001; Borzacchiello et al., 2005; Borzacchiello et al., 2007; Fusco et al., 2007; Borzacchiello et al., 2010). Thanks to its excellent biocompatibility, biodegradability, unique physical, chemical and biological properties and to the ease of chemical functionalisation, HA is already used in several biomedical applications such as regenerative medicine (Mironov et al., 2005) and drug delivery (Auzenne et al., 2007; Peer and Margalit, 2004; Luo et al., 2002; Luo and Prestwich, 1999; Lee et al., 2008). Thanks to HA tropism to CD44 receptor, NPs functionalized with HA are supposed to be able to enter the tumor through the leaky external microvascolature, so that superficial HA binds to CD44 cell receptors and, as a result, a co-internalization of HA and drug occurs, therefore leading to an increased intracellular drug release.

Actually, several HA-based drug carriers have been studied for tumor targeting. Since HA has multiple functional groups available for chemical conjugation, manifold HA-drug conjugates have been developed as macromolecular prodrugs in which the conjugated drugs become active upon release from the backbone of HA (Pouyani and Prestwich, 2007; Coradini et al., 2004; Lee et al., 2007; Auzenne et al., 2007). Other systems comprising HA chemically bound onto various drug-loaded NPs (Eliaz et al., 2001; Eliaz et al., 2004; Peer et al., 2004; Yadav et al., 2010a; Yadav et al., 2007; Choi et al., 2011; Cho et al., 2012). For example, PLGA-grafted HA copolymers were synthesized and utilized as targeted micelle carriers for Doxorubicin. In order to graft hydrophobic PLGA chains onto the backbone of hydrophilic HA, the polysaccharide was preliminarily solubilized in anhydrous DMSO by nano-complexing with dimethoxy-PEG. The carboxylic groups of HA were

chemically grafted with PLGA, producing HA-g-PLGA copolymers. Resulting HA-g-PLGA polymer was able to self-assemble in aqueous solution, thusing form multi-cored micellar aggregates, which were able to encapsulate was Doxorubicin during the self-assembly (Lee et al., 2009). These nano-sized drug carriers exhibited enhanced tumor targeting ability and therapeutic efficacy compared to free anticancer agents. It has been reported that the pharmacokinetics of drug conjugates and NPs are determined by their physicochemical properties such as surface chemistry, size, surface charge, and molecular weight (Nishiyama, 2007; Ferrari, 2008). Despite their attractiveness, the production of these systems involved the development of one or more chemical reaction and, therefore, to the obtainment of new HA-based chemical entities, which may face significant regulatory issues since their toxicological profile must be carefully addressed. Furthermore, the preparation of HA-based or HA-decorated NPs involving a chemical reaction is very likely to face regulatory challenges, in particular when referring to approval by FDA; in addition, serious concerns related to the upscalability of the process exist. Thus, in this context, the aim of this work was to formulate biodegradable NPs characterized by HA interface for the intracellular targeting of chemotherapeutic(s). HA interface was obtained without a chemical reaction and with an easily upscalable process. Also these NPs have been produced starting from PLGA and, to overcome the well known issue of PLGA NP aggregation, the idea was to create a HA shell around the biodegradable core of NP in order to improve the PLGA NPs dimensional stability taking advantage of the negative charge of HA and thus obtaining an electrostatic stabilization due to mutual nanodevice repulsion .

More in detail, the idea was to obtain an external HA shell of NPs by means of a physical binding between hydrophobic PLGA and hydrophilic HA using anphiphilic poloxamer acting as a bridge between the hydrophobic PLGA and the hydrophilic HA as explained in chapter 1 (Figure 1). In this way, it was possible to obtain a stable drug carrier in a simple way avoiding the problems related to a chemical reaction. Thanks to the presence of hydrophobic domains of PLGA, the particles can be stable sites for the encapsulation of poorly-water soluble drugs. On the other side, HA is a natural and biocompatible material that does not trigger adverse reactions when it is injected *in vivo* and, moreover, it endows the particles with a hydrophilic character that allows long circulating times in body fluids (Moghimi and Szebeni, 2003; Kogan et al., 2007). Furthermore, since HA can specifically bind to the cancer cells overexpressing at their surface CD44, an HA binding receptor (Aruffo et al., 1990; Banerji et al., 2007; Entwistle et al., 1996) the particles can be efficiently internalized by the cells by means of both a passive (EPR effect) and an active targeting (Maeda et al., 2000; Brigger et al., 2002; Hashizume et al., 2000). Considering the aforementioned features, these NPs can be considered potentially interesting systems as carriers of active agents. These novel nanoparticulate systems were characterized for their size, morphology and zeta potential. In order to verify their performance as drug carriers, the encapsulation and the release of a chemoterapeutic agent, Irinotecan, was assessed.

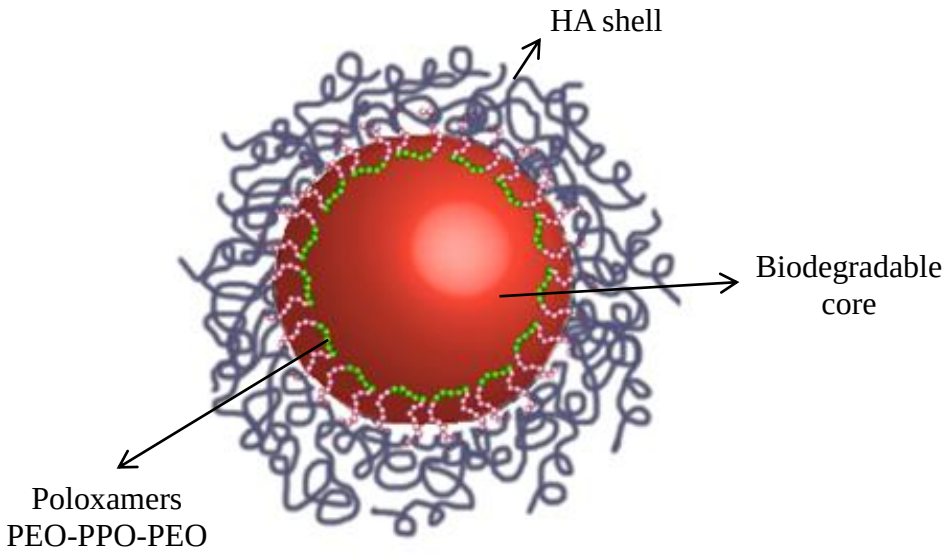

Figure 3.1: Schematic representation of the nanoparticles characterized by HA shell, biodegradable core and poloxamers that act as bridge between PLGA particles and HA

Aim of the Work

In this chapter, we propose a simple method based on single emulsion technique to produce NP. This is clearly advantageous in terms of ease of formulation and possible upscalability of the production process. Here, we have formulated irinotecan (IRIN)-loaded biodegradable PLGA NPs, coated with non-chemically modified HA for tumor targeting toward CD44-overexpressing cell lines. NP stability was evaluated by measuring their size over time and *in vitro* drug release studies have been taken to evaluate the capacity of the produced NPs to control and prolong IRIN release. DSC and ζ potential analyses, along with ELISA tests, were employed to investigate polymer assembly in NP formulations. This work emphasizes the potential of the proposed fabrication technique to obtain NPs decorated with hydrophilic moieties through a single production step. Finally, *in vitro* biological test on both cells overexpressing and not overexpressing CD44 receptor, i.e. human breast carcinoma cells (HS578T) and L-929 cells respectively, were performed to assess NP toxicity and targeting ability to CD44 receptor.

Materials and Methods

Materials

HA with a 850,000 Da weight-average molecular weight (MW) was provided by Novozymes Biopharma (Denmark). IRIN, acetone and dimethyl sulfoxide (DMSO) were obtained from Sigma Aldrich (USA). Phosphate buffer saline (PBS) tablets without calcium and magnesium were obtained from MP Biomedicals Inc. (France). The polymers (PLGA and Poloxamers) are the same described in the *Materials* section of Chapter 1.

Nanoparticle Preparation

Blank and IRIN-loaded NPs were prepared by a single emulsion-solvent evaporation technique (oil in water). Different NP formulations were prepared with different amounts of HA, PLGA and poloxamers; the compositions and the corresponding acronyms are reported in Table 3.1. The NPs have been prepared as schematized in Figure 3.2.

Acronym	**OIL PHASE (O1)**			**WATER PHASE (W1)**		
	PLGA% (w/w)	F68 % (w/w)	F127 % (w/w)	HA % (w/w)	F68 % (w/w)	F127 % (w/w)
P	2	-	-	-	0.05	0.05
PP	1	0.5	0.5	-	0.05	0.05
PPHA30	1	0.5	0.5	2	0.05	0.05
PPHA60	1	1.5	1.5	4	0.05	0.05

Table 3.1: Composition and acronyms of the different NP formulations.

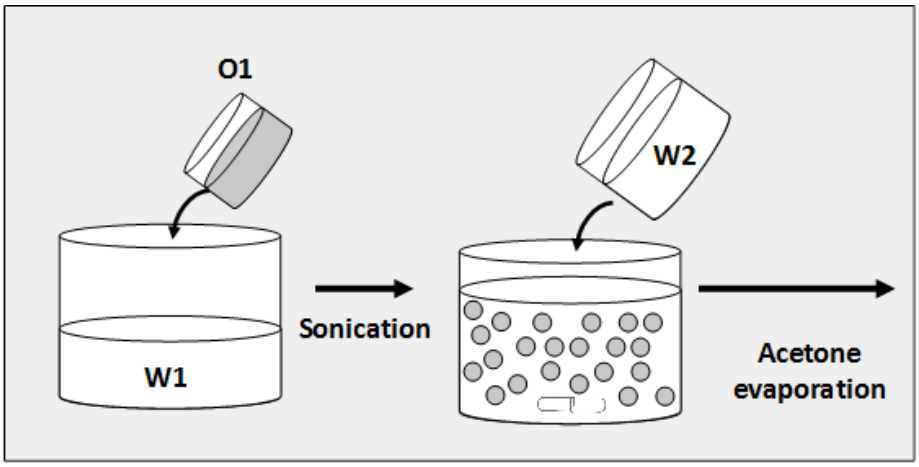

Figure 3.2: Schematic representation of NP preparation through the single emulsion-solvent evaporation technique.

Briefly, a water-in-oil emulsion was obtained by emulsifying 5 mL of an organic phase (O1) with 15 mL of a water phase (W1) by sonication (FALC, Italy, 5 min). Afterwards, a second water phase (W2), made up of pure bidistilled water (25 mL) was added to enhance the separation of the nanodroplets. The organic solvent was evaporated at 35 °C for 35 minutes by means of a rotary evaporator (Laborota 4010 digital, HEIDOLPH). The obtained NP suspension was washed three times by centrifugation (Hettich Zentrifugen, Germany; 13,000 rpm, 60 min) and, once the supernatant was eliminated, NPs were stored at -80 °C. In the case of drug-loaded NPs, IRIN (10 mg) was solubilized in the organic phase.

Nanoparticle Characterization: Morphology, Mean Size, Size Distribution, Yield and ζ Potential

NP morphology was investigated through a transmission electron microscope (TEM, FEI Tecnai G12 Spirit Twin) with emission source LaB6 (120 kV,

spotsize 1) using 400 mesh carbon-coated copper grids at room temperature (RT). The carbon-coated copper grid was immersed in ultradiluted NP suspensions and, after the drying phase, the grid was placed on a rod holder for TEM characterization. Three grids per NP suspension were prepared and a minimum of four micrographs *per* grid were acquired. Surface topography and phase signals of NPs were recorded by atomic force microscopy (NanoWizard II-AFM, standalone top View Optics, JPK Instruments, Germany) by placing one drop of NP suspension (about 1.0 mg/mL) on a freshly cleaved mica surface. For AFM observations, the suspension was air-dried at room temperature. Intensity-average diameters and ζ potentials of NPs were determined *via* dynamic light scattering (DLS) measurements with a Zetasizer Nano (Malvern Instruments, Malvern, UK). For particle size measurements, NPs were suspended in ultrapure water. To study the agglomeration dynamics of NPs in bidistilled water at 4 °C, NP size measurements were taken for ten days. NP yield was gravimetrically calculated after lyophilization for 24 h (Heto PowerDry PL6000 Freeze Dryer, Thermo Electron Corp., USA; -60 °C, 0.73 hPa). ζ-potential assay was also performed at different pH values (from 7.4 to 2) at RT. Results were averaged on at least five measurements.

Thermal Analyses

Aiming to study the interactions between the different polymers in NP formulations, thermoanalytical tests were carried out on PLGA and poloxamer powders, along with freeze-dried P, PP, PPHA30 and PPHA60

NPs. The heat involved in the phase transitions of polymers was determined by a differential scanning calorimeter (DSC; DSC Q20, TA Instruments, U.S.A.), calibrated with a pure indium standard. The samples were placed in aluminum pans and underwent a double scan, from -60 °C to 80 °C. In the case of P NPs, only one scan from 20 to 80 °C was carried out. As for the powders, the first scan was taken to eliminate the thermal history of the samples. Measurements were performed under an inert nitrogen atmosphere, purged at a flow rate of 50.0 mL/min. The heating rate was 5 °C/min in all cases. The heat evolved during polymer crystallization and fusion (W/g) was calculated from the recorded DSC thermograms by integrating the exothermic/endothermic peaks, while the glass transition temperature (Tg) was obtained from thermogram inflection point.

Drug Entrapment Efficiency

Drug entrapment efficiency (EE) was calculated by dissolving freeze-dried NPs (1 mg) in 1 mL of DMSO. The resulting solution was sonicated for 1 h in a water bath at 59 kHz, 100% power. IRIN content was quantified by spectrophotometric assay (UV-1800, UV-VIS spectrophotometer, Shimadzu, Japan) at 370 nm. The linearity of the response was verified on IRIN solutions in DMSO (0.04–10 µg/mL concentration range; $r^2 > 0.99$). Entrapped IRIN percentage was calculated as:

$$EE = 100\frac{D_E}{D_T} \quad (1)$$

where D_E is the amount of entrapped drug in the NPs and D_T is the total amount of the drug used to prepare the NPs. Results were averaged on at least three independent batches.

In vitro Release Kinetic of Irinotecan

For release experiments, NPs were suspended in PBS of release medium (10 mL, pH = 7.4) and incubated at 37 °C in an orbital incubator (SI50, Stuart R, UK) operating at 10,000 rpm. At scheduled time intervals, aliquots of the release medium (1 mL) were withdrawn and replaced with the same volume of fresh medium. The aliquots were ultracentrifuged for 20 minutes at 80,000 rpm (L8-70 ultracentrifuge, Beckam Counter, USA) and the supernatant was analyzed through spectrophotometric analysis (λ = 364.5 nm) to quantify IRIN content. The instrument response was linear over the 0.1–50 μg/mL concentration range ($r^2 > 0.99$). The experiments were run in triplicate.

Quantification of Hyaluronic Acid

The amounts of HA incorporated in/on the NPs were quantified as reported elsewhere (Mondalek et al., 2010). Briefly, HA was determined after conjugation with a specific enzyme provided by a HA ELISA kit (Biorbyt LLC, USA), followed by spectrophotometric analysis at 450 nm after each washing step. More in detail, the amount of HA incorporated in the NP was determined by subtracting, from the initial mass of HA, the amount lost in the

three NP washes. The linearity of the kit response was assessed in the 0–250 ng/mL HA concentration range ($r^2 > 0.96$).

Cell Culture Studies

L929 cells originating from Mouse C34/An connective tissue were obtained from the European Collection of cell cultures (Sigma-Aldrich, USA) and were used at a passage 15–23. CD44-overexpressing human breast carcinoma HS578T cells, kindly gifted by Dr. Olga Zeni (IREA-CNR), were used. The cells were grown at 37 °C and 5% CO_2 in T-75 cell culture flask (Falcon, Italy), using Dulbecco's Modified Eagle's Medium (DMEM, Hyclone, USA) cell culture medium supplemented with 10% fetal bovine serum and antibiotics (penicillin G sodium 100 U/mL, streptomycin 100 μg/mL). In the case of HS578T cells, the culture medium was enriched with 10 μl/mL bovine insulin. When confluent growth was reached, the cells were detached with 0.25% trypsin-EDTA solution and washed twice with fresh PBS. The resulting cell suspensions were centrifuged for 5 min at 10,000 rpm (BRK55/10 Centrifuge, Centurion Scientific Ltd, UK). Finally, the supernatant was separated and the cells resuspended in fresh culture medium. Viable cells were counted using the TC20 automated Cell Counter (Biorad, USA).

In Vitro Cytotoxicity

L929 and HS578T cells were seeded in 48-well plates at a density of 5 x 10^3 cells *per* well in the presence of 200 µL of cell culture medium. Five wells were used as blank control. To determine the 50% inhibitory concentration (IC50) of the drug, the cells were exposed at IRIN solutions at concentrations ranging from 10 to 230 µM. In particular, after 24 h incubation at 37 °C in 5% CO_2 atmosphere, the incubation medium was removed and 200 µL of IRIN solution at the same concentration was added. Afterwards, the cells were incubated for 48 h and their viability assessed by Alamar Blue test. The biocompatibility of void PP and PPHA30 NPs as well as the bio-efficacy of IRIN loaded PP and PPHA30 NPs were estimated using an amount of NPs equivalent to that used to load an IRIN dose correspondent to IRIN IC50. Both L929 and HS578T cells were incubated with the tested NPs for 48 hours, and their viability was assessed by Alamar Blue test. HS578T cells, after the test, were rinsed and an amount of NPs equivalent to IRIN IC50 was added; the cells were then incubated for further 72 hours and their viability assessed by Alamar Blue test.

Alamar Blue test was performed by adding the Alamar Blue (AB) reagent to the samples (at 10% v/v with respect to the medium) and incubated at 37 °C for 4 hours. The absorbance of the samples was measured using a spectrophotometer plate reader (Multilabel Counter, 1420 Victor, Perkin Elmer) at 570 nm and 600 nm. AB is an indicator dye that incorporates an oxidation-reduction indicator whose color changes in response to the

chemical reduction in growth medium resulting from cell viability. Data are calculated as the percentage difference between treated and control samples with the following formula:

$$\%\,reduction = \frac{(O_2 \times A_1) - (O_1 \times A_2)}{(O_2 \times P_1) - (O_1 \times P_2)} \times 100$$

where O_1 is the molar extinction coefficient (E) of oxidized AB at 570 nm; O_2 is the E of oxidized AB at 600 nm; A_1 is the absorbance of test wells at 570 nm; A_2 is the absorbance of test wells at 600 nm; P_1 is the absorbance of positive growth control well at 570 nm; P_2 is the absorbance of positive growth control well at 600 nm.

Statistical Analyses

In all cases, quantitative data are reported as mean value ± standard deviation (SD). The statistical significance of the results has been assessed by one-way analysis of variance ANOVA. A p value < 0.05 was considered to identify statistically different groups.

Results and Discussion

In recent years, many ‘smart’ nanosystems for targeted cancer therapy have been developed, in order to increase the safety of use and the effectiveness of the loaded chemotherapy drugs (Cho et al., 2008; Brigger et al., 2002; Huang et al., 2013; Ding et al., 2012). Furthermore, it is also desirable to endow the produced devices with targeting ability toward cancer cells. A convenient way of developing such NPs can exploit their spontaneous assembly in emulsion, driven by a lipophicity gradient between the core and the external surface of the NPs, which forms core-shell NPs in aqueous environment. Here, we have developed a simple emulsion procedure to obtain amphiphilic PLGA-based NPs decorated with an external HA corona, in which hydrophilic HA was combined to hydrophobic PLGA *via* amphiphilic poloxamer bridging. In particular, HA is the hydrophilic domain of NPs and, therefore, we have hypothesized that it arranges on the outer shell of the devices, while hydrophobic PLGA forms the core of the NPs. These nanosystems have been engineered to combine device stability and targeting ability to CD44-overexpressing cancer cells. HA-decorated NPs have been formulated by dissolving PLGA and poloxamers in acetone and by emulsifying the obtained solution in an aqueous phase containing poloxamers and, in case, HA. The overall polymer concentration (PLGA and poloxamers) in the oil phase has been fixed at 2% w/v, while different amounts of HA and poloxamers in the external aqueous phase have been added. HA is a strong polyanion at physiological pH and, therefore, the robustness of HA self assembly on NP surface can be monitored by ζ potential analyses. Results of

size and ζ potential measurements are summarized in Table 3.2 and shown in Figure 3.3.

Forms.	$PDI_{t=0}$	$d(nm)_{t=0}$	$d(nm)_{t=10\ d}$	ζ potential $(mV)_{t=0}$	ζ potential $(mV)_{t=10\ d}$
P	0.156 ± 0.01	154 ± 2	190 ± 10	-15.0 ± 0.8	-26.1 ± 1.7
PP	0.082 ± 0.01	106 ± 1	110 ± 1	-25.5 ± 1.2	-29.1 ± 1.8
PPHA30	0.884 ± 0.01	184 ± 4	161 ± 2	-49.7 ± 1.4	-49.3 ± 0.9
PPHA60	1.23 ± 0.01	306 ± 14	258 ± 14	-56.2 ± 1.0	-57.0 ± 2.1

Table 3.2: NP intensity-average diameters, polydispersity index and zeta potential in time in bidistilled water at 4 °C. The mean values and standard deviations were calculated from at last three independent experiments.

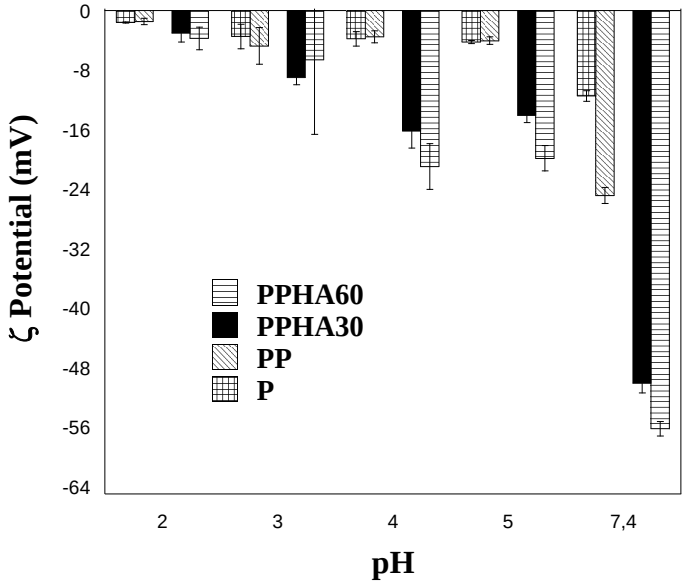

Figure 3.3: Zeta potential values of different NP formulations as a function of pH. The mean values and standard deviations were calculated from at last three independent experiments.

We found single peaks in all size distributions for all formulations. Furthermore, NP size is progressively increasing with increasing HA concentration in the external aqueous phase, while ζ-potential values

significantly decrease from ~ -27mV of PP to ~ -50 mV for PPHA60. These results indicate the formation of an external HA shell, driven by a lipophilicity gradient between the oil and water phases of the emulsion used to produce the NPs. A ζ-potential value of about -50 mV is more negative than the one observed in the case of NPs coated by HA, prepared through LbL procedure (Dreaden et al., 2014), thus suggesting a more uniform and efficacious cover of the polysaccharide on NP surface with the novel production method presented in this work. A negative ζ-potential, which is due to the ionization of the carboxyl groups of HA, can prevent NP aggregation and binding to plasma proteins, therefore possibly promoting their stability and prolonged circulation *in vivo*. Furthermore, the ζ-potential of NPs was found to be increasing with decreasing pH and, in particular, a *quasi*-neutral surface charge was found in the case of PPHA NPs, at a pH close to pKa value of HA (~ 2), due to the protonation of the carboxyl groups on HA under decreasing pH (Figure 3.3) (Huang et al., 2014). Differently, HA-free NPs neutralize their superficial charge at the pKa of PLGA (~ 4) (Yoo and Mitragotri, 2010). These results support the hypothesis of HA exposed on NP surface, which can be reasonably ascribed to the 'bridging' action of poloxamers between the inner hydrophobic PLGA and the outer hydrophilic HA domains. Indeed, it can be easily hypothesized that the surfactant properties of poloxamers help creating a gradient of lipophilicity, which encourages the interaction and arrangement of HA chains on the surface of P NPs. In the clinical administration of NPs, the phenomenon of particle aggregation represents, of course, a crucial issue, affecting the drug release profile and possibly increasing the risk of vessel occlusion. For these

reasons, the electrostatic and/or steric stabilization of NPs is an important aspect to be considered. As it can be noticed in Table 3.2, after 10 days the diameter of P NPs increases from about 154 to about 190 nm, indicating that a significant aggregation occurs. On the contrary, the presence of hydrophilic moieties on PP, PPHA30 and PPHA60 NP surface confers higher dimensional stability to the nanodevices, being their size almost constant in the time frame of the experiment. Moreover, in the case of PPHA30 and PPHA60 NPs, the stabilizing effect can be also ascribed to a higher electrostatic repulsion which, in turn, depends on the lower ζ-potential values, i.e., a higher density of negative charges at NP surface after 10 days at 4 °C. Table 3.3 reports the polymer-to-drug weight ratio and drug encapsulation efficiency, along with the NP yield.

Form.	Polymer:drug ratio	Drug encapsulation efficiency (%)	NP yield (%)
P	10.5 ± 0.4	62.6 ± 2.5	65.9 ± 4.2
PP	8.2 ± 0.5	64.9 ± 3.3	53.0 ± 7.8
PPHA30	10.0 ± 0.5	62.7 ± 3.4	48.0 ± 6.8
PPHA60	9.7 ± 0.3	64.1 ± 1.8	38.9 ± 10.0

Table 3.3: Polymer-to-drug ratio, drug encapsulation efficiency and NP yield. The mean values and standard deviations were calculated from at last three independent experiments.

Results indicate that the presence of HA does not affect the drug encapsulation efficiency, which is higher than 60% in all cases. Moreover, even if HA presence reduces NP yield from 65.9% for P NPs to 48.0% for PPHA30 NPs, the polymer-to-drug ratio is around 10 for both formulations. This result, together with their smaller size compared to PPHA60 NPs, leads us to choose PPHA30 NPs as the optimized formulation to be further

investigated. TEM images were taken to study the morphology of the optimized PPHA30 NP formulation. Selected micrographs of P, PP and PPHA30 NPs are reported in figures 3.4, 3.5 and 3.6, respectively. The images revealed discrete, spherical particles for all NP formulations and, in particular, PP and PPHA30 NPs exhibited a core–shell structure due to their surface exposing hydrophilic PEO and/or HA chain segments. The shape of NPs and outer HA corona were also visible in AFM images (Figure 3.6 B).

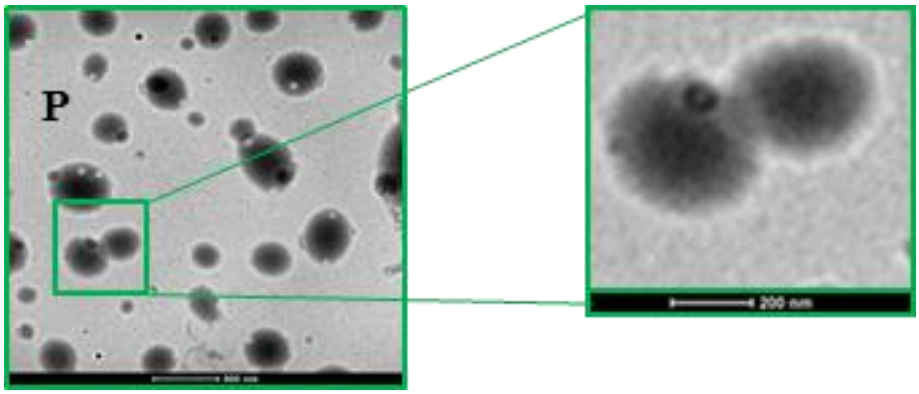

Figures 3.4: Selected TEM micrographs of P NPs

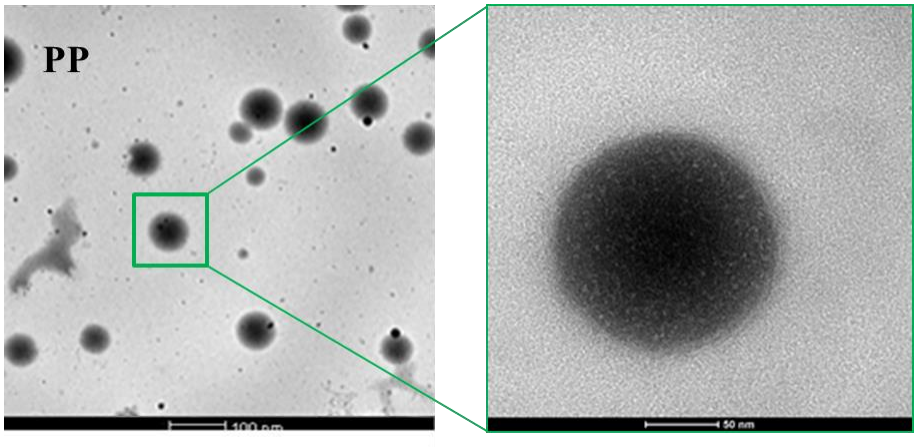

Figures 3.5: Selected TEM micrographs of PP NPs

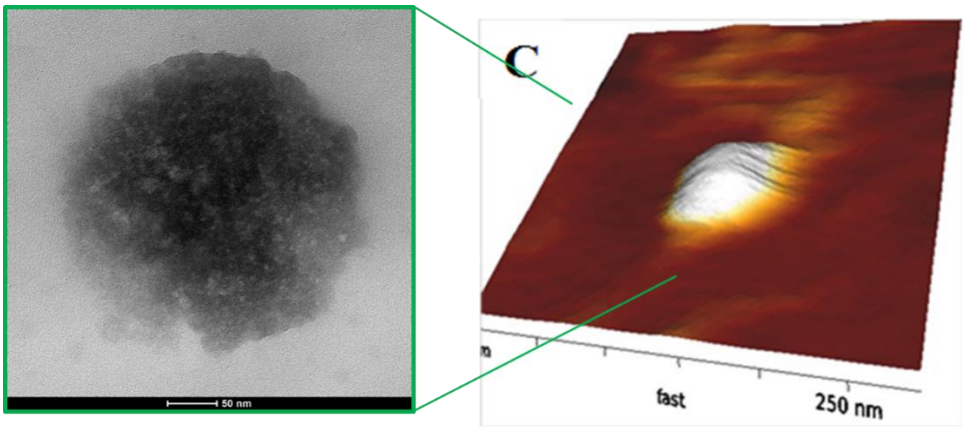

Figures 3.6: Selected TEM (A) and AFM (B) micrographs of PPHA30 NPs**.**

The results of thermal analyses are shown in Figures 3.7 and summarized in Table 3.4.

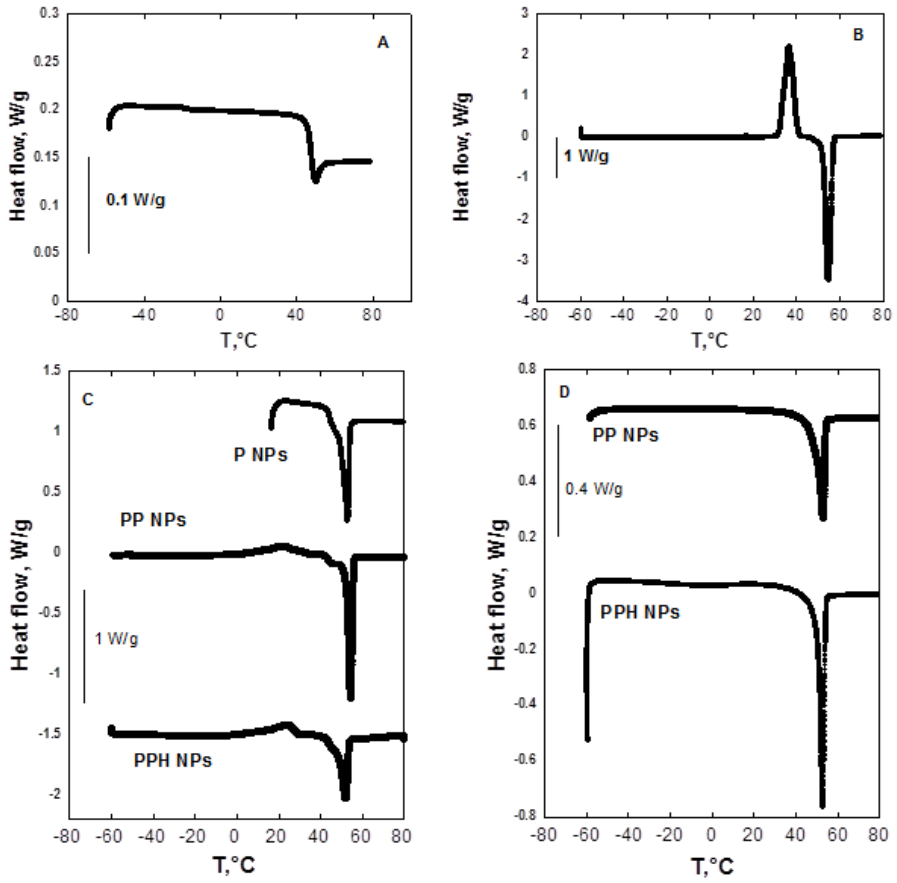

Figures 3.7: DSC thermograms of PLGA powder (A) and Poloxamer powder (B); P, PP and PPHA NPs first scan (C); P, PP and PPHA NPs, second scan (D). Results were obtained from at last three independent experiments.

	T_g, °C	T_f, °C	ΔH_f, J/g	T_c, °C	ΔH_c, J/g
PLGA powder	47.7 ± 0.1	-	-	-	-
Poloxamers	-	54.2 ± 0.1	140 ± 3	36.3 ± 0.2	127 ± 3
P NPs	44.0 ± 0.5	-	-	-	-
PP NPs	43.3 ± 0.3	54.3 ± 0.2	28.1 ± 9.4	27.8 ± 4.8	23.3 ± 9.2
PPHA NPs	43.6 ± 0.8	51.7 ± 0.2	37.3 ± 4.2	26.8 ± 3.2	28.6 ± 15.1

Table 3.4: Results of thermal analyses. The mean values and standard deviations were calculated from at last three independent experiments.

As it can be seen in Figure 3.7A, the thermogram of PLGA powder shows a glass transition temperature (Tg) around 48 °C, while, as for the poloxamers (Figure 3.7B), crystallization and melting are shown at about 36 °C and 54

°C, respectively. As for HA powder, DSC traces showed no thermodynamic transition in the temperature range here examined. In the case of P NPs (Figure 3.7C), the Tg is lower than that of PLGA powder (~ 44 °C instead of ~ 48 °C), therefore pointing at a possible plasticizing effect of the poloxamers used as surfactants in the aqueous phase of the emulsion. The Tg values were found to be very similar also when the poloxamers had been blended in the organic phase of the emulsion (i.e. for PP and PPHA30 NPs), therefore indicating the same plasticizing effect of poloxamers also when they are within the bulk of NPs. Furthermore, as depicted in Figure 3.7, when analyzing PP NPs, a broadening of poloxamer crystallization peak, along with a decrease of their crystallization heat (ΔHc) and temperature (Tc), has been observed. This suggests an amorphous interaction between the polymeric chains of PLGA and poloxamers when they are solubilized into the organic phase of the emulsion used to produce the NPs. In actual fact, as we have previously hypothesized, due to the amphiphilic nature of poloxamers, the hydrophobic PO segments preferentially self-orient towards the PLGA core of the NPs, while the hydrophilic EO segments direct towards the aqueous phase (Mayol et al., 2015). In the presence of HA in NP formulation, melting and crystallization do not significantly change compared to PP NPs, therefore indicating that poloxamer crystallization is not further hampered. Moreover, it must be underlined that, in the first heating ramp, the Tg of PLGA is observable in NPs while, in the second scan (Figure. 3.7D), after poloxamer melting, PLGA Tg and poloxamer crystallization peak are no longer visible. This may support the hypothesis that, in PPHA30 NPs, PLGA and HA do not interact since PLGA constitutes

NP bulk while HA is superficially exposed, with the poloxamers acting as a bridge between the PLGA and HA. After poloxamer melting, this configuration is lost and a polymeric blend, with thermal properties different from the ones of the starting polymers, is formed. This hypothesis of polymer self-assembly into the NPs is also corroborated by the previously shown morphologic and ζ potential results. PPHA30 drug entrapment efficiency was found to be 61.2 % (w/w), while for P NP it was 58.8 % (w/w). Results of ELISA assay showed a loss of 34.3% w/w of HA in the supernatant. Experimental in vitro release profiles of IRIN from P and PPHA30 NPs are reported in Figure 3.8.

The results demonstrated that IRIN is completely released in less than two weeks, with > 85% of the loaded drug eluted within 7 days. In both formulations, a strong burst is evidenced. It can also be seen that IRIN release is slightly slower in the case of HA-containing NPs. This can be probably ascribed to a slightly higher affinity of IRIN for the amphiphilic HA-containing NPs compared to simple P NPs.

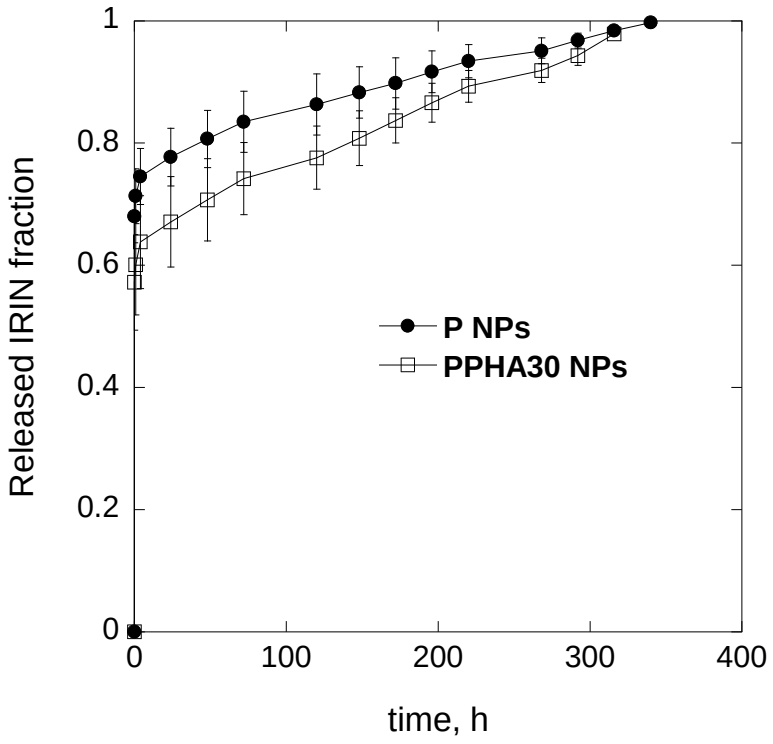

Figure 3.8: In vitro IRIN release profiles from P and PPHA30 NPs.

HS578T and L929 cell lines were employed to investigate the cytotoxicity of PP NP and PPHA30 NPs using Alamar blue assay. The IRIN IC50 for L929 cells was found to be 51.7 μM, while the IRIN IC50 for HS578T cells was 100.5 μM. The NP concentrations used in the experiments were chosen as those able to load IRIN at a dose equivalent to its IC50. Results from cell culture studies related to *in vitro* bioefficacy of IRIN-loaded PPHA30 NPs and PP NPs are presented in Figure 3.9.

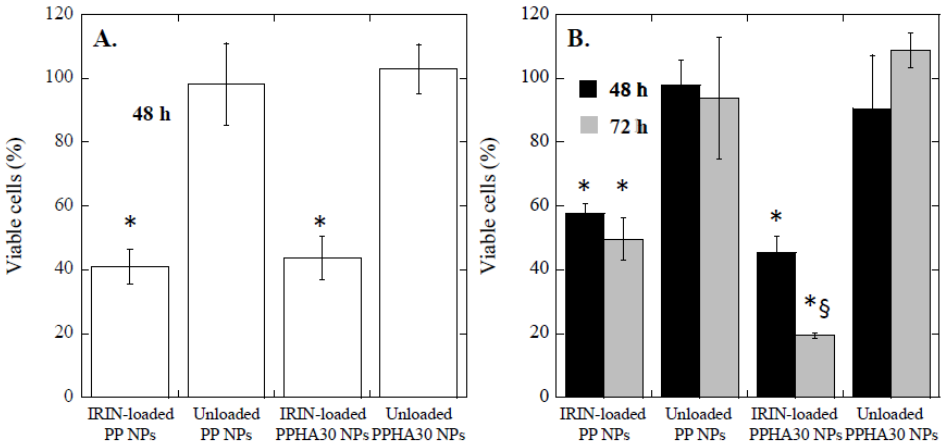

Figures 3.9: Results of cytotoxicity assay. Percentage of viable L929 cells after 48 h incubation (A) and of HS578T cells after 48 and 72 h of incubation (B). Cell viability was calculated with respect to the non-treated control cells.
*P < 0.05 vs the respective unloaded NP ; § P < 0.05 vs IRIN-loaded PP NPs

As to L929 cells (Figure 3.9A) it is possible to observe unloaded NPs are not toxic. Indeed, the percentage of viability, compared to the control, for PP and PPHA30 is almost 100%. Differently, for both the IRIN-loaded particles, the percentage of viability is about 40%. This result indicates that PP and PPHA30 particles are able to inhibit the cells growth and that HA coating does not influence this ability. Also in the case of HS578T cells (figure 3.9B), the unloaded NPs are not cytotoxic. Interestingly, in the case of IRIN-loaded NPs, the behaviors of PPHA30 and PP NPs are different both at 48 and, in a significant way, at 72 hours. In particular, the percentage of cell viability is about 60% and 45% after 48 hours for PP and PPHA30 NPs, respectively, therefore indicating that HA-coated NPs can inhibit cellular growth more effectively compared to PP NPs. A more evident result was obtained at 72 hours, being the percentage of viable cells about 20% and 50% for PPHA30 and PP NPs, respectively. Taken all together, these results suggest that PPHA30 NPs can deliver more drugs into cancer cells and

resulting in a stronger cell killing effect, probably due to the HA receptor-mediated endocytosis and therefore a better NP cellular uptake in CD44+ cells.

Conclusions

In this study, a novel and easily upscalable method to directed the self-assembly of tumor targeting HA moieties on IRIN-loaded PLGA NPs is proposed. Thermal analyses revealed that in the produced NP formulations PLGA, poloxamer and HA act as independent entities and not as a polymeric blend. These results, together with the results of ζ-potential analyses, suggest a polymer self-organization driven by a gradient of lypophilicity between the oil and water phases of the emulsion used to prepare the NPs. The HA cover enhances NP size stability over time, due to an enhanced electrostatic repulsion of HA coated NPs and also to a higher degree of hydration and/or to a steric stability caused by the presence of flexible HA chains on NP surface. The *in vitro* release profiles of IRIN showed a sustained drug release up to 7-13 days. Cell cytotoxicity tests showed that PPHA30 NPs can deliver more drugs into cancer cells resulting in a stronger cell killing effect on CD44-overexpressing cells, probably due a positive effect of HA on NP internalization.

Taken all together, these results designate PPHA30 NPs as promising candidates for targeted drug delivery to solid tumors for a number of significant cancer types.

References

Aggarwal B.B., Sung B. Pharmacological basis for the role of curcumin in chronic diseases: an age-old spice with modern targets. Tr Pharmacol Sci. 2009; 30 (2), 85-94.

Ahrens T., Assmann V., Fieber C., Termeer C.C., Herrlich P., Hofmann M., Simon J.C. CD44 is the principal mediator of hyaluronic-acid-induced melanoma cell proliferation. J Invest Dermatol. 2001; 116, 93–101.

Alemany C. Etirinotecan pegol: development of a novel conjugated topoisomerase I inhibitor. Curr Oncol Rep. 2014; 16(2), 367.

Alho A.M., Underhill C.B. The hyaluronate receptor is referentially expressed on proliferating epithelial cells. J Cell Biol. 1989; 108(4), 1557–1565.

Ambrosio L., Borzacchiello A., Netti P.A., Nicolais L. Rheological properties of hyaluronic acid based solutions. Polym Mater Sci Engin. 1999a; 79, 244-245.

Ambrosio L., Borzacchiello A., Netti P.A., Nicolais L. Rheological study on Hyaluronic acid and its derivatives solutions. J Macromol Sci - Pure Appl Chem. 1999b; A36(7-8), 991-1000.

Anand P., Kunnumakkara A.B., Newman R.A., Aggarwal B.B. Bioavailability of curcumin: poblems and promises. Mol Pharm. 2007; 4 (6), 807-818.

Anand P., Thomas S.G., Kunnumakkara A.B., Sundaram C., Harikumar K.B., Sung B., Tharakan S.T., Misra K, Privadarsini I.K., Rajasekharan K.N., Aggarwala B.B. Biological activities of curcumin and its analogues (Congeners) made by man and Mother Nature. Biochem Pharmacol. 2008; 76(11), 1590–1611.

Anand P., Nair H.B., Sung B.K., Kunnumakkara A.B., Yadav V.R., Tekmal R.R., Aggarwal B.B. Design of curcumin-loaded PLGA nanoparticles formulation with enhanced cellular uptake, and increased bioactivity in vitro and superior bioavailability in vivo. Biochem Pharmacol. 2010; 79 (3), 330-338.

Apetz N., Munch G., Govindaraghavan S., Gyengesi E. Natural compounds and plant extracts as therapeutics against chronic inflammation in Alzheimer's diseasea translational perspective, CNS Neurol Disord Drug Targets. 2014; 13 (7), 1175–1191.

Aruffo A., Stamenkovic I., Melnick M., Underhill C.B., Seed, B. CD44 is the principal cell surface receptor for hyaluronate. Cell. 1990; 61(7), 1303–1313.

Asayama S., Nogawa M., Takei Y., Akaike T., Maruyama A. Synthesis of novel polyampholyte comb-type copolymers consisting of a poly(L-lysine)

backbone and hyaluronic acid side chains for a DNA carrier. Bioconj Chem. 1998; 9(4), 476 –481.

Auzenne E., Ghosh S.C., Khodadadian M., Rivera B., Farquhar D., Price R.E., Ravoori M., Kundra V., Freedman R.S., Klostergaard J. Hyaluronic acid-paclitaxel: antitumor efficacy against CD44(+) human ovarian carcinoma xenografts. Neoplasia. 2007; 9(6), 479–486.

Aziz K.J. Clinical molecular biology: concepts and applications. Adv Clin Chem. 1996; 32, 39–72.

Baban D., Seymour L.W. Control of tumor vascular permeability. Adv Drug Deliv Rev. 1998; 34, 109–19.

Bae K.H., Chung H.J., Park T.G. Nanomaterials for cancer therapy and imaging. Mol Cells. 2011; 31(4), 295-302.

Balasubramanian S., Eckert R.L. Curcumin suppresses AP1 transcription factor-dependent differentiation and activates apoptosis in human epidermal keratinocytes. J Biol Chem. 2007; 282 (9), 6707-6715.

Banerji S., Wright A.J., Noble M., Mahoney D.J., Campbell I.D., Day A.J., Jackson D.G. Structures of the Cd44-hyaluronan complex provide insight into a fundamental carbohydrate-protein interaction. Nat Struct Mol Biol. 2007; 14(3), 234-239.

Banerjee M.; Singh P.; Panda D. Curcumin suppresses the dynamic instability of microtubules, activates the mitotic checkpoint and induces apoptosis in MCF-7 cells. Febs Journal. 2010, 277 (16), 3437-3448.

Barbucci R., Rappuoli R., Borzacchiello A., Ambrosio L. Synthesis, chemical and rheological characterisation of new hyaluronic based hydrogels, J Biomater Sci Polym Ed, 2000; 11(4), 383-399.

Barbucci R., Lamponi S., Borzacchiello A., Ambrosio L., Fini M., Torricelli P., Giardino R. Hyaluronic acid hydrogel in the treatment of osteoarthritis. Biomaterials. 2002; 23(23), 4503-4513.

Bhattacharyya, S.; Mandal, D.; Saha, B.; Sen G.S., Das T., Sa G. Curcumin prevents tumor-induced T cell apoptosis through Stat-5a-mediated Bcl-2 induction. J Biol Chem. 2007a; 282 (22), 15954-15964.

Bhattacharyya S.; Mandal D.; Sen G.S.; Pal S.; Banerjee S.; Lahiry L.; Finke J.H., Tannenbaum C.S., Das T., Sa G. Tumor-induced oxidative stress perturbs nuclear factorr-kappa B activity-augmenting tumor necrosis factor-alpha-mediated T-cell death: Protection by curcumin. Cancer Res. 2007b; 67 (1), 362-370.

Bies C., Lehr C.M., Woodley J.F. Lectin-mediated drug targeting: history and applications. Adv Drug Deliv Rev, 2004; 56(4), 425–435.

Biondi M., Fusco S., Lewis A.L., Netti P.A. Investigation of the mechanisms governing doxorubicin and irinotecan release from drug-eluting beads:

mathematical modeling and experimental verification. 2013a; 24(10), 2359-2370.

Biondi M., Guarnieri D., Yu H.; Belli V., Netti P.A. Sub-100 nm biodegradable nanoparticles: in vitro release features and toxicity testing in 2D and 3D cell cultures. Nanotechnology. 2013b; 24 (4), 045101.

Bisht S., Feldmann G, Soni S, Ravi R, Karikar C, Maitra A, Maitra A. Polymeric nanoparticle encapsulated curcumin ("nanocurcumin"): a novel strategy for human cancer therapy. J Nanobiotech. 2007; 5, 3.

Bonelli M.A., Fumarola C., La Monica S., Alfieri R. New therapeutic strategies for malignant pleural mesothelioma. Biochem Pharmacol. 2016, in press

Borzacchiello A., Netti P.A., Ambrosio L., Nicolais L. Hyaluronic acid derivatives mimic the rheological properties of vitreous body. New Frontiers in Medical Sciences: Redefining Hyaluronan. 2000; 195-202.

Borzacchiello A., Ambrosio L. Network formation of low molecular weight hyaluronic acid derivatives. J Biomat Sci Polym Ed. 2001; 12(3), 307-316.

Borzacchiello A., Mayol L., Gaerskog O., Dahlqvist A., Ambrosio L. Evaluation of injection augmentation treatment of hyaluronic acid based materials on rabbit vocal folds viscoelasticity. J Mater Sci Mater Med. 2005; 16(6), 553-557.

Borzacchiello A., Mayol L., Ramires P.A., Di Bartolo C., Pastorello A., Ambrosio L., Milella E. Structural and rheological characterization of hyaluronic acid-based scaffolds for adipose tissue engineering. Biomaterials. 2007; 28, 4399–4408.

Borzacchiello A., Mayol L., Schiavinato A., Ambrosio L. Effect of hyaluronic acid amide derivative on equine synovial fluid viscoelasticity. J Biomed Mater Res. 2010; 92(3), 1162-1170.

Bozzuto G., Molinari A. Liposomes as biomedical devices. Int J Nanomed. 2015; 10, 975-99.

Brigger I., Dubernet C., Couvreur P. Nanoparticles in cancer therapy and diagnosis. Adv Drug Deliv Rev. 2002; 54(5), 631-651.

Byrne J.D., Betancourt T., Brannon-Peppas L. Active targeting schemes for nanoparticle systems in cancer therapeutics. Adv Drug Deliv Rev. 2008; 60(15), 1615–1626.

Cao G. Nanostructures and Nanomaterials: synthesis, properties and applications. Imperial College Press, London. 2004.

Chen Y., Wu Q, Zhang Z, Yuan L, Liu X, Zhou L. Preparation of curcumin loaded liposomes and evaluation of their skin permeation and pharmacodynamics. Molecules. 2012; 17, 5972–5987.

Chen X., Zou L.Q., Niu J., Liu W., Peng S.F., Liu C.M. The stability, sustained release and cellular antioxidant activity of curcumin nanoliposomes. Molecules. 2015; 20(8):14293-311.

Chiu S., Terpstra K.J., Bureau Y., Hou J., Raheb H., Cernvosky Z., Badmeav V., Copen J., Husni M., Woodbury-Farina M. Liposomal-formulated curcumin [Lipocurc] targeting HDAC (histone deacetylase) prevents apoptosis and improves motor deficits in Park 7 (DJ-1)-knockout rat model of Parkinson's disease: implications for epigenetics-based nanotechnology-driven drug platform. J Complement Integr. Med. 2013;10.

Cho K., Wang X., Nie S., Chen Z., Shin D.M. Therapeutic nanoparticles for drug delivery in cancer. Clin Cancer Res. 2008; 14, 1310-1316.

Cho H.J., Yoon H.Y., Koo H., Ko S.H., Shim J.S., Lee J.H., Kim K., Kwon I.C., Kim D.D. Self-assembled nanoparticles based on hyaluronic acid-ceramide (HA-CE) and Pluronic® for tumor-targeted delivery of docetaxel. Biomaterials. 2011; 32(29), 7181-90.

Cho H.J., Yoon I., Yoon H.Y., Koo H., Jin Y., Ko S., Shim J., Kim K., Kwon I.C., Kim D. Polyethylene glycol-conjugated hyaluronic acid-ceramide self-assembled nanoparticles for targeted delivery of doxorubicin. Biomaterials. 2012; 33(4), 1190-1200.

Choi K.Y., Min K.H., Na J.H., Choi K., Ki K. Park J.H., Kwon, I.C., Jeong S.Y. Self-assembled hyaluronic acid nanoparticles as a potential drug carrier for cancer therapy: synthesis, characterization, and in vivo biodistribution. J Mater Chem. 2009; 19, 4102–4107.

Choi K.Y., Chung H., Min K.H., Yoon H.Y., Kim K., ParkJ .H., Kwon I.C., Jeong S.Y. Self-assembled hyaluronic acid nanoparticles for active tumor targeting. Biomaterials. 2010; 31(1), 106–114.

Choi K.Y., Min K.H., Yoon H.Y:, Kim K., Park J.H., Kwon I.C:, Choi K., Jeong S.Y. PEGylation of hyaluronic acid nanoparticles improves tumor targetability in vivo. Biomaterials. 2011; 32(7), 1880-1889.

Coradini D., Zorzet S., Rossin R., Scarlata I., Pellizzaro C., Turrin C., Bello M., Cantoni S., Speranza A., Sava G., Mazzi U., Perbellini A. Inhibition of hepatocellular carcinomas in vitro and hepatic metastases in vivo in mice by the histone deacetylase inhibitor HA-But. Clin Cancer Res. 2004; 10(14), 4822–4830.

Davis M.E., Chen Z., Shin D.M. Nanoparticle therapeutics: an emerging treatment modality for cancer. Nat Rev Drug Discovery. 2008; 7, 771-782.

de Gennaro B., Catalanotti L., Cappelletti P., Langella A., Mercurio M., Serri C., Biondi M., Mayol L. Surface modified natural zeolite as a carrier for sustained diclofenac release: A preliminary feasibility study. Colloids Surf B - Biointerfaces. 2015; 130, 101-109.

De Jong W.H., Borm P.J. Drug delivery and nanoparticles: applications and hazards. Int J Nanomed. 2008; 3(2):133–149.

Dilnawaz F., Singh A., Sahoo S.K. Transferrin-conjugated curcumin-loaded superparamagnetic iron oxide nanoparticles induce augmented cellular uptake and apoptosis in K562 cells. Acta Biomater. 2012; 8, 704–719.

Ding H., Wang X.J., Zhang S., & Liu, X. L. Applications of polymeric micelles with tumor targeted in chemotherapy. J Nanoparticle Res. 2012; 14, 1254-1.

Doty A.C., Zhang Y., Weinstein D.G, Wang Y., Choi S., Qu W., Mittal S., Schwendeman SP. Mechanistic analysis of triamcinolone acetonide release from PLGA 5 microspheres as a function of varying in vitro release conditions. Eur J Pharm Biopharm. 2016. S0939-6411(16), 30387-3.

Dreaden E.C., Morton, S.W., Shopsowitz K.E., Choi J.H., Deng Z.J., Cho N.J. Hammond P.T.. Bimodal tumor-targeting from microenvironment responsive hyaluronan layer-by-layer (LbL) nanoparticles. ACS Nano. 2014; (8), 8374-8382.

Duncan R. The dawning era of polymer therapeutics. Nat Rev Drug Discovery. 2003; 2, 347-360.

Duncan R. Polymer conjugates as anticancer nanomedicines. Nat Rev Cancer. 2006; 6, 688–701.

Ehdaie B. Application of Nanotechnology in Cancer Research: Review of Progress in the National Cancer Institute's Alliance for Nanotechnology. Int J Biol Sci. 2007; 3(2): 108–110.

Eliaz R.E., Szoka F.C.J. Liposome-encapsulated doxorubicin targeted to CD44: a strategy to kill CD44-overexpressing tumor cells. Cancer Res. 2001; 61(6), 2592–2601.

Eliaz R.E., Nir S., Marty C., Szoka F.C.J. Determination and modeling of kinetics of cancer cell killing by doxorubicin and doxorubicin encapsulated in targeted liposomes. Cancer Res.2004; 64, 711–718.

Entwistle J., Hall C.L., Turley E.A. HA receptors: regulators of signaling to the cytoskeleton. J Cell Biochem. 1996; 61(4), 569 –577.

Estlin E.J., Veal G.J. Clinical and cellular pharmacology in relation to solidtumours of childhood. Cancer Treat Rev. 2003; 29(4), 253-73.

Falconieri M.C., Adamo M., Monasterolo C., Bergonzi M.C., Coronnello M., Bilia A.R. New dendrimer based nanoparticles enhance curcumin solubility. Planta Med. 2016 in press.

Fang J.G.; Lu J.; Holmgren A. Thioredoxin reductase is irreversibly modified by curcumin - A novel molecular mechanism for its anticancer activity. J Biol Chem. 2005; 280 (26), 25284-25290.

Fang J.; Nakamura H.; Maeda H. The EPR effect: Unique features of tumor blood vessels for drug delivery, factors involved, and limitations and augmentation of the effect. Adv Drug Deliv Rev. 2011; 63 (3), 136-151.

Farokhzad O.C., Jon S., Khademhosseini A., Tran T.N., Lavan D.A., Langer R. Nanoparticle-aptamer bioconjugates: a new approach for targeting prostate cancer cells. Cancer Res. 2004; 64(21), 7668–7672.

Farokhzad O.C., Cheng J., Teply B.A., Sherifi I., Jon S., Kantoff P.W., Richie J.P., Langer R. Targeted nanoparticle-aptamer bioconjugates for cancer chemotherapy in vivo. Proc Natl Acad Sci. 2006; 103(16), 6315–6320.

Farokhzad O.C. Nanotechnology for drug delivery: the perfect partnership. Expert Opinion on Drug Delivery. 2008; 5 (9), 927-929.

Ferrari M. Cancer nanotechnology: opportunities and challenges. Nat Rev Cancer. 2005; 5, 161-171.

Ferrari M. Nanogeometry: Beyond drug delivery. Nat Nanotechnol. 2008; 3, 131–132.

Ferreira V.H, Nazli A., Dizzell S.E., Mueller K., Kaushic C. The antiinflammatory activity of curcumin protects the genital mucosal epithelial barrier from disruption and blocks replication of HIV-1 and HSV-2. Plos One 2015; 10 (4),0124903.

Feynman R.P. There's plenty of room at the bottom. Engineering and Science. 1960; 23 (5), 22-36.

Forte M., Iachetta G., Tussellino M., Carotenuto R., Prisco M., De ,F.M., Laforgia,V., Valiante,S. Polystyrene nanoparticles internalization in human gastric adenocarcinoma cells. Toxicol In Vitro. 2016; 31, 126-136.

Freitas R.A. Current status of nano medicine and medical nanorobotics. Comput Theor Nanosci. 2005; 2, 1-25.

FDA. ‘‘Poloxamer 407’’. U.S. Food and Drug Administration, 2013.

Fusco S., Borzacchiello A., Miccio L., Pesce G., Rusciano G., Sasso A., Netti P.A. High frequency viscoelastic behaviour of low molecular weight hyaluronic acid water solutions. Biorheology. 2007; 44(5-6), 403-418.

Gao Y., Chen L., Gu W., Xi Y., Lin L., Li Y. Targeted nanoassembly loaded with docetaxel improves intracellular drug delivery and efficacy in murine breast cancer model. Mol Pharmacol. 2008; 5(6), 1044-1054.

Gandapu U., Chaitanya R.K., Kishore G., Reddy R.C., Kondapi A.K. Curcumin-loaded apotransferrin nanoparticles provide efficient cellular uptake and effectively inhibit HIV-1 replication in vitro. PLoS One. 2011; 6, e23388.

Garcia-Carbonero R., Supko J.G. Current perspectives on the clinical experience, pharmacology, and continued development of the camptothecins. Clin Cancer Res. 2002; 8(3), 641-61.

Goel A., Kunnumakkara A.B., Aggarwal B.B. Curcumin as Curecumin: from kitchen to clinic. Biochem Pharmacol. 2008; 75(4):787-809.

Gonçalves C., Pereira P., Schellenberg P., Coutinho P.J., Gama F.M., Self-assembled dextrin nanogel as curcumin delivery system. J Biomater Nanobiotechnol. 2012; 3, 178–184.

Gotte M., Yip G.W. Heparanase, hyaluronan, and cd44 in cancers: a breast carcinoma perspective. Cancer Res. 2006; 66, 10233–10237.

Gullotti E., Yeo Y. Extracellularly activated nanocarriers: a new paradigm of tumor targeted drug delivery. Mol Pharm. 2009; 6, 1041-51.

Gupta E., Mick R., Ramirez J., Wang X., Lestingi T. M., Vokes E. E. and Ratain M. J. Pharmacokinetic and pharmacodynamic evaluation of the topoisomerase inhibitor irinotecan in cancer patients. J Clin Oncol. 1997; 15(4), 1502–1510.

Hardman J.G., Limbird L.E., Goodman G.A. The pharmacological basis of therapeutics. 10th edition McGraw Hill, 2001.

Hasan S.T., Zingg J.M., Kwan P., Noble T., Smith D., Meydani M. Curcumin modulation of high fat diet-induced atherosclerosis and steatohepatosis in LDL receptor deficient mice. Atherosclerosis. 2014; 23, 240–51.

Hashizume H., Baluk P., Morikawa S., McLean J.W., Thurston G., Roberge S., Jain R.K., McDonald D.M. Openings between defective endothelial cells explain tumor vessel leakiness. Am J Pathol. 2000; 156(4), 1363-1380.

Hatcher H.; Planalp, R.; Cho J.,Tortia F.M.; Torti S.V. Curcumin: From ancient medicine to current clinical trials. Cell Molec Life Sci. 2008; 65 (11), 1631-1652.

He Q., Gao Y., Zhang L., Zhang Z., Gao F., Ji X., Li Y., Shi J. A pH-responsive mesoporous silica nanoparticles-based multi-drug delivery system for overcoming multi-drug resistance. Biomaterials. 2011; 32(30), 7711-20.

Huang S., Shao K., Liu Y., Kuang Y., Li J., An S., Guo Y., Ma H., Jiang C. Tumor-targeting and microenvironment-responsive smart nanoparticles for combination therapy of antiangiogenesis and apoptosis. ACS Nano. 2013; 7, 2860-2871.

Huang J., Zhang H., Yu,Y., Chen Y., Wang D., Zhang G, Zhou G., Liu J., Sun Z., Sun D., Lu Y., Zhong Y. Biodegradable self-assembled nanoparticles of poly (D,L-lactide-co-glycolide)/hyaluronic acid block copolymers for target delivery of docetaxel to breast cancer. Biomaterials. 2014; 35, 550-566.

Isacke C.M., Yarwood H. The hyaluronan receptor, CD44. Int J Biochem Cell Biol. 2002; 34(7), 718-721.

Jain R.A. The manufacturing techniques of various drug loaded biodegradable poly(lactide-co-glycolide) (PLGA) devices. Biomaterials. 2000; 21, 2475-2490.

Jaracz S., Chen J., Kuznetsova L.V., Ojima I. Recent advances in tumor-targeting anticancer drug conjugates. Bioorg Med Chem. 2005; 13(17), 5043–5054.

Jee J.P., Na J.H., Lee S., Kim S.H., Choi K., Yeo Y., Kwon I.C. Cancer targeting strategies in nanomedicine: Design and application of chitosan nanoparticles. Curr Opin Solid State Mater Sci. 2012; 16, 333–342.

Jiang H., Wang Z., Wang Y., Xie K., Zhang Q., Luan Q., Chen W., Liu D., Antidepressant-like effects of curcumin in chronic mild stress of rats: involvement of its anti-inflammatory action. Prog Neuro-Psychopharmacol Biol Psychiatry. 2013; 47, 33–39.

Jurenka J.S, MT(ASCP): Anti-inflammatory properties of curcumin, a major constituent of *Curcuma longa*: a review of preclinical and clinical research. Altern Med Rev. 2009; 14 (2), 141-53.

Kasi P.D., Tamilselvam R., Skalicka-Woźniak K., Nabavi S.F., Daglia M., Bishayee A.,Pazoki-Toroudi H., Nabavi S.M.. Molecular targets of curcumin for cancer therapy: an updated review. Tumour Biol. 2016; 37(10), 13017-13028.

Kehrer D.F., Sparreboom A., Verweij J., de Bruijn P., Nierop C.A., van de Schraaf J., Ruijgrok E.J., de Jonge M.J. Modulation of irinotecan-induced diarrhea by cotreatment with neomycin in cancer patients. Clin Cancer Res. 2001; 7, 1136–1141.

Kerdsakundee N., Mahattanadul S., Wiwattanapatapee R., Development and evaluation of gastroretentive raft forming systems incorporating curcuminEudragit(R) EPO solid dispersions for gastric ulcer treatment. Eur J Pharm Biopharm. 2015, 94:513-20.

Kiuchi F., Goto Y., Sugimoto N., Akao N., Kondo K., Tsuda Y. Nematocidal activity of turmeric: synergistic action of curcuminoids. Chem Pharm Bull. 1993; (41), 1640–1643.

Ko A.H. Nanomedicine developments in the treatment of metastatic pancreatic cancer: focus on nanoliposomal irinotecan. Int J Nanomedicine. 2016; 11:1225-35.

Kochi A., Lee H.J., Vithanarachchi S.M., Padmini V., Allen M.J., Lim M.H. Inhibitory activity of curcumin derivatives towards metal-free and metal-induced amyloidbeta aggregation. Curr Alzheimer Res. 2015 (12) 415–423.

Kogan G., Šoltés L., Stern R., Gemeiner P. Hyaluronic acid: a natural biopolymer with a broad range of biomedical and industrial applications. Biotechnol Lett. 2007; 29, 17-25.

Lampe V., Milobedeska J.. Studien über curcumin. Ber Dtsch Chem Ges 1913; 46, 2235–2240.

Lao C.D., Ruffin M.T., Normolle D., Heath D.D., MurrayS.I., Bailey J.M., Boggs M.E., Crowell J., Rock C.L., Brenner D.E. Dose escalation of a curcuminoid formulation. BMC Complement Altern Med. 2006; 6, 10.

Lavergne O., Lesueur-Ginot L., Pla Rodas F., Kasprzyk P.G., Pommier J., Demarquay D.,Prévost G., Ulibarri G., Rolland A., Schiano-Liberatore A.M., Harnett J., Pons D.,Camara J., Bigg D.C. Homocamptothecins: synthesis and antitumor activity of novel E-ring-modified camptothecin analogues. J Med Chem. 1998, 41, 5410-5419.

Lee R.J., Low P.S. Delivery of liposomes into cultured KB cells via folate receptor mediated endocytosis. J Biol Chem. 1994; 269(5), 3198–3204.

Lee H., Mok H., Lee S., Oh Y.K., Park T.G. Target-specific intracellular delivery of siRNA using degradable hyaluronic acid nanogels. J Controlled Release. 2007; 119(2), 245-252.

Lee H., Lee K., Park T.G. Hyaluronic acid-paclitaxel conjugate micelles: synthesis, characterization, and antitumor activity. Bioconjug Chem. 2008; 19(6), 1319–1325.

Lee H., Ahn C., Park T.G. Poly[lactic-co-(glycolic acid)]-grafted hyaluronic acid copolymer micelle nanoparticles for target-specific delivery of doxorubicin. Macromol Biosci. 2009; 9(4), 336–342.

Li Y., Kong D., Bao B., Ahmad A., Sarkar F.H. Induction of cancer cell death by isoflavone: the role of multiple signaling pathways. Nutrients. 2011; 3, 877-896.

Li X., Zhen D., Lu X., Xu H., Shao Y., Xue Q., Hu Y., Liu B., Sun W. Enhanced cytotoxicity and activation of ROS-dependent c-Jun NH2-terminal kinase and caspase-3 by low doses of tetrandrine-loaded nanoparticles in Lovo cells--a possible Trojan strategy against cancer. Eur J Pharm Biopharm. 2010; 75 (3), 334-340.

Limtrakul P., Chearwae W., Shukla S. Phisalphong, C., Ambudkar S.V. Modulation of function of three ABC drug transporters, P-glycoprotein (ABCB1), mitoxantrone resistance protein (ABCG2) and multidrug resistance protein 1 (ABCC1) by tetrahydrocurcumin, a major metabolite of curcumin. Mol Cell Biochem. 2007; 296 (1-2), 85-95.

López-Miranda E., Cortés J. Etirinotecan pegol for the treatment of breast cancer. Expert Opin Pharmacother. 2016;17(5),727-34.

Lu Y., Low P.S. Folate-mediated delivery of macromolecular anticancer therapeutic agents. Adv Drug Deliv Rev. 2002; 54(5), 675–693.

Luo Y., Prestwich G.D. Synthesis and selective cytotoxicity of a hyaluronic acid-antitumor bioconjugate. Bioconjug Chem. 1999; 10(5), 755–763.

Luo Y., Bernshaw N.J., Lu Z.R., Kopecek J., Prestwich G.D. Targeted delivery of doxorubicin by HPMA copolymer-hyaluronan bioconjugates. Pharm Res. 2002; 19(4), 396–402.

Lukyanov A.N., Elbayoumi T.A., Chakilam A.R., Torchilin V.P. Tumor-targeted liposomes: doxorubicin-loaded long-circulating liposomes modified with anticancer antibody. J Controlled Release. 2004; 100(1), 135–44.

Lv H., Liu J., Wang L., Zhang H., Yu S., Li Z., Jiang F., Niu Y., Yuan J., Cui X., Wang W. Ameliorating effects of combined curcumin and desferrioxamine on 6-OHDA-induced rat mode of Parkinson's disease. Cell Biochem Biophys. 2014; (70), 1433–1438.

Maeda H., Wu J., Sawa T., Hori K. Tumor vascular permeability and the EPR effect in macromolecular therapeutics. J Controlled Release. 2000; 65(1-2), 271-284.

Mahajanakatti A.B., Murthy G., Sharma N., Skariyachan S.. Exploring inhibitory potential of curcumin against various cancer targets by in silico virtual screening. Interdiscip Sci. 2014; 6(1),13-24.

Mainardes R.M., Gremiao M.P., Brunetti I.L., da Fonseca L.M., Khalil N.M. Zidovudine-loaded PLA and PLA-PEG blend nanoparticles: influence of polymer type on phagocytic uptake by polymorphonuclear cells. J Pharm Sci. 2009; 98 (1), 257-267.

Malam Y., Loizidou M., Seifalian A.M. Liposomes and nanoparticles: nanosized vehicles for drug delivery in cancer. Tr Pharmacol Sci. 2009; 30 (11), 592-599.

Martin R.C.G., Locatelli E., Li Y., Zhang W.Z., Li S.P., Monaco, I., Franchini M.C. Gold nanorods and curcumin-loaded nanomicelles for efficient in vivo photothermal therapy of Barrett's esophagus. Nanomedicine. 2015; 10 (11), 1723-1733.

Masson M., Loftsson T., Jonsdottir S., Fridriksdottir H., Petersen D.S. Stabilisation of ionic drugs through complexation with non-ionic and ionic cyclodextrins. Int J Pharm. 1998; 164, 45-55.

Mayol L., Biondi M., Quaglia F., Fusco S., Borzacchiello A., Ambrosio L., La Rotonda M.I. Injectable thermally responsive mucoadhesive gel for sustained protein delivery. Biomacromolecules. 2011; 12 (1), 28-33.

Mayol L., Serri C., Menale C., Crispi S., Piccolo M.T., Mita L., Giarra S., Forte M, Saija A, Biondi M. Mita D.G.. Curcumin loaded PLGA–poloxamer blend nanoparticles induce cell cycle arrest in mesothelioma cells. Eur J Pharm Biopharm. 2015; 93, 37–45.

Mehanny M., Hathout R.M., Geneidi A.S., Mansour S. Exploring the use of nanocarrier systems to deliver the magical molecule; curcumin and its derivatives. J Controlled Release. 2016; 225, 1-30.

Meyer K., Palmer J. The polysaccharide of the vitreous humor. J Biol Chem. 1934; 107, 629-634.

Mikami K., Haseba T., Ohno Y. Ethanol induces transient arrest of cell division (G(2)+M block) followed by G(0)/G(1) block: Dose effects of short- and longer-term ethanol exposure on cell cycle and cell functions. Alcohol and Alcoholism. 1997; 32 (2), 145-152.

Miller J.M., Thompson J.K., MacPherson M.B., Beuschel S.L., Westbom C.M., Sayan M., Shukla A. Curcumin: a double hit on malignant mesothelioma. Cancer Prev Res (Phila). 2014; 7(3), 330-340.

Milobedeska J., Kostanecki V., Lampe V. Structure of curcumin. Ber Dtsch Chem Ges. 1910, 43, 2163–2170.

Minko T. Drug targeting to the colon with lectins and neoglycoconjugates. Adv Drug Deliv Rev. 2004; 56 (4), 491–509.

Mironov V., Kasyanov V., Zheng Shu X., Eisenberg C., Eisenberg L., Gonda S., Trusk T., Markwald R.R., Prestwich G.D. Fabrication of tubular tissue constructs by centrifugal casting of cells suspended in an in situ crosslinkable hyaluronan-gelatin hydrogel. Biomaterials. 2005; 26 (36), 7628–7635.

Moghimi S.M., Szebeni J. Stealth liposomes and long circulating nanoparticles: critical issues in pharmacokinetics, opsonization and protein-binding properties. Progr Lipid Res. 2003; 42 (6), 463-478.

Mohanraj V.J., Chen Y. Nanoparticles – A Review. Trop J Pharm Res. 2006; 5 (1), 561-573.

Mondalek F.G., Ashley R.A:, Roth C.C., KibarY., Shakir N. Ihnat, M.A., Fung, K., Grady, B.P., Kropp, B.P., Lin, H. Enhanced angiogenesis of modified porcine small intestinal submucosa with hyaluronic acid-poly(lactide-co-glycolide) nanoparticles: from fabrication to preclinical validation. J Biomed Mater Res. 2010; 94A, 712-719.

Monheit G.D. Coleman K.M. Hyaluronic acid fillers. Dermatologic Therapy. 2006; 19(3), 141–150.

Mori M., Yamaguchi M., Sumitomo S., Takai Y. Hyaluronic-based biomaterials in tissue engineering. Acta Histochem Cytochem. 2004; 37(1), 1-5.

Morton C.L., Wadkins R.M., Danks M.K., Potter P.M. The anticancer prodrug CPT-11 is a potent inhibitor of acetylcholinesterase but is rapidly catalyzed to SN-38 by butyrylcholinesterase. Cancer Res. 1999; 59, 1458–1463.

Mulik R.S., Mönkkönen J., Juvonen R.O., Mahadik K.R., Paradkar A.R. Transferrin mediated solid lipid nanoparticles containing curcumin: enhanced in vitro anticancer activity by induction of apoptosis. Int J Pharm. 2010; 398, 190–203.

Nishiyama N. Nanomedicine: nanocarriers shape up for long life. Nat Nanotechnol. 2007; 2(4), 203–204.

Noble P.W. Hyaluronan and its catabolic products in tissue injury and repair. Matrix Biology. 2002; 21(1), 25–29.

Owens D.E. 3rd, Peppas N.A. Opsonization, biodistribution, and pharmacokinetics of polymeric nanoparticles. Int J Pharm. 2006; 307 (1), 93-102.

Pan M.H., Huang T.M., Lin J.K. Biotransformation of curcumin through reduction and glucuronidation in mice. Drug Metab Dispos. 1999; 27 (4), 486-494.

Parajo Y., d'Angelo I., Horvath A., Vantus T., Gyorgy K., Welle A., Garcia-Fuentes M.; Alonso M.J. PLGA:poloxamer blend micro- and nanoparticles as controlled release systems for synthetic proangiogenic factors. Eur J Pharm Sci. 2010, 41 (5), 644-649.

Park J.W., Kirpotin D.B., Hong K., Shalaby R., Shao Y., Nielsen U.B., Marks J.D., Papahadjopoulos D., Benz C.C. Tumor targeting using anti-her2 immunoliposomes. J Controlled Release. 2001; 74(1- 3), 95–113.

Pari L., Tewas D., Eckel J., Role of curcumin in health and disease. Arch Physiol Biochem. 2008 ; (114), 127–149.

Peer D., Margalit R. Loading mitomycin C inside long circulating hyaluronan targeted nano-liposomes increases its antitumor activity in three mice tumor models. Int J Cancer. 2004; 108(5), 780–789.

Peer D., Karp J.M., Hong S., Farokhzad O.C., Margalit R., Langer R. Nanocarriers as an emerging platform for cancer therapy. Nature Nanotechnology. 2007; 2, 751-760.

Peresa C., Matosa A.I., Conniota J., Sainza , Zupančiča E., Silvaa J.M., Graçac L., SáGaspara R., Préatb V., Helena, Florindoa F. Poly(lactic acid)-based particulate systems are promising tools for immune modulation. Acta Biomater. 2016; in press.

Prakash P., Misra A., Surin WR., Jain M., Bhatta RS, Pal R., Raj K., Barthwal M.K., Dikshit M. Anti-platelet effects of curcuma oil in experimental models of myocardial ischemia–reperfusion and thrombosis, Thromb Res. 2011; (127), 111–118.

Poudel B.K., Gupta B., Ramasamy T., Thapa R.K., Youn Y.S., Choi H.G., Yong C.S., Kim J.O. Development of polymeric irinotecan nanoparticles using a novel lactone preservation strategy. Int J Pharm. 2016; 512, 75–86.

Pouyani T., Prestwich G.D. Functionalized derivatives of hyaluronic acid oligosaccharides: drug carriers and novel biomaterials. Bioconjugate Chem. 2007; 5(4), 339-347.

Qian Z.M., Li H., Sun H., Ho K. Targeted drug delivery via the transferrin receptor mediated endocytosis pathway. Pharmacol Rev. 2002; 54(4), 561–587.

Ranall M.V., Gabrielli B.G., Gonda T.J. High-content imaging of neutral lipid droplets with 1,6-diphenylhexatriene. Biotechniques. 2011; 51 (1), 35-42.

Rao W., Zhang W., Poventud-Fuentes I., Wang Y, Lei Y, Agarwal P., Weekes B., Li C., Lu X., Yu J., He X. Thermally responsive nanoparticle-encapsulated curcumin and its combination with mild hyperthermia for enhanced cancer cell destruction. Acta Biomater. 2014; (10), 831–842.

Robbins. Basic Pathology, 8ª edition, Saunders/Elsevier 2007, chapter 6.

Rosen H., Abribat T. The rise and rise of drug delivery. Nat Rev Drug Discov. 2005, 4 (5), 381-385.

Ross J.S., Schenkein D.P., Pietrusko R., Rolfe M., Linette G., Stec J., Stagliano N.E., Ginsburg G.S., Symmans W.F., Pusztai L., Hortobagyi G.N. Targeted therapies for cancer. Am J Clin Pathol. 2004; 122, 598- 609.

Sa G., Das T. Anti cancer effects of curcumin: cycle of life and death. Cell Division. 2008; 3, 14.

Sahin K., Pala R., Tuzcu M., Ozdemir O., Orhan C., Sahin N., Juturu V. Curcumin prevents muscle damage by regulating NF-κB and Nrf2 pathways and improves performance: an in vivo model. J Inflam Res. 2016; 9, 147–154.

Sahoo S.K., Labhasetwar V. Enhanced antiproliferative activity of transferring conjugated paclitaxel-loaded nanoparticles is mediated via sustained intracellular drug retention. Mol Pharm. 2005; 2(5), 373–383.

Saltz L.B., The role of irinotecan in colorectal cancer. Curr Oncol Rep. 1999; 1, 155–160.

Santander-Ortega M.J., Jódar-Reyes A.B., Csaba N., Bastos-Gonzáleza D., Ortega-Vinuesa J.L.. Colloidal stability of Pluronic F68-coated PLGA nanoparticles: a variety of stabilisation mechanisms. J Colloid Interface Sci. 2006; 302 (2), 522–529.

Sapra P., Allen T.M. Internalizing antibodies are necessary for improved therapeutic efficacy of antibody-targeted liposomal drugs. Cancer Res. 2002; 62(24), 7190–7194.

Sarkar A, De R, Mukhopadhyay AK. Curcumin as a potential therapeutic candidate for *Helicobacter pylori* associated diseases. World J Gastroenterol. 2016; 22(9), 2736-2748.

Sawant V.J., Bamane S.R., Patil S.B. PEG-cyclodextrin coated curcumin loaded zinc ferrite core nanocomposites as pH-responsive drug delivery system for antiinflammation and anticancer application. Arch Appl Sci Res. 2014; 6, 44–54.

Schledzewski K., Falkowski M., Moldenhauer G., Metharom P., Kzhyshkowska J., Ganss R.,. Demory A., Falkowska-Hansen B., Kurzen H., Ugurel S., Geginat G., Arnold B., Goerdt S. Lymphatic endothelium-specific

hyaluronan receptor LYVE- 1 is expressed by stabilin-1+, F4/80+, CD11b+ macrophages in malign ant tumors and wound healing tissue in vivo and in bone marrow cultures in vitro: implications for the assessment of lymphangiogenesis. J Pathol. 2006; 209(1), 67–77.

Shah B.H, Nawaz Z., Pertani S.A., Roomi A., Mahmood H., Saeed S.A., Gilani A.H. Inhibitory effect of curcumin, a food spice from turmeric, on platelet-activating factor- and arachidonic acid-mediated platelet aggregation through inhibition of thromboxane formation and Ca2+ signaling. Biochem Pharmacol. 1999 (58) 1167–1172.

Shaikh J., Ankola D.D., Beniwal V., Singh D., Kumar M.N. Nanoparticle encapsulation improves oral bioavailability of curcumin by at least 9-fold when compared to curcumin administered with piperine as absorption enhancer. Eur J Pharm Sci. 2009; 37 (3-4), 223-230.

Shanmugam M.K., Rane G., Kanchi M.M., Arfuso F., Chinnathambi A., Zayed M.E., Alharbi S.A., Tan B.K., Kumar A.P., Sethi G. The multifaceted role of curcumin in cancer prevention and treatment. Molecules. 2015; 20(2), 2728-69.

Shen H., Hu X., Szymusiak M., Wang Z.J. Liu Y. Orally administered nanocurcumin to attenuate morphine tolerance: comparison between negatively charged PLGA and partially and fully PEGylated nanoparticles. Mol Pharm. 2013; 10 (12), 4546-4551.

Shishodia S., Amin H.M., Lai R., Aggarwal B.B. Curcumin (diferuloylmethane) inhibits constitutive NF-kappaB activation, induces G1/S arrest, suppresses proliferation, and induces apoptosis in mantle cell lymphoma. Biochem Pharmacol. 2005; 70 (5), 700-713.

Shome S., Talukdar A.D., Choudhury M.D., Bhattacharya M.K., Upadhyaya H. Curcumin as potential therapeutic natural product: a nanobiotechnological perspective. J Pharm Pharmacol. 2016; 68(12), 1481-1500.

Some S., Gwon A.R., Hwang E., Bahn G.H., Yoon Y., Kim Y., Kim S.H., Bak S., Yang J., Jo D.G., Lee H. Cancer therapy using ultrahigh hydrophobic drug-loaded graphene derivatives. Sci Rep. 2014; 4, 6314.

Srivastava R., Dikshit M., Srimal R.C., Dhawan B.N., Anti-thrombotic effect of curcumin. Thromb Res. 1985; (40), 413–417.

Stacy K.M. Therapeutics MAbs: saving lives and making billions. The Scientist. 2005; 19(3), 17–19.

Subhashini, Chauhan P.S., Kumari S., Kumar J.P., Chawla R., Dash D., Singh M., Singh, R. Intranasal curcumin and its evaluation in murine model of asthma. Int Immunopharmacol. 2013; 17(3), 733-743.

Takei Y., Maruyama A., Ferdous A., Nishimura Y., Kawano S., Ikejima K., Okumura S., Asayama S., Nogawa M., Hashimoto M., Makino Y., Kinoshita M., Watanabe S., Akaike T., Lemasters J.J., Sato N. Targeted gene delivery

to sinusoidal endothelial cells: DNA nanoassociate bearing hyaluronan–glycocalyx. FASEB J. 2004; 18(6), 699–701.

Tang N., Du G., Wang N., Liu C., Hang H., Liang W. Improving penetration in tumors with nanoassemblies of phospholipids and doxorubicin. J. Natl Cancer Inst. 2007; 99(13), 1004-1015.

Toole B.P., Wight T.N., Tammi M.I. Hyaluronan-cell interactions in cancer and vascular disease. J Biol Chem. 2002; 277, 4593–4596.

Toole B.P. Hyaluronan: from extracellular glue to pericellular cue. Nat Rev Cancer. 2004; 4, 528–539.

Torchilin V.P. Multifunctional nanocarriers. Adv Drug Deliv Rev. 2006; 58(14), 1532–1555.

Torchilin V.P. Targeted pharmaceutical nanocarriers for cancer therapy and imaging. The AAPS Journal. 2007; 11, 9(2), E128-47.

Tsai Y.M., Chien C.F., Lin L.C., Tsai T.H. Curcumin and its nano-formulation: the kinetics of tissue distribution and blood-brain barrier penetration. Int J Pharm. 2011; 416(1), 331-338.

Ur Rehman S.S., Lim K., Wang-Gillam A. Nanoliposomal irinotecan plus fluorouracil and folinic acid: a new treatment option in metastatic pancreatic cancer. Expert Rev Anticancer Ther. 2016;16(5), 485-92.

Ventura C.A., Puglisi G., Zappala M., Mazzone G.A. physico-chemical study on the interaction between papaverine and natural and modified beta-cyclodextrins. Int J Pharm. 1998; 160(2), 163-172.

Vergara D., Bellomo C., Zhang X., Vergaro V., Tinelli A., Lorusso V., Rinaldi R., Lvov Y.M., Leporatti S. Maffia M. Lapatinib/Paclitaxel polyelectrolyte nanocapsules for overcoming multidrug resistance in ovarian cancer. Nanomedicine. 2012; 8(6), 891-899.

Vogel H.A., Pelletier J. Curcumin-biological and medicinal properties. J Pharmacol. 1815, 2, p. 50.

Wang J., Mongayt D., Torchilin V.P. Polymeric micelles for delivery of poorly soluble drugs: Preparation and anticancer activity in vitro of paclitaxel incorporated into mixed micelles based on poly(ethylene glycol)-lipid conjugate and positively charged lipids. J Drug Targeting. 2005; 13(1), 73-80.

Wang Y., Rishi A.K., Wu W., Polin L., Sharma S., Levi E., Albelda S., Pass H.I., Wali A. Curcumin suppresses growth of mesothelioma cells in vitro and in vivo, in part, by stimulating apoptosis. Mol Cell Biochem. 2011; 357(1-2), 83-94.

Wang A.W., Langer R., Farokhzad O.C. Nanoparticle delivery of cancer Drugs. Ann Rev Med. 2012; 63, 185-198.

Weissman B., Meyer K. The structure of hyalobiuronic acid and of hyaluronic acid from umbilical cord. J Am Chem Soc. 1954; 76(7), 1753-1757.

Whatmore R.W. Nanotechnology - what is it? Should we be worried? Occup Med. 2006; 56(5), 295–299.

Willis R.A. The Spread of Tumors in the Human Body, London, Butterworth. 1952.

World Health Organization; World Cancer Report. 2014.

World Health Organization. (2015). Cancer. Fact sheet N°297 Updated February. 2015.

Xiao L., Xiong X.Q., Sun X.H., Zhu Y.H., Yang H., Chen H.B., Gan L., Xu H.B., Yang X.L. Role of cellular uptake in the reversal of multidrug resistance by PEG-b-PLA polymeric micelles. Biomaterials. 2011; 32, 5148-5157.

Xu Y., Villalona-Calero M.A. Irinotecan: mechanisms of tumor resistance and novel strategies for modulating its activity. Ann Oncol. 2002; (13), 1841-1851.

Xuejun X., Borzacchiello A., Netti P.A., Ambrosio L., Nicolais L. Hyaluronic Acid Based Semi Interpenetrating Materials. J Biomater Sci Polymer Edn, 2004; 15(9), 1223-1236.

Yadav A.K., Mishra P., Mishra A.K., Mishra P., Jain S., Agrawal G.P. Development and characterization of hyaluronic acid–anchored PLGA nanoparticulate carriers of doxorubicin. Nanomedicine: Nanotechnology, Biology, and Medicine. 2007; 3(4), 246–257.

Yadav A.K., Agarwal A., Rai G., Mishra P., Jain S., Mishra A.K., Agrawal H., Agrawal G.P. Development and characterization of hyaluronic acid decorated PLGA nanoparticles for delivery of 5-fluorouracil. Drug Delivery. 2010a; 17 (8), 561–572.

Yadav V.R., Prasad S.; Kannappan R., Ravindran J., Chaturvedi M.M., Vaahtera L., Parkkinen J., Aggarwal B.B. Cyclodextrin-complexed curcumin exhibits anti-inflammatory and antiproliferative activities superior to those of curcumin through higher cellular uptake. Biochem Pharmacol. 2010b; 80 (7), 1021-1032.

Yadav S.K., Sah A.K., Jha R.K., Sah P., Shah D.K., Turmeric (curcumin) remedies gastroprotective action, Pharmacogn Rev. 2013; 7, 42–46.

Yallapu M.M., Jaggi M., Chauhan S.C. beta-Cyclodextrin-curcumin self-assembly enhances curcumin delivery in prostate cancer cells. Colloids Surf B Biointerfaces. 2010; 79(1), 113-125.

Yallapu M.M., Ebeling M.C., Khan S., Sundram V., Chauhan N., Gupta B.K., Puumala S.E., Jaggi M., Chauhan S.C. Novel curcumin loaded

magnetic nanoparticles for pancreatic cancer treatment. Mol Cancer Ther. 2013; 12, 1471–1480.

Yallapu M.M., Nagesh P.K., Jaggi M., Chauhan S.C. Therapeutic Applications of Curcumin Nanoformulations. AAPS J. 2015;17 (6):1341-56.

Yamauchi Y., Izumi Y., Asakura K., Hayashi Y., Nomori H. Curcumin induces autophagy in ACC-MESO-1 cells. Phytother Res. 2012; 26(12), 1779-83.

Yoo J. W., Mitragotri S. Polymer particles that switch shape in response to a stimulus. Proc Natl Acad Sci USA. 2010; 107, 11205-11210.

Zhang X., Yang X., Ji J., Liu A., Zhai G. Tumor targeting strategies for chitosan-based nanoparticles. Colloids Surf B Biointerfaces. 2016, 148, 460–473.

Acknowledgements

To achieve the PhD degree at the University of Messina has been a truly life-changing experience for me and it would not have been possible to do without the support and guidance that I received from many people.

I would like to thank my PhD Tutor, Prof. Antonella Saija, and the components of her team, especially Dr. Francesco Cimino, Dr. Mariateresa Cristani and Dr. Antonio Speciale, from the University of Messina, and my co-tutor Dr. Marco Biondi and his collegues, Dr. Laura Mayol and Prof. Giuseppe De Rosa, from the University of naples Federico II, for their continous support during these three years.

My special thanks also to Prof. Arto Urtti and Prof. Marika Rupponen for having invited me to work for 6 months in their research group at the School of Pharmacy, University of Eastern Finland, Kuopio. It was a great opportunity for my professional growth.

Finally, last but certainly not least, I want to mention and thank all people who have collaborated for carrying out my research work, in particular Prof. Damiano Gustavo Mita (Interuniversity Consortium INBB, National Laboratory Endocrine Disrupters, Naples, Italy), Prof. Assunta Borzacchiello (Institute for Polymers, Composites and Biomaterials, National Research Council, CNR, Naples, Italy), Prof. Bruno De Gennaro (Dept. Chemical Engineering, Materials and Industrial Production, Univ. of Naples Federico II, Italy) and Prof. Rosario Vincenzo Iaffaioli (Dept. Abdominal Oncology, Istituto Nazionale per lo Studio e la Cura dei Tumori, Fondazione "G. Pascale"-IRCCS, Naples, Italy).